KINETICS OF THE METALLOTHERMIC REDUCTION OF MAGNESIA IN MOLTEN SLAGS

by

JOSÉ DEODORO TRANI CAPOCCHI, B.Sc., M.Sc.

July, 1977

A thesis submitted for the degree of Doctor of Philosophy of the University of London and for the Diploma of Imperial College.

John Percy Research Group
Department of Metallurgy and Materials Science
Imperial College
London, S.W.7

BEST COPY

AVAILABLE

Variable print quality

ABSTRACT

Molten slags of the composition 5.6% MgO, 48.1% Al_2O_3 and 46.3% CaO were reacted with ferroaluminium (80% Al and 35% Al), in graphite crucibles, at 1435 - 1450 C and reduced pressure (28 - 63 mm Hg). Experiments were also made with bubbling of argon through the slag/metal melt (argon flow rate = 1040 - 2040 $ml.min^{-1}$ STP). A new technique was developed for measuring the rate of evolution of magnesium vapour transported from the reaction zone to a condenser which was continuously weighed by means of a load cell.

In the reduced-pressure experiments it was found that, in the range of operating pressures and compositions studied, the final yield of magnesium increased linearly as the pressure decreased. Values of the standard free energy change, ΔG^0_T. for the reaction

$$(MgO) + \frac{2}{3}[Al] \rightarrow Mg_{(g)} + \frac{1}{3}(Al_2O_3)$$

were estimated to be in the range -2.6 to 5.5 kcal/mole MgO at 1708 - 1723 K and these are well within the uncertainty of ΔG^0_T calculated from existing data.

The rate per unit driving force with the 80% Al-alloy was 4.7 times that with the 35% Al-alloy mainly because of the larger slag/metal interfacial area when the 80% Al-alloy was used. In this case the metal phase existed as a dispersion of droplets whereas with the 35% Al-alloy it existed as a distinct layer below the slag. The overall process appears to be controlled by transport in the slag phase and/or by a first order, reversible reaction taking place at the slag/metal interface.

It was possible to recover magnesium from slags by bubbling argon through the melt at atmospheric pressure, although rates were

one to three orders of magnitude lower than those obtained at reduced pressures. A continuous process for producing magnesium from molten slags by bubbling inert gas could be of potential industrial interest, since operation at atmospheric pressure is very desirable.

The deposits of magnesium produced by reduction of $MgO - Al_2O_3 - CaO$ slags with ferroaluminium were more than 98.5 atomic percent pure. However, reduction of MgO from silicate slags with ferrosilicon yielded magnesium which was heavily contaminated with silicon and carbon.

To Silvia, Eduardo and Roberto

CONTENTS

	Page
CHAPTER 1 - INTRODUCTION	17
CHAPTER 2 - THEORETICAL BACKGROUND	20
2.1 - Chemistry and Thermodynamics	20
2.1.1 - Reduction of solid MgO-bearing raw materials with metals	20
2.1.1.1 - Aluminothermic reduction	20
2.1.1.2 - Silicothermic reduction	22
2.1.1.3 - Conclusions from the thermochemical assessment of the reduction of solid MgO-bearing materials with aluminium and silicon	27
2.1.2 - Reduction of molten MgO-bearing slags with ferroalloys	29
2.1.2.1 - Reduction with ferroaluminium	33
2.1.2.2 - Reactions of CaO and Al_2O_3 from the slag with ferroaluminium	42
2.1.2.3 - Reactions of $Mg_{(g)}$ with Al_2O_3 and CaO present in the slag and solution of magnesium in ferroaluminium	44
2.1.2.4 - Reduction with ferrosilicon	44
2.1.2.5 - Reactions of SiO_2, CaO and Al_2O_3 present in the slag with ferrosilicon	48
2.1.2.6 - Reactions of $Mg_{(g)}$ with SiO_2 present in the slag phase and the solution of magnesium in ferrosilicon	52
2.1.2.7 - Reactions of MgO, CaO and Al_2O_3 with carbon	52
2.1.2.8 - Formation of carbides	54
2.1.2.9 - Evaporation of metals, oxides and carbides	54

Page

2.1.2.10 - Conclusions from the thermodynamic assessment of reduction of molten MgO-bearing slags with ferroalloys 56

2.2 - Kinetics of Reduction of MgO-Bearing Solid Materials With Metals 60

2.3 - Kinetics of Slag/Metal/Gas Reactions 62

CHAPTER 3 - EXPERIMENTAL WORK 71

3.1 - Apparatus and Technique used for Measuring Rates of Evolution of Magnesium 71

3.1.1 - Furnace 75

3.1.2 - Retort assembly 77

3.1.3 - Probe for collecting and weighing the deposit of magnesium 79

3.1.4 - Pressure control for reduced pressure experiments 83

3.1.5 - Procedures for conducting experiments 87

3.1.5.1 - Preparation for an experiment 87

3.1.5.2 - Heating cycle 89

3.1.5.3 - Experiments on reduction of slags at reduced pressures 89

3.1.5.4 - Experiments on reduction of slags at atmospheric pressure with bubbling of argon through the melt 91

3.2 - Preparation of Slags and Ferroalloys 91

3.3 - Visual Observation of the Surface of the Slag/Metal Melt 93

3.3.1 - Apparatus 93

3.3.2 - Experimental procedure 93

3.4 - Reduction of SiO_2 - MgO-Bearing Slags with Ferrosilicon 95

3.4.1 - Apparatus 97

3.4.2 - Experimental procedure 97

Page

CHAPTER 4 - RESULTS

4.1 - Reduction of Molten MgO - Al_2O_3 - CaO Slags with Ferroaluminium 105

4.1.1 - Effect of reduced pressures 105

4.1.2 - Pressure at which magnesium vapour boiled off the slag/metal melt 116

4.1.3 - The effect of argon flow rate 120

4.2 - Reduction of MgO from Silicate Slags with Ferrosilicon 122

CHAPTER 5 - DISCUSSION 133

5.1 - Reduction of MgO from Molten MgO - Al_2O_3 - CaO Slags with Ferroaluminium 133

5.1.1 - Equilibrium between slag and alloy at reduced pressures 133

5.1.2 - Effect of pressure on rate 141

5.1.3 - Effect of argon flow rate bubbled through the melt on the rate of reduction of MgO 147

5.1.4 - Purity of the deposits of magnesium 153

5.2 - Reaction of MgO Dissolved in Silicate Slags with Ferrosilicon at Reduced Pressures 154

CHAPTER 6 - CONCLUSIONS 156

APPENDICES 159

Appendix 1 - Metallothermic processes of production of magnesium 160

Appendix 2 - Activity of aluminium in Fe-Al and Fe-Al-C alloys 165

Appendix 3 - Power supply 172

Appendix 4 - Phase Diagrams 174

REFERENCES 179

ACKNOWLEDGEMENTS 185

LIST OF FIGURES

		Page
Figure 2.1	- p_{Mg} vs. temperature for reduction of solid MgO and CaO.MgO with aluminium and Al-alloys	23
Figure 2.2	- Activities of Al and Si in Fe-Al and Fe-Si alloys	34
Figure 2.3	- Variation of the equilibrium constant cf reaction (2.18) with temperature	38
Figure 2.4	- p_{Mg} vs. yield of magnesium for reaction of slags with ferroaluminium alloys (calculated values)	40
Figure 2.5	- p_{Mg} vs. yield of magnesium for reaction of slags with Fe-75% Si (calculated values)	47
Figure 2.6	- Standard free energies of formation of carbides	55
Figure 2.7	- Vapour pressure of Mg, Ca, Al, Si and Fe	57
Figure 2.8	- Generalised representation of concentration gradients across a slag/metal system	65
Figure 3.1	- Schematic diagram of the apparatus used for measuring rates of evolution of magnesium	72
Figure 3.2	- Layout of the furnace; (a) elevation; (b) plan	74
Figure 3.3	- Circuit diagram of the furnace	76
Figure 3.4	- Maximum permissible loading of the heating elements	78
Figure 3.5	- Supporting for the tube of the furnace and for locating the probe	80
Figure 3.6	- View of the upper part of the 140 mm × 120 mm tube furnace	82
Figure 3.7	- General view of the furnaces	80
Figure 3.8	- Retort assembly (a)- lance (b)	84
Figure 3.9	- Temperature at the bottom of the crucible vs. temperature in the hot chamber	86

Page

Figure 3.10 - Types of condenser which were tried 88

Figure 3.11 - Crown of crystals of magnesium 90

Figure 3.12 - Probe for collecting and weighing the deposit of magnesium 92

Figure 3.13 - (a) Probe; (b) load cell; (c) condenser 94

Figure 3.14 - Calibration curve of the load cell 96

Figure 3.15 - Typical example of procedure for obtaining a required pressure in the furnace 98

Figure 3.16 - Calibration curve of the pressure transducer 100

Figure 3.17 - Schematic diagram of the apparatus used for visual observation of the surface of the melt 102

Figure 3.18 - View of the upper part of the apparatus used for visual observation of the melt 82

Figure 3.19 - Schematic diagram of the apparatus used for studies on the reduction of MgO from silicate slags 104

Figure 4.1a - Effect of reduced pressure on the yield of magnesium; 80% Al-alloy; 1435C 107

Figure 4.1b - Effect of reduced pressure on the yield of magnesium; 35% Al-alloy; 1460 C 109

Figure 4.2a - Effect of reduced pressure on the reduction of MgO; 80% Al-alloy; 1435 C 111

Figure 4.2b - Effect of reduced pressure on the reduction of MgO; 35% Al-alloy; 1460 C 113

Figure 4.3a - Semi-log plot $\log\{[(\%MgO)_t - (\%MgO)_{eq}] / [(\%MgO)_0 - (\%MgO)_{eq}]\} = - Kt$; 80% Al-alloy; 1435 C 115

Figure 4.3b - Semi-log plot $\log\{[(\%MgO)_t - (\%MgO)_{eq}] / [(\%MgO)_0 - (\%MgO)_{eq}]\} = - Kt$; 35% Al-alloy; 1460 C 117

Page

Figure 4.4 - Pressure drop from 113 mm Hg to 38 mm Hg (Experiment A-2) 119

Figure 4.5 - Frozen melt; 80% Al-alloy; 30 mm Hg pressure 121

Figure 4.6 - Frozen melt; 80% Al-alloy; 63 mm Hg pressure 121

Figure 4.7 - Frozen melt; 35% Al-alloy; 28 mm Hg pressure 121

Figure 4.8 - Frozen melt; 35% Al-alloy; 39 mm Hg pressure 121

Figure 4.9 - Droplets of aluminium alloy (80% Al-Fe) 123

Figure 4.10 - Effect of reduced pressure on the expansion of the slag/metal melt 123

Figure 4.11 - Variation of the final yield of magnesium with pressure . 125

Figure 4.12a - Yield of magnesium versus time; argon-bubbling; 80% Al-alloy; 1450 C 127

Figure 4.12b - Yield of magnesium versus time; argon-bubbling; 35% Al-alloy; 1455 C 129

Figure 4.13a - Reduction of MgO at atmospheric pressure with bubbling of argon through the melt; 80% Al-alloy; 1450 C 131

Figure 4.13b - Reduction of MgO at atmospheric pressure with bubbling of argon through the melt; 35% Al-alloy; 1455C 132

Figure 4.14 - Cross-section of crucible containing slag + metal after bubbling of argon 123

Figure 5.1 - Activities of Al_2O_3 and CaO in CaO - Al_2O_3 melts at 1500 C 135

Page

Figure 5.2 - Variation of p_{Mg} with x_{MgO} 138

Figure 5.3 - Evolution of $Mg_{(g)}$ per unit volume of slag in experiments A-4 and A-5 145

Figure 5.4 - Schematic flow diagram for the gas-bubbling process 152

Figure A2.1 - Activity coefficient of aluminium for Fe-Al and Fe-Al-C alloys at 1600 C 166

Figure A2.2 - Solubility of carbon in liquid Fe-Al alloys 168

Figure A2.3 - Effect of carbon on activity coefficient of aluminium in Fe-Al-C alloys 170

Figure A4.1a - System CaO - MgO - Al_2O_3 175

Figure A4.1b - System CaO - MgO - Al_2O_3 (stability field of $3CaO.MgO.2Al_2O_3$) 176

Figure A4.2 - The Fe-Al system 177

Figure A4.3 - The Fe-Si system 178

LIST OF TABLES

Page

Table 2.1 - p_{Mg} and ΔH^0_T for the reduction of solid MgO and CaO.MgO with Al and Si 28

Table 2.2 - Equilibrium constants of reaction (2.18) and (2.19) at 1700 K 32

Table 2.3 - Standard free energy and standard enthalpy of formation of hypothetical liquid oxides 36

Table 2.4 - Properties of slag and ferroaluminium 37

Table 2.5 - Calculated values of p_{Mg} at yield = 90% (reduction of slags) 41

Table 2.6 - Standard free energy of formation of aluminium and silicon sub-oxides 43

Table 2.7 - Proerties of slag and ferrosilicon 46

Table 2.8 - Calculated values of p_{SiO} and p_{Mg} 49

Table 2.9 - Distribution of Ca and Mg among phases present in the smelting of Fe-Si-Ca-Mg alloys 51

Table 2.10 - Vapour pressures of oxides and carbides 58

Table 4.1 - Reduction of slag with ferroaluminium; reduced-pressure experiments; series A and series B 106

Table 4.2 - Values of K (defined by equation (4.11)) for various experiments 114

Table 4.3 - Composition of the magnesium deposits 118

Table 4.4 - Visual observation of the slag/metal surface 124

Table 4.5 - Reduction of slag with ferroaluminium; argon-bubbling experiments; series C and series D 126

Table 4.6 - Chemical analysis of the deposits produced when silicate slags were reacted with Fe-75% Si at reduced pressures 128

Page

Table 5.1 - Values of the equilibrium constant of reaction (2.18) derived from experimental points 140

Table 5.2 - Comparison between values for ΔG^0_T of reaction (2.18) derived from experimental points with those calculated from the standard free energies of formation of hypothetical liquid MgO and Al_2O_3 142

Table 5.3 - Volumetric flow rate of $Mg_{(g)}$ observed in experiments of series A and series B 146

Table 5.4 - Rates of reduction of MgO at reduced pressures and at atmospheric pressure with bubbling of argon through the Slag/metal melt 148

Table 5.5 - p_{Mg} in Ar + $Mg_{(g)}$ mixtures 150

Table 5.6 - Calculated values for p_{Mg} and p_{SiO} at various temperatures and activities of MgO and SiO_2 in the slags 155

Table A2.1 - Activity of Al in Fe-Al and Fe-Al-C alloys at 1600 C 171

LIST OF SYMBOLS

a	activity	
A	interfacial area	cm^2
A_s	slag/metal interfacial area	cm^2
A_g	metal/gas interfacial area	cm^2
C	concentration	$mols.cm^{-3}$
C_t	concentration at any time t	$mols.cm^{-3}$
C_o	concentration at time t=0	$mols.cm^{-3}$
C_{eq}	concentration at the equilibrium	$mols.cm^{-3}$
d	diameter	cm
D	diffusion coefficient	$cm^2.s^{-1}$
E	voltage	mV
f	as subscript, relating to formation	
fus	as subscript, relating to fusion	
(g),g	as subscript, relating to gas	
ΔG^0_T	standard free energy change at temperature T	cal/mole
ΔH^0_T	standard enthalpy change at temperature T	cal/mole
i	as subscript, relating to interface	
k	mass transfer coefficient	$cm.s^{-1}$
k_M	mass transfer coefficient relating to metal	$cm.s^{-1}$
k_{sl}	mass transfer coefficient relating to slag	$cm.s^{-1}$
k_g	mass transfer coefficient relating to gas	$cm.s^{-1}$
k'_M	mass transfer coefficient relating to metal (equation (2.66))	$cm.s^{-1}$
K	equilibrium constant	

K(=kA/2.303V)	proportionality constant (equation (4.11))	s^{-1}
K_a	equilibrium constant for absorption	
K_1, K_2, K_1', K_2'	chemical rate constants	
(l)	as subscript, relating to liquid	
M	as subscript, relating to metal	
$\dot{n}$	rate	$mols.cm^{-3}.s^{-1}$
p	pressure	atm or mm Hg
$\hat{p}_R$	resultant pressure (equation (3.1))	mm Hg
p_R	resultant pressure (Section 3.1.4)	mm Hg
p_D	pressure in the tube of the furnace (equation (3.1))	mm Hg
$p_{l'}$	pressure in the surge tank (equation (3.1))	mm Hg
Q	gas flow rate	$m\ell min^{-1}$ or $cm^3.s^{-1}$
r	residual (Section 3.1.4)	
r	product moment correlation coefficient (Section 4.1.1)	
R	gas constant (=1.987 $calK^{-1}mole^{-1}$)	
R	total resistance (equation (A3.1))	ohms
s,sl	as subscript, relating to slag	
(s)	as subscript, relating to solid	
T	absolute temperature	K
t	time	min or s
V	volume	cm^3
V	nominal full lead (equation (A3.3))	V
V_{max}	maximum output voltage of the transformer (equation (A3.4))	V
x	molar fraction or atom fraction	
Y	yield	%

w_{Mg_t}	weight of magnesium at any time t	g
$w_{(MgO)_0}$	weight of MgO in the slag at t=0	g
$w_{(Al_2O_3)_0}$	weight of Al_2O_3 in the slag at t=0	g
$w_{(CaO)_0}$	weight of CaO in the slag at t=0	g
$w_{(MgO)_t}$	weight of MgO in the slag at time t	g
$w_{(Al_2O_3)_t}$	weight of Al_2O_3 in the slag at time t	g
$w_{(CaO)_t}$	weight of CaO in the slag at time t	g
$(\%MgO)_t$	wt.pct. MgO in the slag at time t	%
$(\%Al_2O_3)_t$	wt.pct. Al_2O_3 in the slag at time t	%
$(\%CaO)_t$	wt.pct. CaO in the slag at time t	%
[ ]	solute in the metal phase	
( )	solute in the slag	
< >	solid	
□	site	
θ	fraction of occupied sites	
γ, γ'	activity coefficient	

CHAPTER 1

INTRODUCTION

Most of the magnesium is, at present, produced by processes which are based on the electrolysis of anhydrous magnesium chloride baths but there are points to be considered which might make a metallothermic route very attractive. Electrolytic plants are heavy energy - consuming units; they require between 6.3×10^{10} and 7.2×10^{10} Joules (17500 - 20000 kWhr) per metric ton of metal, which is twice that for a Pidgeon plant [1] producing magnesium by the reduction of calcined dolomite with ferrosilicon (75% Si-alloy). Moreover, maintenance costs of electrolytic units are higher than those of a retort plant, mainly due to the corrosion of the electrical equipment by the electrolyte [2]. They are, in general, relatively large integrated units producing not less than 15000 metric tons of magnesium per year. On the other hand, a silicothermic unit (retort process) for example, situated near the dolomite mine, can be operated economically even with a production of less than 10000 metric tons per year and the capacity of the plant can be varied easily by changing the number of retorts.

The retort process however, has limitations. It is a labour intensive batch process which involves elaborate unit operations for the preparation of the charge including calcination and briquetting. It must be operated at temperatures below 1200C because of the limited heat resistance above this temperature of the nickel-chromium steel used for making the retorts. The output of magnesium per retort, which is about 50 kg per day, cannot be increased without using larger retorts. This is not a practical solution for enlarging the capacity of production, unfortunately, as the process is controlled by heat transfer to the pile of briquettes inside the retorts.

Despite its shortcomings, the retort process has always been an attractive alternative to the electrolytic ones, particularly where dolomite and ferrosilicon are available and the demand for primary magnesium does not justify the installation of a large electrolytic plant. For this reason, since the second World War a fair amount of effort has been put into the improvement of the Pidgeon process and the invention of new pyrometallurgical processes for the extraction of magnesium. These processes involve reduction of MgO-bearing raw materials (mainly dolomite) with metals (ferrosilicon, Fe-Al-Si alloys, Al-Si alloys and calcium), carbon and calcium carbide. Presently there are plants based on the following processes [3]:

(a) Retort process (Pidgeon process);

(b) Rotary furnace process;

(c) Knapsack process;

(d) Magnetherm process.

A literature survey on the various proposed metallothermic processes is presented in Appendix 1. The fundamental aspects concerning Chemical Metallurgy and Process Engineering are well known in the case of the Pidgeon process. Thermochemical studies of the reduction of magnesia and calcined dolomite with aluminium have also been reported. However, most of the information on the new processes is available in patents or papers which give only broad descriptions. There is a lack of scientific information on the thermodynamics of the reactions and phases involved. Molten slags are formed at high temperatures and it would appear that activities of MgO in these slags have not been determined. No data is available on the kinetics of reduction in liquid state. Even the Process Engineering aspects are far from clear. For instance, published information on the Magnetherm process, in which calcined dolomite is reduced with ferrosilicon under reduced pressures in an electric furnace, reveals several uncertainties and contradictions.

It is not clear whether reduction takes place entirely in the liquid state or in the solid state. According to the French practice [4] the composition of the charge should be controlled in such a way as to obtain a slag with the molecular ratios CaO/SiO_2 and Al_2O_3/SiO_2 greater than 1.8 and 0.26 respectively. It is claimed that this procedure avoided carbothermic reductions of MgO and SiO_2 and prevented the evolution of silicon monoxide due to the reaction of silica with silicon. The products of the side reactions are undesirable as they contaminate the magnesium with carbon, silicon, silica and magnesia. Japanese patents [5, 6] describe procedures by which the process was operated successfully with alumina-free slag at 1600C or, if alumina was added, the process could be carried out at 1300 - 1400C, using any MgO-bearing raw material. No information is given on the purity of the magnesium product obtained in their experiments.

The present research programme was devised to obtain data on the rate of reduction of molten magnesia-bearing slags with ferroalloys. The influence of reduced pressure on the rate of reduction and the yield of magnesium would allow a useful analysis of the chemical and transport phenomena involved. Existing processes rely exclusively on the application of reduced pressure to recover magnesium by batch operations. It was felt that, in principle, magnesium could be recovered also by bubbling an inert gas at atmospheric pressure through slag/metal melts. The comparison of the yield and rate of reduction between the two methods would also be of value in assessing the potential applications of the processes. This research could improve the state of knowledge of the existing and proposed processes for extraction of magnesium and provide a scientific basis for the assessment of further developments in the field.

Accordingly, the theoretical background for the present work will be dealt with in Chapter 2. This will be followed in Chapter 3 by the description of the apparatus and special techniques developed to study the kinetics of reduction. The results, their analysis and discussion will be presented in Chapters 4 and 5

CHAPTER 2

THEORETICAL BACKGROUND

This chapter deals with the theoretical background relevant to the experimental programme. A review of previous work on the chemical metallurgy of the reduction of solid briquettes of magnesia and calcined dolomite with aluminium and with silicon is followed by thermodynamic calculations for the reduction of magnesia from molten slags. The results of these calculations, which are based on existing thermodynamic data for hypothetical liquid oxides, have not been presented elsewhere. The possibility of the occurrence of side reactions and evaporation of various species are also discussed. This is followed by a survey of the literature on the kinetics of metallothermic reduction of MgO-bearing materials. Finally, chemical and transport kinetics of slag/metal and slag/metal/gas reactions are discussed.

2.1 CHEMISTRY AND THERMODYNAMICS

Metallothermic reduction of solid MgO-bearing raw materials and molten slags will be discussed separately in this section.

2.1.1 Reduction of solid MgO-bearing raw materials with metals

The two cases which have been comprehensively investigated are the reduction with aluminium and with silicon. Products of reaction have been identified and equilibrium vapour pressures of magnesium have been measured for various reactions by several research workers.

2.1.1.1 Aluminothermic reduction

The reduction of solid MgO-bearing materials with pure aluminium or its alloys at temperatures less than 1300C was investigated by Grjotheim et al. [7] Taitz [8] and Komatsu & Senda [9, 10] Briquetted mixtures of solid reactants were used but at the reaction temperatures the reducing metal was actually molten. Magnesium vapour was produced leaving a solid residue which contained aluminates. Magnesium aluminate

($MgAl_2O_4$) [7] and calcium aluminates [7-10] were obtained with pure magnesia and calcined dolomite respectively. Grjotheim et al. [7] concluded that the compound $12CaO.7Al_2O_3$ was the stable calcium aluminate in equilibrium with CaO in the temperatures range 850 - 1100C. At higher temperatures, i.e. between 1100C and 1300C, however, Taitz [8] suggested the formation of the compound $5CaO.3Al_2O_3$. Komatsu and Senda [9, 10] detected mainly the aluminate $3CaO.Al_2O_3$, but they also found the compound $5CaO.3Al_2O_3$ in the residue. Grjotheim et al. [7] investigated the stability of the aluminate $3CaO.Al_2O_3$ by analysing samples quenched from temperatures up to 1350C to room temperature. They found that below 1200C traces of the compound $12CaO.7Al_2O_3$ were present. Again, when samples of calcined dolomite and aluminium were heated above 1200C both aluminates appeared in the X-ray patterns of the samples, the amount of $3CaO.Al_2O_3$ increasing with time of holding at a given temperature. Thus they concluded that this compound must be formed at temperatures above 1200C below which it dissociates according to the solid state reaction

$$7\langle 3CaO.Al_2O_3\rangle \rightarrow \langle 12CaO.7Al_2O_3\rangle + 9\langle CaO\rangle \qquad (2.1)$$

The Al-Mg phase diagram shows complete miscibility of these metals in the liquid state. Therefore some magnesium was expected to enter into solution in the reducing metal. In fact, it has been reported [7] that the droplets of aluminium present in the reacted briquettes contained up to 10.4 ± 5 mole percent (approximately 9.7 wt. pct.) of magnesium, which corresponds to the activity of magnesium equal to 0.1. The reduction was carried out at 1000C and magnesium was removed from the reaction interface by means of a carrier gas (argon).

Although intermetallic compounds of calcium and aluminium are formed during the aluminothermic reduction of pure lime [11, 12], their formation has not been reported when calcined dolomite is used.

Equilibrium vapour pressures of magnesium have been determined by

several workers by means of the carrier gas technique. The results are summarised in Figure 2.1. Calculated curves, derived from existing thermodynamic data on the standard free energies of formation of solid oxides [13] magnesium aluminate [14] and calcium aluminates [15], are also plotted for the following reactions:

$$\langle MgO\rangle + \tfrac{1}{2}[Al] \rightarrow \tfrac{1}{4}\langle MgAl_2O_4\rangle + \tfrac{3}{4} Mg_{(g)} \quad (2.2)$$

$$\langle MgO\rangle + 4/7\langle CaO\rangle + 2/3[Al] \rightarrow 1/21\langle 12CaO.7Al_2O_3\rangle + Mg_{(g)} \quad (2.3)$$

$$\langle MgO\rangle + \langle CaO\rangle + 2/3[Al] \rightarrow 1/3\ \langle 3CaO.Al_2O_3\rangle + Mg_{(g)} \quad (2.4)$$

The equilibrium vapour pressures for the reduction of calcined dolomite are higher than those for pure magnesia because the formation of magnesium aluminate does not occur in the presence of lime. It is interesting to note that the calculated values of the equilibrium vapour pressure for reactions (2.3) and (2.4) are within one per cent of each other. The experimentally determined values of the vapour pressure are in good agreement with the theoretically predicted ones, considering the uncertainties inherent in the determinatiom of the standard free energies of formation of oxides and aluminates. When Al-alloys were used, the activity of aluminium would be decreased so that vapour pressures were lower than with pure aluminium, as expected.

The reduction of magnesia and calcined dolomite with aluminium is endothermic. In the range of temperatures 1127 - 1527C (1400 - 1800K) the standard enthalpies for reactions (2.2), (2.3) and (2.4) are 29 kcal/mole MgO, 42 kcal/mole MgO and 39 kcal/mole MgO respectively. These values were calculated from the standard enthalpies of formation of solid oxides [14] magnesium aluminate [14] and calcium aluminates [15].

2.1.1.2 Silicothermic reduction

The chemistry and thermodynamics of the reduction of briquettes of magnesia or calcined dolomite with ferrosilicon have been extensively

Figure 2.1 - Equilibrium vapour pressures of magnesium for the reduction of solid MgO and CaO.MgO with aluminium and its alloys. Calculated values for the reduction of MgO and CaO.MgO according to reactions (2.2), (2.3) and (2.4) are plotted as full lines above the boiling point of magnesium.

MgO + Al (Ref. 7)

CaO.MgO + Al (Ref. 7)

CaO.MgO + Al (Ref. 9)

CaO.MgO + Al - 50% Si (Ref. 9)

CaO.MgO + Al - 51% Si - 15% Fe (Ref. 7)

CaO.MgO + Al - 40% Si - 43% Fe (Ref. 9)

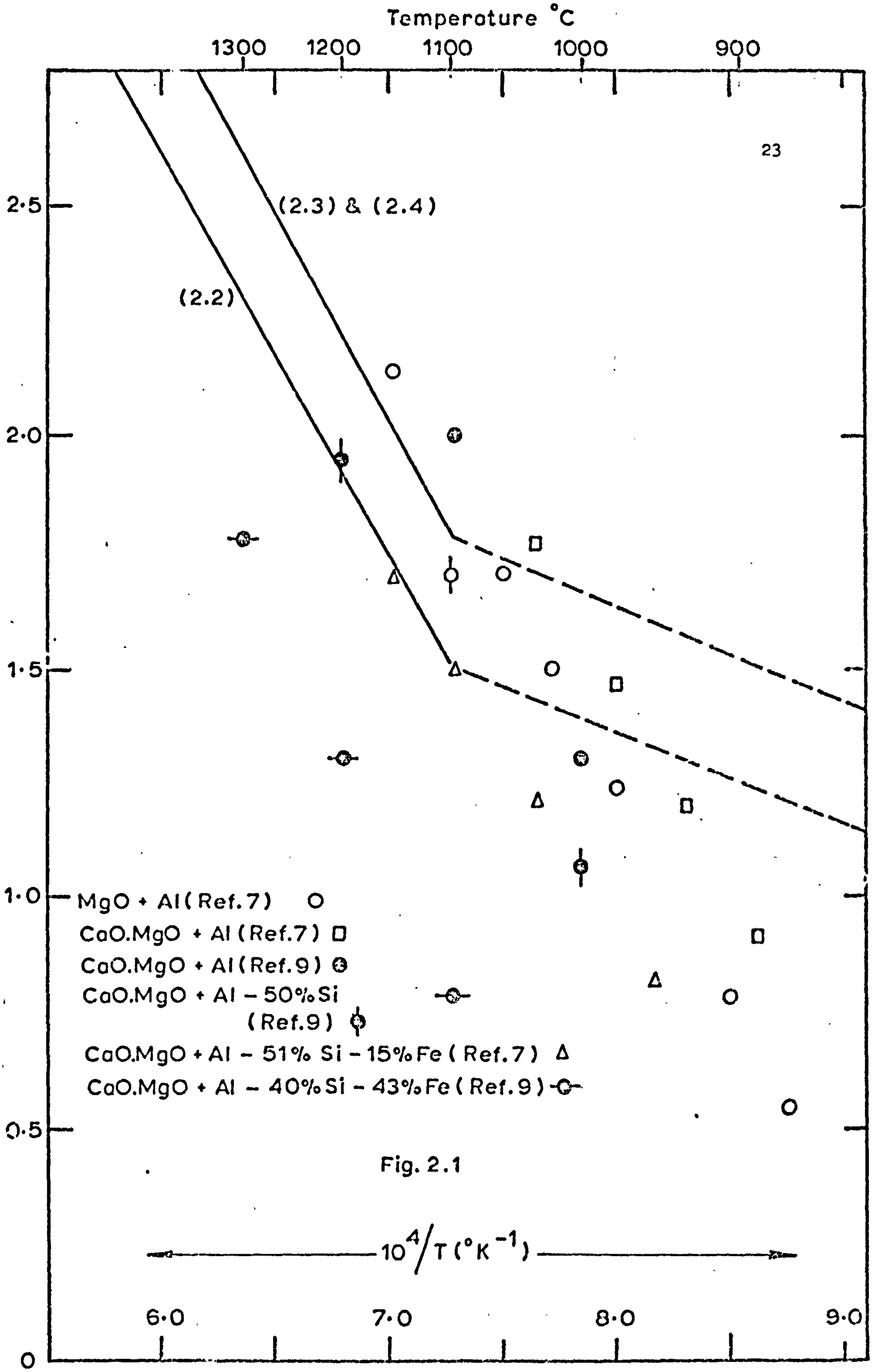

Temperature °C
1300
1200
1100
1000
900
2·5
2·0
1·5
1·0
0·5
0
Log p_{Mg} (m.m.Hg)
(2.3) & (2.4)
(2.2)
MgO + Al (Ref. 7) O
CaO.MgO + Al (Ref. 7) □
CaO.MgO + Al (Ref. 9) ⊕
CaO.MgO + Al – 50% Si (Ref. 9) ⊖
CaO.MgO + Al – 51% Si – 15% Fe (Ref. 7) △
CaO.MgO + Al – 40% Si – 43% Fe (Ref. 9) -O-
$10^4/T\ (°K^{-1})$
6·0
7·0
8·0
9·0

Fig. 2.1

studied since 1940. From X-ray analysis of the products from the reduction of magnesia with silicon Schneider & Hesse [16] established that magnesium orthosilicate was formed according to the reaction

$$\langle MgO\rangle + \tfrac{1}{4}\, Si_{(s,l)} \rightarrow \tfrac{1}{2}\, Mg_{(g)} + \tfrac{1}{4}\langle Mg_2SiO_4\rangle \qquad (2.5)$$

Pidgeon & King [17] suggested that this reaction would proceed in the solid state at temperatures up to 1200C. However, Toguri & Pidgeon [18] have shown that the reduction of MgO with silicon cannot be described by a single solid - state diffusion mechanism. The reduction proceeds by solid/solid and solid/gas reactions involving the formation of silicon monoxide particularly above 1280C. The proposed [18] reaction for the evolution of $SiO_{(g)}$ is

$$\langle MgO\rangle + Si_{(s,l)} \rightarrow Mg_{(g)} + SiO_{(g)} \qquad (2.6)$$

The formation of magnesium orthosilicate would take place according to the reaction

$$\langle MgO\rangle + SiO_{(g)} \rightarrow \tfrac{1}{2}\langle Mg_2SiO_4\rangle + \tfrac{1}{2}\, Si_{(s,l)} \qquad (2.7)$$

It has been suggested by Kroll [19,20] that magnesium silicide is formed as an intermediate product during the process but Toguri & Pidgeon [18] were not able to detect this compound even at the earlier stages of the reaction. The production of Mg_2Si is thermodynamically more favourable than that of magnesium vapour at temperatures up to 1900C [21,23], although for both reactions the standard free energy change is positive.

The reaction

$$MgO_{(s,l)} + \tfrac{1}{2}\,[Si] \rightarrow \tfrac{1}{4}\,[Mg_2Si] + \tfrac{1}{4}\, Mg_2SiO_{4\ (s,l)} \qquad (2.8)$$

occurs during the smelting of Fe-Si-Mg alloys at 1800-1900C and at atmospheric pressure. In this case the transfer of magnesium to the metal

phase is attributed to the formation of magnesium silicide [21-23]. It is difficult to confirm whether or not this compound is produced at reduced pressures because it could decompose liberating magnesium vapour according to the reaction

$$\tfrac{1}{2}\ MgSi_{2\ (s,l)} \rightarrow Mg_{(g)} + \tfrac{1}{2}\ Si_{\ (s,l)} \qquad (2.9)$$

The reduction of calcined dolomite produces several intermediate compounds. The overall reaction, however, could be described by

$$\langle CaO.MgO\rangle + \tfrac{1}{2}\ Si_{(s,l)} \rightarrow \tfrac{1}{2}\langle Ca_2SiO_4\rangle + Mg_{(g)} \qquad (2.10)$$

A valuable contribution to the explanation of the chemical steps in the silicothermic reduction of calcined dolomite was made by Schneider [24,25]. Their investigation established the following mechanism:

In the range of temperatures 600-1000C calcium di-silicide can be formed according to the reaction

$$\langle CaO\rangle + \tfrac{1}{2}\langle Si\rangle \rightarrow 1/5\langle CaSi_2\rangle + 1/10\langle Ca_2SiO_4\rangle + 3/5\langle CaO\rangle \qquad (2.11)$$

Reduction of MgO subsequently takes place by:

$$\langle MgO\rangle + 1/5\langle CaSi_2\rangle + 3/5\langle CaO\rangle \rightarrow Mg_{(g)} + 2/5\langle Ca_2SiO_4\rangle \qquad (2.12)$$

The sum of equations (2.11) plus (2.12) will give reaction (2.10).

At 1020C $CaSi_2$ decomposes according to the peritectic reaction

$$\langle CaSi_2\rangle \rightarrow \langle CaSi\rangle + \text{Liquid} \qquad (2.13)$$

At 1245C calcium monosilicide melts congruently producing a Ca-Si alloy. In the presence of ferrosilicon a ternary alloy results. The eutectic point of the Fe-Si-Ca system is at 890C and it corresponds to the 55% Si - 25% Fe - 20% Ca alloy. At this stage the reducing alloy is molten and contains also calcium which might then play an effective role in the reduction process of magnesium oxide according to the reaction

$$Ca_{(l,g)} + \langle MgO\rangle \rightarrow \langle CaO\rangle + Mg_{(g)} \qquad (2.14)$$

The production of calcium silicides which is more favoured to that of calcium vapour in the reduction of pure lime at atmospheric pressure, is also relevant for the smelting of Fe-Si-Ca alloys [21]. It has been shown [21] that, in the smelting of Fe-Si-Ca-Mg alloys from dolomite and ferrosilicon, calcium will be distributed almost entirely between the slag and the metal phases, whereas most of the magnesium reduced will be lost as vapour.

Hughes et al. [26] detected the compound $Ca_3Mg(SiO_4)_2$ in partly reacted briquettes of calcined dolomite and ferrosilicon and suggested that the reaction may proceed in accordance with equation (2.15):

$$\langle MgO\rangle + 1/3\ \langle CaO\rangle + 1/6\ \langle CaSi_2\rangle \rightarrow 1/6\ \langle Ca_3Mg(SiO_4)_2\rangle + 5/6\ Mg_{(g)} \qquad (2.15)$$

In fully reacted briquettes they also found Ca_2SiO_4 which would be formed according to the reaction

$$5/6\ \langle Ca_3Mg(SiO_4)_2\rangle + 1/6\ \langle CaSi_2\rangle + 4/3\ \langle CaO\rangle \rightarrow 2\ \langle Ca_2SiO_4\rangle + 5/6\ Mg_{(g)} \qquad (2.16)$$

The formation of $CaSi_2$ is described by a reaction which differs from (2.11) in the sense that no free lime is regenerated, but the silicate Ca_3SiO_5 is produced with $CaSi_2$ according to (2.17):

$$\langle CaO\rangle + \langle Si\rangle \rightarrow 2/5\ \langle CaSi_2\rangle + 1/5\ \langle Ca_3SiO_5\rangle \qquad (2.17)$$

The conclusions from the previous work on the reduction of calcined dolomite with ferrosilicon demonstrate clearly that the reaction (2.10) cannot possibly describe the actual process, as it proceeds through several other chemical steps which involve solid/solid, solid/liquid and solid/gas reactions. Reaction (2.10) however, may be used for the calculation of the equilibrium vapour pressure of magnesium in the overall process. Similarly, reaction (2.5) only describes the overall process of reduction of pure magnesia and may also be used for the calculation of the equilibrium vapour pressure of magnesium in that case.

The equilibrium vapour pressure of magnesium above reaction mixtures containing magnesia or calcined dolomite and ferrosilicon have been determined by several research workers. The results have been reviewed by Akerman et al. [27] and, more recently, by Krüger [28]. For this reason they are not going to be presented here. In general, the experimentally determined values are in good agreement with those predicted from the standard free energy change for reactions (2.5) and (2.10). Calculated values of the equilibrium vapour pressure are tabulated in Table 2.1 for temperatures which are of relevance to existing and proposed processes for extraction of magnesium. The standard free energies of formation of MgO [13], Al_2O_3 [13], SiO_2 [13], $MgAl_2O_4$ [14], $12CaO.Al_2O_3$ [15], $3CaO.Al_2O_3$ [15], Mg_2SiO_4 [14] and Ca_2SiO_4 [13] were used in the calculations. The enthalpy changes for the silicothermic reduction, according to reactions (2.5) and (2.10), are also tabulated together with the figures for the aluminothermic reduction of magnesia and calcined dolomite, for comparison. Standard heats of formation of solid oxides (MgO and SiO_2) [14], magnesium silicate (Mg_2SiO_4) [15] and calcium silicate (Ca_2SiO_4) [15] were used for the calculation of the heats of reaction. As would be expected, the equilibrium vapour pressures for the reduction of calcined dolomite with silicon are higher than those generated when pure magnesia is reduced, since magnesium silicate is not produced. Silicothermic reduction is also endothermic.

2.1.1.3 Conclusions from the thermochemical assessment of the reduction of solid MgO-bearing materials with aluminium and silicon

The thermochemical assessment of previous work on the reduction of briquettes of magnesia and calcined dolomite with aluminium and silicon may be summarized as follows:

(a) Reactions (2.2), (2.3), (2.4), (2.5) and (2.10) are over-simplified representations of the reduction processes. However, they are useful for thermodynamic calculations which are in good agreement with experimental results obtained by various research workers.

Table 2.1

Calculated values of the equilibrium vapour pressure of magnesium and heat of reaction for the reduction of solid magnesia and calcined dolomite with aluminium and silicon

Reaction	Reactants	Equilibrium vapour pressures (in mm Hg) @ :			Heat of reaction (kcal/mol MgO)
		1400 K	1600 K	1800 K	@ 1400 - 1800 K
(2.2)	MgO + Al	41.6	258.9	1009.6	29
(2.3)	CaO.MgO + Al	82.1	530.2	-	42
(2.4)	CaO.MgO + Al	83.4	535.7	2210.1	39
(2.5)	MgO + Si	0.156	2.6	20.8	34
(2.10)	CaO.MgO + Si	6.2	69.5	396.8	54

(b) From a pure thermodynamic point of view, aluminium is a better reducing agent than silicon for magnesia and calcined dolomite, as it generates magnesium at higher vapour pressures and the reactions are less endothermic. Moreover aluminothermic processes may be carried out at atmospheric pressure, provided that the temperatures are higher than 1480C for magnesia and 1370C for calcined dolomite, and the activities of the species involved are equal to unity. For the silicothermic reduction, the temperatures at which the calculated vapour pressures of magnesium exceeds 760mmHg are 2010C and 1590C for magnesia and calcined dolomite respectively.

(c) Reduction of calcined dolomite is thermodynamically more favourable than the reduction of pure magnesia. When pure magnesia is reduced, 25% and 50% of the magnesium atoms are consumed for the production of $MgAl_2O_4$ and Mg_2SiO_4 respectively, whereas with calcined dolomite the calcium aluminate and calcium silicate are produced instead.

(d) The vapour pressure of magnesium increases greatly with temperature, particularly for the silicothermic reduction.

(e) Calculated values of the equilibrium vapour pressure of magnesium generated according to reactions (2.3) and (2.4) are very close to each other. Both reactions may be used to describe the overall process of reduction of calcined dolomite with aluminium. However, above 1200C, as the aluminate $3CaO.Al_2O_3$ is stable, reaction (2.4) will occur.

2.1.2 Reduction of molten MgO-bearing slags with ferroalloys

Granulated raw materials are charged into electric reduction furnaces for the extraction of magnesium or smelting of Fe-Si-Ca-Mg alloys. When the temperature of the charge reaches approximately 1400C, slags containing MgO and CaO start to form. At this stage, reduction of slag with already existing liquid metal commences. The extent of reduction in the liquid

state will depend on the amount of slag, which is governed by the rate of heat transfer to the solids, their heat capacity and chemical composition. Coarse raw materials and the addition of alumina, for example, could help the formation of molten slags at relatively low temperatures. Under these circumstances reduction in the liquid state would play an importart role in the overall process [4].

An accurate thermodynamic assessment of the reduction of MgO-bearing slags in the liquid state is not possible, as relevant scientific information required is not available at present. For example, activities of MgO in such slags have not been determined, the actual ionic species involved in the reduction process are still a matter of speculation and values for the standard free energy of formation of liquid oxides are not precisely known. Despite all these difficulties an attempt to estimate the equilibrium vapour pressure of magnesium which would be generated by the reduction of slags with ferroaluminium and ferrosilicon will be made on the basis of the following assumptions:

(a) The aluminothermic and silicothermic reduction of molten MgO-bearing slags are decribed, respectively, by reactions (2.18) and (2.19):

$$(MgO) + 2/3[Al] \rightarrow Mg_{(g)} + 1/3(Al_2O_3) \qquad (2.18)$$

$$(MgO) + \tfrac{1}{2}[Si] \rightarrow Mg_{(g)} + \tfrac{1}{2}(SiO_2) \qquad (2.19)$$

(b) Molar fractions of MgO, Al_2O_3 and SiO_2 are used in the calculations, instead of the corresponding activities in the slag phase.

(c) Extrapolated values for the activities of aluminium are used for the alloy compositions and temperatures at which they have not been determined.

(d) Standard free energies of formation of hypothetical liquid oxides are used to calculate the free energies of reactions (2.18) and (2.19).

Assumption (a) was made bearing in mind that the actual ionic species which participate in the processes and the nature of the interface reactions are unknown. Therefore, reactions (2.18) and (2.19) describe overall processes. Absorption-desorption mechanisms and eletrochemical reactions occurring at the slag/metal/gas interface are not considered. Assumption (b) implies that activity coefficients (γ) of the oxides are equal to unity. Existing data on the activities of aluminium and silicon in their alloys with iron may be extrapolated to find the required values at the temperatures and compositions studied. Standard free energies of formation of hypothetical liquid oxides may be derived from data on solid oxides and from measurements of the melting properties.

The expressions for calculation of the equilibrium vapour pressure of magnesium are

$$P_{Mg} = (x_{MgO} \cdot a_{Al}^{2/3} / x_{Al_2O_3}^{1/3}) \cdot \exp(-\Delta G_T^\circ / R.T) \qquad (2.20)$$

and

$$P_{Mg} = (x_{MgO} \cdot a_{Si}^{1/2} / x_{SiO_2}^{1/2}) \cdot \exp(-\Delta G_T^\circ / R.T) \qquad (2.21)$$

for reactions (2.18) and (2.19) respectively.

The values of the standard free energy of formation of liquid oxides are less accurately known than those of solid oxides. Richardson [29] has suggested that the uncertainties in the values of $\Delta G_{T,f}^\circ$ for solid MgO and Al_2O_3 are ± 10 kcal/mole O_2 and ± 3 kcal/mole O_2 respectively. For solid SiO_2 the suggested accuracy is also ± 3 kcal/mole O_2. Even using the same values of uncertainties for the liquid oxides, the standard free energy changes for reactions (2.18) and (2.19) would only be accurate to within ± 6.5 kcal/mole MgO. Examples are given in Table 2.2 where it is assumed that hypothetical liquid MgO is reduced with liquid aluminium (or liquid silicon) to produce magnesium vapour and hypothetical liquid Al_2O_3 (or liquid SiO_2). The scatter in the calculated values of the equilibrium constant shown in the table results from this uncertainty in

Table 2.2

Equilibrium constants of reactions (2.18) and (2.19) at 1700 K

$\Delta G^0_{T,f}$ Al_2O_3 (cal/mole)	$\Delta G^0_{T,f}$ SiO_2 (cal/mole)	$\Delta G^0_{T,f}$ MgO (cal/mole)	ΔG^0_T reaction (cal/mole MgO)	$K_{(2.18)}$	$K_{(2.19)}$
-264006	-145106	-87381	- 621	-	-
± 4500	± 3000	± 5000	±6500	-	-
-259506	-	-92381	5879	0.175	-
-264006	-	-87381	- 621	1.202	
-268506	-	-82381	-7121	8.233	-
-	-142106	-92381	21328	-	0.002
-	-145106	-87381	14828	-	0.012
-	-148106	-82381	8328	-	0.085

the free energies for formation.

Equations (2.20) and (2.21) show that the equilibrium vapour pressure at which magnesium is generated decreases as the isothermal reduction proceeds, due to the depletion of the reactants. In industrial processes the activities of the reducing metals change considerably as aluminium or silicon are consumed by the reaction.

In the M.C. process [30] which uses calcined dolomite and ferro-aluminium (Appendix 1), the concentration of aluminium in the alloy decreases from 20-25% at the start to 7-8% at the end of reduction and the activity of aluminium would drop to 1/4 of its initial value. For the Magnetherm process [31, 32] Fe-75% Si is used and the alloy at the end of a heat contains only 20-30% Si. In this case, the activity of silicon could drop from 0.9 to 0.2. The concentration of magnesia in the slag probably drops from around 10-15% to about 3% in the case of the Magnetherm process. The concentrations of alumina and silica do not vary greatly during the heat as only 0.33 mole of alumina and 0.5 mole of silica are produced for each mole of magnesia reduced. If a great excess of ferroalloy is present, then the change in the activities of aluminium or silicon will be negligible so that the equilibrium vapour pressure will decrease linearly with the yield of magnesium.

The activities of aluminium [33, 34] and silicon [35-37] in alloys with iron are given in Figure 2.2 (see also Appendix 2). Standard free energies of formation and heats of formation of hypothetical liquid oxides are given in Table 2.3 [14, 38-40].

2.1.2.1 Reduction with ferroaluminium

Reduction of magnesia from molten slags with ferroaluminium according to reaction (2.18) will be dealt with in this section. Results of calculations of equilibrium constant derived from different sets of thermodynamic data will be discussed. Theoretical curves of the variation of

Figure 2.2 - Activities of aluminium and silicon in alloys of the binary systems Fe-Al and Fe-Si.

Al, @ 1600 C, (Ref. 34)

Al, @ 1600 C, (Ref. 33)

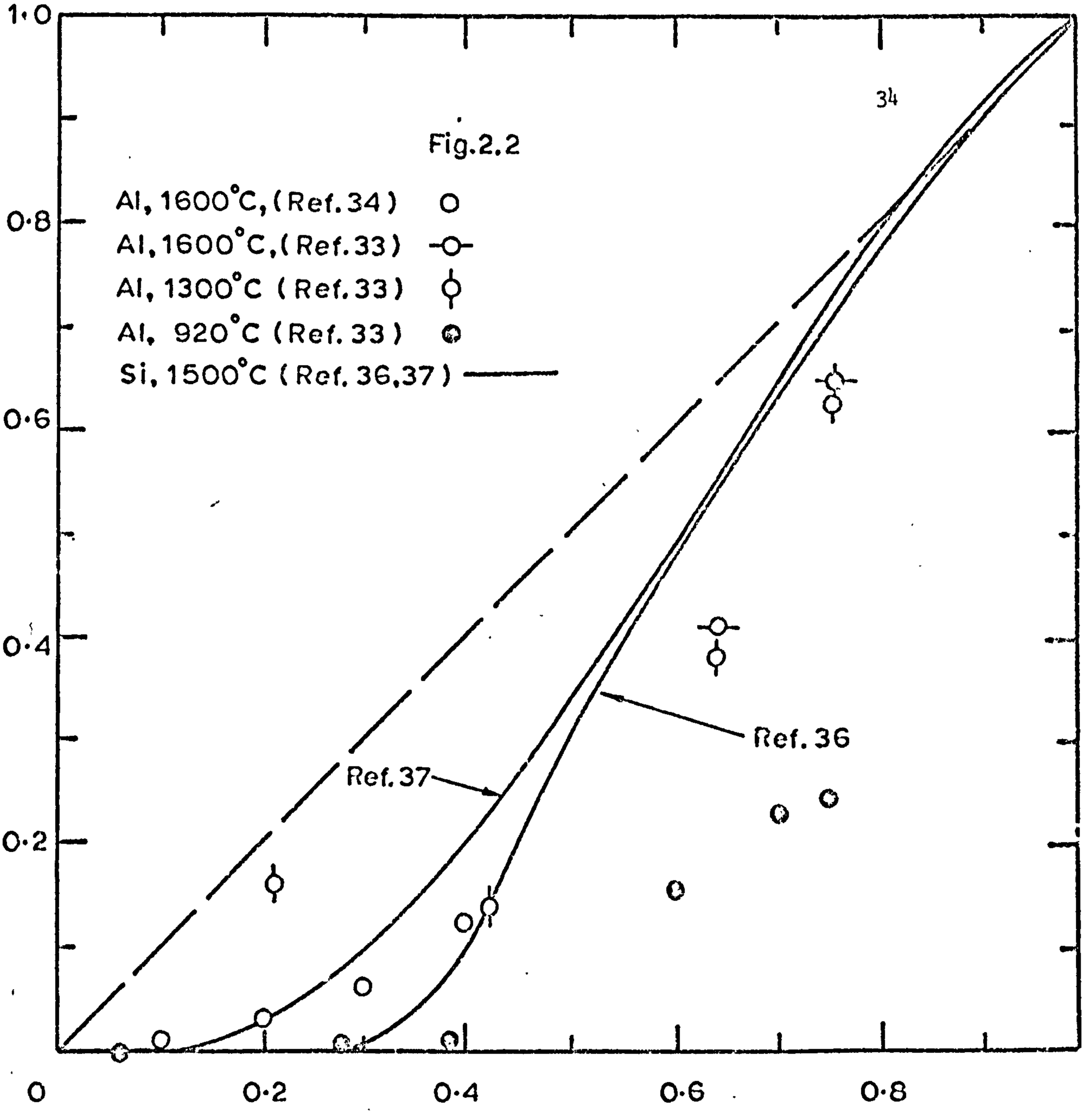
Al, @ 1300 C, (Ref. 33)

Al, @ 920 C, (Ref. 33)

Si, @ 1500 C, (Ref. 36, 37)

Note: a_{Si} in Fe-Si alloys at 1200 C (Ref. 35)

Fig.2.2


Al, 1600°C, (Ref. 34)
Al, 1600°C, (Ref. 33)
Al, 1300°C (Ref. 33)
Al, 920°C (Ref. 33)
Si, 1500°C (Ref. 36,37)
Ref. 37
Ref. 36
1·0
0·8
0·6
0·4
0·2
0
0·2
0·4
0·6
0·8
a_{Si} or a_{Al}
N_{Si} or N_{Al}

equilibrium vapour pressure with temperature and concentration of aluminium in the ferroalloys will be presented. The properties of the slag and ferroaluminium are presented in Table 2.4. The compositions of the slag and ferroalloys used in the experiments were chosen for the following reasons:

a) A silica-free slag must be used in order to avoid undesirable side reactions.

b) The slag and ferroalloys must melt at less than 1400 C due to the limitation of the maximum operating temperature of the furnace.

c) The influence of the activity of aluminium is an important experimental factor to investigate.

d) Alloys with different densities produce different slag/metal interfacial areas.

A detailed discussion of the various side reactions will be presented in following sections. The 20% Al-alloy was not used in the experimental programme, but it is relevant for industrial processes.

The equilibrium constant $K_{(2.18)}$ for reaction (2.18) was calculated and the results are plotted in Fig. 2.3. Curves A, B and C were obtained from sets of thermodynamic data which appear in the corresponding columns of Table 2.3. The calculations show that $K_{(2.18)}$ increases with temperature as expected although this increase is small for curve C. Curve CD, which is derived from data compiled in column C for Al_2O_3 and D for MgO is not consistent with the general trend shown by the other curves.

It is worth noting that the values of $\Delta G^0_{T,f}$ for MgO which appear in column D were obtained assuming $\Delta H^0_{T,fus}$ = 31.7 kcal/mole MgO, whereas for those of columns A, B and C the value assumed was $\Delta H^0_{T,fus}$ = 18.5 kcal/mole MgO. The first of these figures appear to be abnormally high when it is compared with the values of the standard enthalpy of fusion for other oxides (2.3 kcal/mole SiO_2[14], 2.6 kcal/mole SiO_2[38], 28.3 kcal/mole Al_2O_3[14], 26.5 kcal/mole Al_2O_3[38], 16.6 kcal/mole CaO[38]).

References for Table 2.3:

(A) Ref. 14

(B) Ref. 38

(C) Ref. 38 Data on hypothetical liquid oxides derived from the corresponding values for solid oxides given in Ref. (39).

$\Delta H^0_{T,fus}\ MgO_{(l)}$ = 18.5 kcal/mole; $\Delta H^0_{T,fus}\ Al_2O_{3(l)}$ = 26.5 kcal/mole

(D) Ref. 38 $\Delta H^0_{T,fus}\ MgO_{(l)}$ = 31.7 kcal/mole

(E) Ref. 38 Data on hypothetical liquid Al_2O_3 calculated from the corresponding values for solid Al_2O_3 given in Ref. 40.

$\Delta H^0_{T,fus}\ Al_2O_{3(l)}$ = 25.7 kcal/mole

(F) Ref. 38 $\Delta H^0_{T,fus}\ SiO_{2(l)}$ = 2.6 kcal/mole

(G) Ref. 38 $\Delta H^0_{T,fus}\ CaO_{(l)}$ = 16.6 kcal/mole

Table 2.3

Standard free energy and standard enthalpy of formation of hypothetical liquid oxides

	Temperature (°K)	Hypothetical liquid oxide										
		MgO				Al_2O_3				SiO_2		CaO
		A	B	C	D	A	B	C	E	A	F	G
$\Delta G^0_{T\,f}$ (cal/mole of oxide)	1000	-105810	-107866	-106512	-97578	-309805	-316356	-317066	-313388	-173921	-173744	-116832
	1200	-101372	-102917	-101854	-93773	-296335	-300729	-301273	-299085	-165772	-165400	-112666
	1400	- 96448	- 98100	-97280	-90053	-282990	-285704	-286113	-285005	-157699	-157244	-108398
	1600	- 87636	- 93393	- 92776	-86403	-269766	-271189	-271484	-271107	-149691	-149241	-104236
	1800	- 78911	- 88771	- 88333	-82814	-256693	-257114	-257313	-257365	-140952	-140542	-100165
	2000	- 70265	- 84253	- 83941	-79277	-243780	-243428	-243543	-243758	-131719	-131357	- 96172
$\Delta H^0_{T,f}$ (cal/mole of oxide)	1000	-128017	-132985	-130048	-116849	-377483	-396206	-397206	-385543	-214875	-216016	-136965
	1200	-128014	-132188	-129532	-116333	-376781	-392573	-394013	-384186	-214427	-214860	-138621
	1400	-158455	-131412	-129036	-115833	-375971	-389001	-390272	-382890	-213972	-213767	-137881
	1600	-157774	-130651	-128555	-115346	-375070	-385472	-386599	-381637	-213489	-212730	-137155
	1800	-157074	-129898	-128082	-114873	-373602	-381970	-382975	-380411	-224542	-223742	-136441
	2000	-156353	-129155	-127619	-114410	-372170	-378497	-379404	-379214	-223537	-222637	-135739

Table 2.4

Properties of slag and ferroaluminium

	Slag	Al - alloys		
% MgO	5.6	-	-	-
% Al_2O_3	48.1	-	-	-
% CaO	46.3	-	-	-
% Al	-	80	35	20
x_{MgO}	0.097	-	-	-
$x_{Al_2O_3}$	0.328	-	-	-
x_{CaO}	0.575	-	-	-
x_{Al}	-	0.89	0.53	0.34
a_{Al}	-	0.87	0.29	0.10
Liquidus (°C)	<1345	1020	1300	1450
Density @ 20C (g/cm^3)	2.9	3.7	6.0	6.7

Figure 2.3 - Variation of the equilibrium constant of reaction (2.18) with temperature. Curves A, B and C are based on data given in columns A, B and C of Table 2.3. Curve (CD) was plotted using data from column C (for Al_2O_3) and D (for MgO). The dotted line is derived from the average values of $\Delta G^0_{T,f}$ for hypothetical liquid Al_2O_3 and MgO

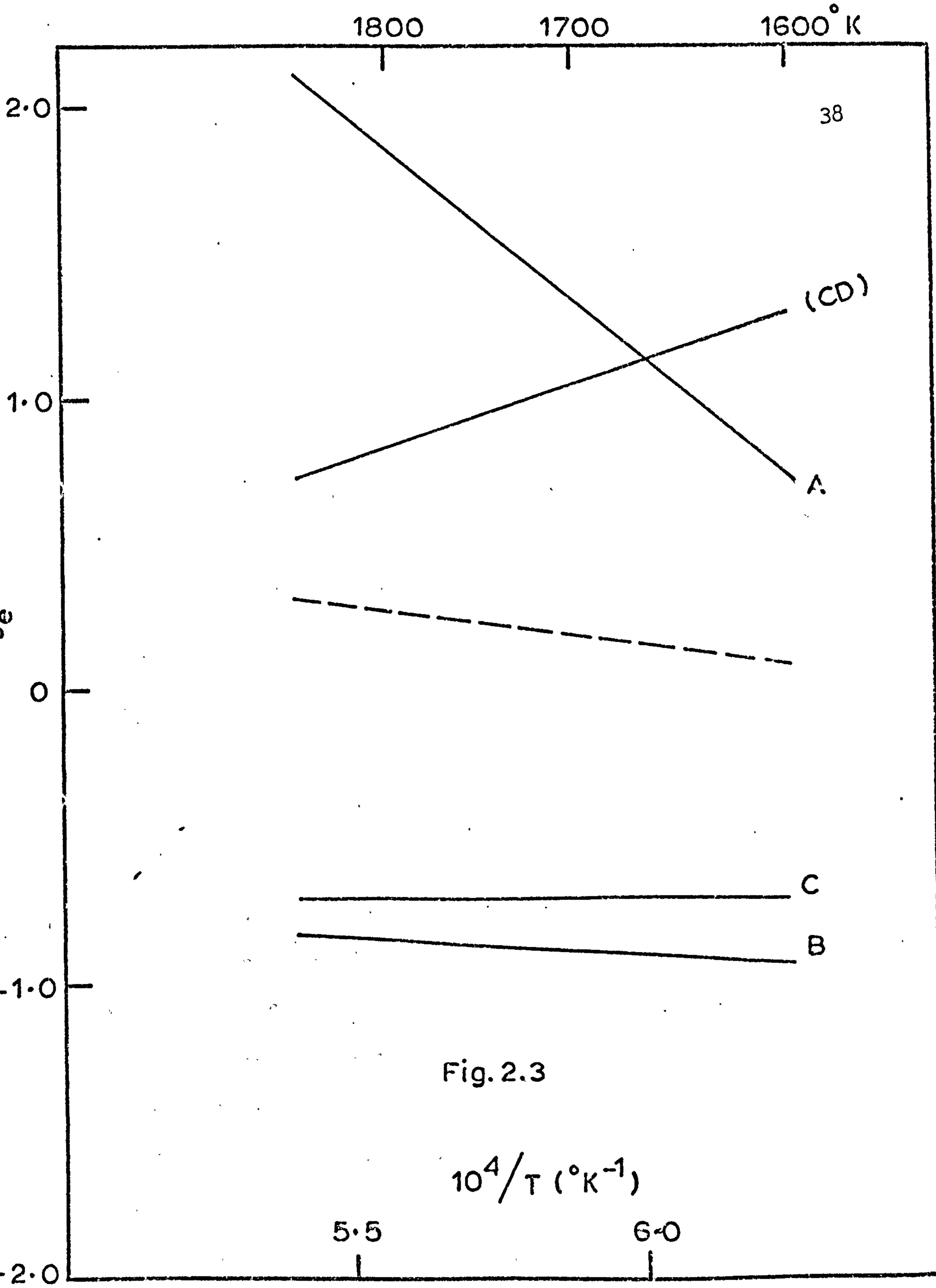


Fig. 2.3

Enthalpies of fusion and heat capacities of liquid oxides are still inadequately known, therefore discrepancies in calculations derived from values of the Gibbs energy of formation of liquid MgO, Al_2O_3, CaO and SiO_2 are unavoidable.

The values for the equilibrium vapour pressure of magnesium were calculated at various stages of reduction. Calculations were made for isothermal reduction at 1700 K and 1800 K. Activities of aluminium in the ferroalloys were assumed to be constant, but increases in the values of $x_{Al_2O_3}$ were allowed for. The average values for $\Delta G^0_{T,f}$ of MgO and Al_2O_3 from Table 2.3 were used for the calculation of the exponential term of equation (2.20). Curves for equilibrium vapour pressure against yield of magnesium for reduction with 80% -, 35% - and 20% - Al alloys are plotted in Fig. 2.4. The curves indicate that, in industrial processes operating at 1400 - 1500 C, it is essential to use alloys containing much more than 20% - Al in order to extract more than 90 per-cent of the magnesium from the slag at operating pressures of 5 - 30 mm Hg. When thermodynamic data from columns A, B and C from Table 2.3 were used, the calculated values of p_{Mg} at the slag/metal interface corresponding to 90% yield of magnesium are given in Table 2.5. Comparison between values of the equilibrium vapour pressure of magnesium given in Table 2.1 with those derived from Fig. 2.4 and Table 2.5 clearly shows that, for any aluminothermic process operating at pressures near atmospheric, no reduction in the liquid state would be expected to occur in the range of temperature 1700 - 1800 K.

The heat of reaction at 1700 K, derived from the average values of the standard enthalpy of formation of liquid MgO and Al_2O_3, is 5.8 kcal/mole MgO. This is small when compared with that for the reduction of solid magnesia and calcined dolomite with aluminium given in Table 2.1. Nevertheless, depending on the amounts of slag and metal present, the drop in temperature, if the reaction is carried out under adiabatic

Figure 2.4 - Equilibrium vapour pressure of magnesium as function of the yield of magnesium at 1700 K and 1800 K, for the 80% Al-, 35% Al- and 20% Al-alloys. The average values of $\Delta G^0_{T,f}$ of hypothetical liquid Al_2O_3 and MgO were used for the calculation of the exponential term of equation (2.20).

80% Al-alloy ——————

35% Al-alloy ----------

20% Al-alloy - . - . - .

Fig.2.4

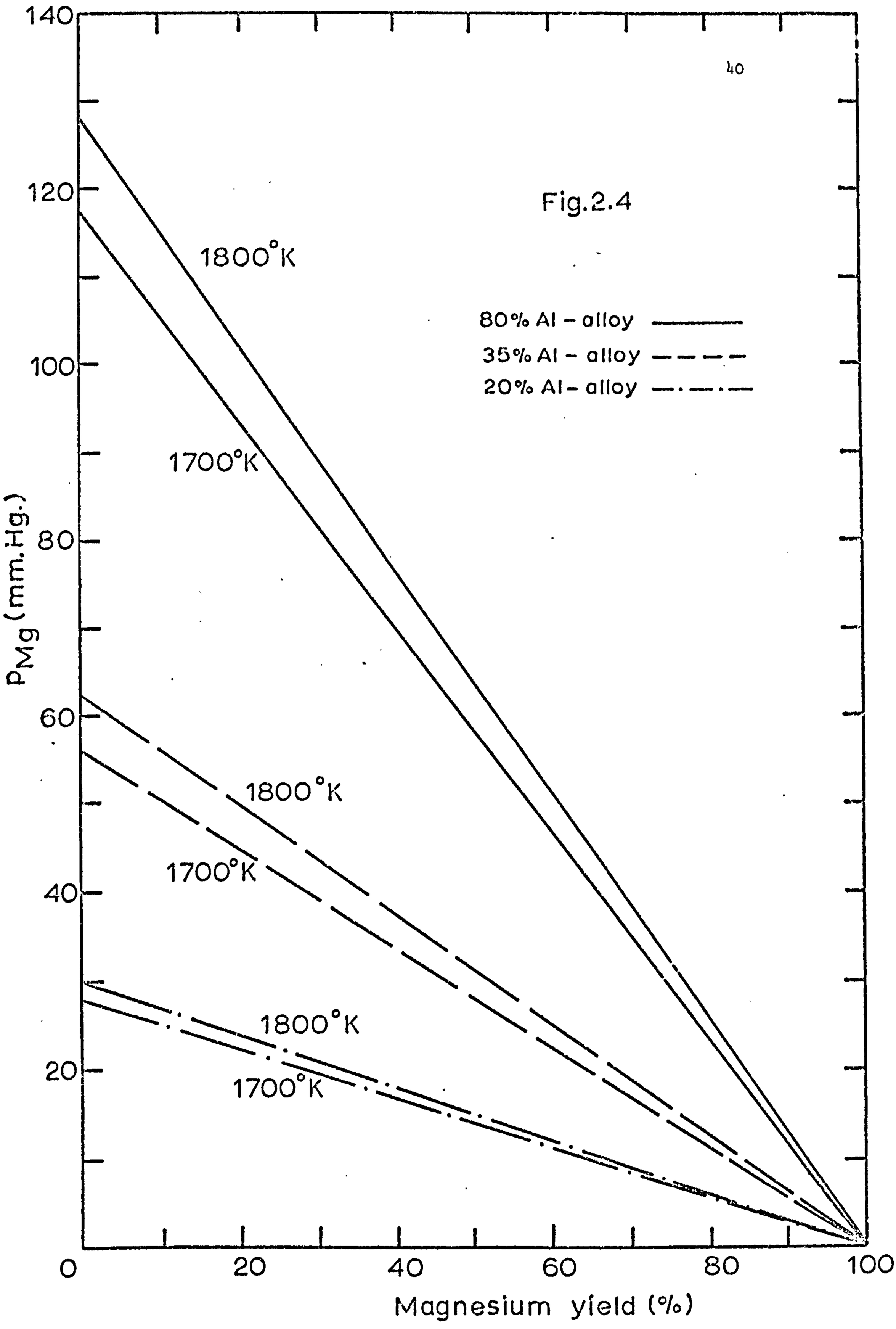

140
120
100
80
60
40
20
P_{Mg} (m.m.Hg.)
1800°K
1700°K
1800°K
1700°K
1800°K
1700°K
80% Al – alloy
35% Al – alloy
20% Al – alloy
0
20
40
60
80
100
Magnesium yield (%)

Table 2.5

Vapour pressures of magnesium in equilibrium with the slag at 1700 K after 90 percent of the magnesium has been removed. Thermodynamic data from columns A, B and C of Table 2.4 were used in the calculations.

Al - alloy	Vapour pressure P_{Mg} (in mm Mg)		
	A	B	C
Al - 80%	39.3	4.0	4.8
Al - 35%	14.1	1.7	2.0
Al - 20%	7.1	0.8	1.0

conditions, could be large enough to cool the melt to undesirably low levels. For example, assuming that the heat capacities of slag and ferroaluminium (80% - Al) are 0.3 and 0.15 cal/C.g respectively, the temperature of a sample containing 70 grams of slag and 30 grams of ferroaluminium, originally at 1700 K, could drop by about 9 - 10 C/g of magnesium produced.

2.1.2.2 - Reactions of CaO and Al_2O_3 from the slag with ferroaluminium

Besides magnesia, lime and alumina are the oxides present in the slag; therefore, it is necessary to assess the thermodynamic conditions for their reduction with aluminium. The equilibrium constant at 1800 K were calculated for the following reactions:

$$(CaO) + \frac{2}{3}\,[Al] \rightarrow Ca_{(g)} + \frac{1}{3}\,(Al_2O_3) \quad ; \quad K_{(2.22)} = 1.76 \times 10^{-2} \qquad (2.22)$$

$$\frac{1}{3}\,(Al_2O_3) + 4/3\,[Al] \rightarrow Al_2O_{(g)} \quad ; \quad K_{(2.23)} = 1.25 \times 10^{-3} \qquad (2.23)$$

$$\frac{1}{3}\,(Al_2O_3) + \frac{1}{3}\,[Al] \rightarrow AlO_{(g)} \quad ; \quad K_{(2.24)} = 9.04 \times 10^{-10} \qquad (2.24)$$

$$\frac{2}{3}\,(Al_2O_3) + \frac{2}{3}\,[Al] \rightarrow Al_2O_{2(g)} \quad ; \quad K_{(2.25)} = 4.52 \times 10^{-11} \qquad (2.25)$$

Reactions of CaO with ferroaluminium may also produce calcium aluminides which would be present in the metal phase. However, vapour producing reactions, which could compete with the evolution of magnesium vapour, are of primary concern. Values of $\Delta\, G^0_{T,f}$ for aluminium and silicon sub-oxides are given in Table 2.6. Values of the equilibrium vapour pressures of $Ca_{(g)}$, $Al_2O_{(g)}$, $AlO_{(g)}$ and $Al_2O_{2(g)}$ were calculated for the reduction with the 80% Al-alloy at 1800 K. It was found that ferro-aluminium reduces magnesia selectively at pressures greater than 10 mm Hg at this temperature.

Table 2.6

Values of the standard free energy of formation of aluminium and silicon sub-oxides (Ref. 14)

Sub-oxide vapour	$\Delta G^0_{T,f}$ (cal/mole)					
	1000 K	1200 K	1400 K	1600 K	1800 K	2000 K
$AlO_{(g)}$	380	- 2635	- 5559	- 8419	-11229	-14005
$Al_2O_{(g)}$	-52725	-55207	-57533	-59721	-61796	-63762
$Al_2O_{2(g)}$	-95255	-93157	-90940	-88621	-86218	-83734
$SiO_{(g)}$	-44782	-48672	-52491	-56244	-59118	-61341

2.1.2.3 - Reactions of $Mg_{(g)}$ with Al_2O_3 and CaO present in the slag and the solution of magnesium in ferroaluminium

Reduction of magnesia in the liquid state produces magnesium vapour at slag/metal interfaces. Therefore, it is worth considering reactions of Mg vapour with oxides present in the slag in order to determine the possibility of the metal's reoxidation or dissolution in the metal phase. The following reactions were considered and their equilibrium constants calculated at 1800 K are given below:

$$Mg_{(g)} + \frac{1}{3}(Al_2O_3) \rightarrow \frac{2}{3}[Al] + (MgO) \; ; K_{(2.26)} = 7.57 \times 10^{-1} \qquad (2.26)$$

$$Mg_{(g)} + \frac{1}{2}(Al_2O_3) \rightarrow \frac{1}{2}Al_2O_{(g)} + (MgO); K_{(2.27)} = 2.70 \times 10^{-2} \qquad (2.27)$$

$$Mg_{(g)} + (Al_2O_3) \rightarrow 2\,AlO_{(g)} + (MgO) \; ; K_{(2.28)} = 6.19 \times 10^{-19} \qquad (2.28)$$

$$Mg_{(g)} + (Al_2O_3) \rightarrow Al_2O_{2(g)} + (MgO) \; ; K_{(2.29)} = 3.40 \times 10^{-11} \qquad (2.29)$$

$$Mg_{(g)} + (CaO) \rightarrow Ca_{(g)} + (MgO) \; ; K_{(2.30)} = 13.3 \times 10^{-3} \qquad (2.30)$$

The low values of K for reactions (2.26) - (2.30) indicate that reoxidation of magnesium vapour brought into contact with the bulk of the slag phase is thermodynamically unlikely.

Very little, if any, magnesium is expected to remain in the metal phase. The reasons for this are twofold. Firstly, the solubility of magnesium in ferroaluminium decreases with the increase of the iron concentration in the alloy because the solubility of magnesium in iron is very low [78]. Secondly, high temperatures and reduced pressures favour distillation of magnesium from the metal phase (see Figure 2.7).

2.1.2.4 - Reduction with ferrosilicon

Reduction of magnesia from molten slags with ferrosilicon will be dealt with in this section. The compositions of slags and ferrosilicon

for the two cases which will be examined are given in Table 2.7. The Fe-75% Si alloy was selected since it is used in industrial processes. The slag compositions, one of them being alumina-free, were chosen to investigate the effect of activity of silica on the vapour pressure of silicon monoxide produced by a reaction which takes place simultaneously with the reduction of magnesia. The formation of $SiO_{(g)}$ will be discussed in the next section. The molecular ratios CaO/SiO_2 and Al_2O_3/SiO_2 for the quarternary slag are equal to 2.09 and0.74 respectively. This should prevent the evolution of large quantities of silicon monoxide, according to French practice [4]. An alumina-free slag was also considered because Japanese inventors [5,6] have claimed that extraction of magnesium may be successfully carried out with no alumina present in the charge.

The equilibrium vapour pressure of magnesium was calculated using the average values for the standard free energy of formation of MgO and SiO_2 from Table 2.3 and values of x_{MgO}, x_{SiO_2} and a_{Si} from Table 2.7. Curves of p_{Mg} versus yield of magnesium are plotted in Fig. 2.5. The curves show that, in the 1700 - 1800 K range, the values of the equilibrium vapour pressure of magnesium are lower than those obtained when ferroaluminium is used. For the particular slags considered, reduction in the liquid state at 1700-1800 K would take place only when the pressure of magnesium at the slag/metal interface was lower than 5 mm Hg, which is the lowest value at which the Magnetherm process is operated [4].

Reduction with silicon is endothermic. The change of standard enthalpy for reaction (2.19) is 20.4 kcal/mole MgO at 1800 K. This is approximately 3.5 times that for reduction with ferroaluminium. Greater falls in temperature in small samples would be expected per gram of magnesium produced.

Table 2.7

Properties of slags and ferrosilicon

	Slags		Ferrosilicon
% S_i02	22.00	52.00	-
% Al_2O3	25.00	0.00	-
% CaO	43.00	35.33	-
% MgO	10.00	12.67	-
x_{SiO_2}	0.23	0.48	-
$x_{Al_2 3}$	0.15	0.00	-
x_{CaO}	0.47	0.35	-
x_{MgO}	0.15	0.17	-
a_{SiO_2}	0.01*	0.4**	
% Si	-	-	75.0
x_{Si}	-	-	0.86
a_{Si}	-	-	0.86***
L.T. (^oC)	1428****	1350****	1330
Density ($g\ cm^{-3}$)	~3	~3	~3.7

* @ 1600° C (Ref. 41)

** @ 1600° C (Ref. 44)

*** @ 1500° C (Ref. 36,37)

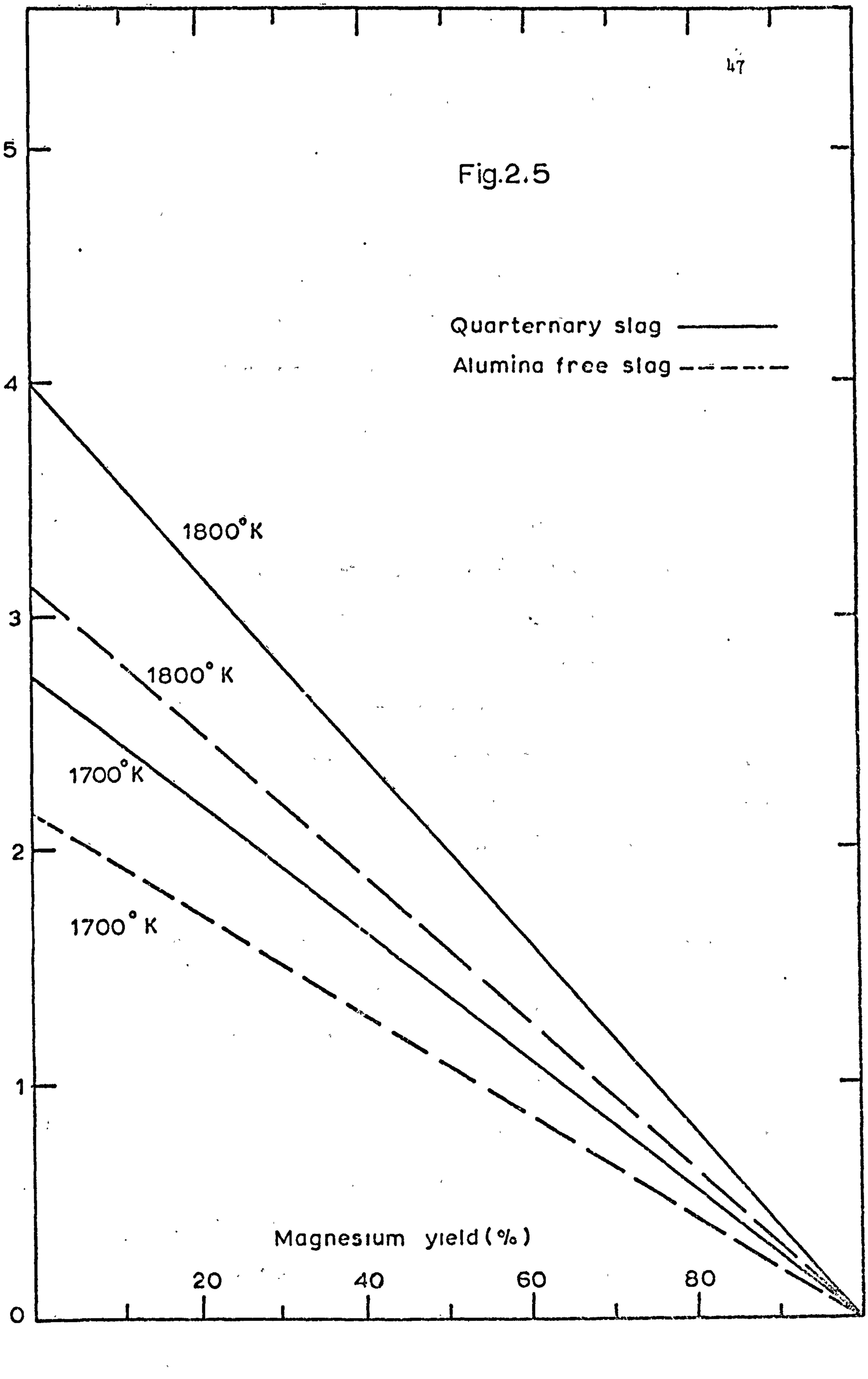
**** Ref (42)

Figure 2.5 - Equilibrium vapour pressure of magnesium as function of the yield of magnesium at 1700 K and 1800 K, for the 75% Si-Fe alloy. The average values of $\Delta G^{\circ}_{T,f}$ of hypothetical liquid SiO_2 and MgO were used for the calculation of the exponential term of equation (2.21).

Quarternary slag ————————

Alumina-free slag ----------

Fig.2.5


Quarternary slag
Alumina free slag
1800°K
1800° K
1700°K
1700° K
P_{Mg} (mm.Hg)
Magnesium yield (%)
0
1
2
3
4
5
20
40
60
80

2.1.2.5 - Reactions of SiO_2, CaO and Al_2O_3 present in the slag with ferrosilicon

The reaction of silica with silicon from the metal phase produces silicon monoxide according to

$$\tfrac{1}{2}\ (SiO_2) + \tfrac{1}{2}\ [Si] \rightarrow SiO_{(g)} \qquad (2.31)$$

When silicon monoxide leaves the reaction zone it is transported together with magnesium vapour to the condensation zone. Below 1200 C,[79] $SiO_{(g)}$ disproportionates according to the reaction:

$$SiO_{(g)} \rightarrow \langle Si \rangle + \langle SiO_2 \rangle \qquad (2.32)$$

Disproportionation of silicon monoxide causes contamination of magnesium with silicon and silica. Therefore, formation of $SiO_{(g)}$ must be minimized during the operation of industrial processes. One way[4] of achieving this is by providing a properly balanced burden consisting of ferrosilicon, calcined dolomite and alumina which produces slags in which the activity of silica is low. As reduction of magnesia proceeds, however, the concentration of SiO_2 and its activity in the slag increase; therefore more alumina must be fed into the furnace to lower the activity of silica and the melting point of the slag.

Two examples are presented in Table 2.8, where values of the equilibrium vapour pressures of $Mg_{(g)}$ and $SiO_{(g)}$ were calculated for reduction of slags with ferrosilicon. Equilibrium values at the start of reduction as well as the final values for $SiO_{(g)}$ are given. The results clearly show that, unless the activity of silica is maintained at very low levels (less than 0.01), the reduction of SiO_2 is more favourable than that of MgO and large quantities of silicon monoxide are generated. In the Magnetherm process the evolution of $SiO_{(g)}$ is bound to occur to some extent. The silicon monoxide vapour could react with lime in the solid burden according to

Table 2.8

Calculated values of the equilibrium vapour pressures of SiO(g) and Mg(g) for reduction of slags with ferrosilicon (75% Si) at 1800 K

Yield of Magnesium (%)	Slag composition (%)				x_{SiO2}	a_{SiO2}	p_{SiO} (mm Hg)	p_{Mg} (mm Hg)
	SiO_2	Al_2O_3	CaO	MgO				
0	52.00	-	35.33	12.67	0.478	0.35	17.9	3.2
100	63.52	-	36.48	-	0.619	0.90	28.7	-
0	22.00	25.00	43.00	10.00	0.225	0.01	3.0	4.0
100	30.26	25.64	44.10	-	0.327	0.10	9.6	-

a_{SiO2} @ 1600° C (Ref. 41, 44-47)

a_{Si} assumed to be constant during the process (excess of Fe-Si)

The average values of $\Delta G^0_{T,f}$ (SiO_2) at 1800 K from Table 2.3 were used in the calculations.

$$2\,SiO_{(g)} + 2(CaO) \rightarrow \langle Ca_2SiO_4 \rangle + [Si] \qquad (2.33)$$

as experimentally confirmed by Kuslov and Mikulinskii [43].

Other reactions may produce $SiO_{(g)}$ as, for example, the reduction of silica with carbon (from the electrodes) and the reaction of magnesia itself with silicon (reaction 2.6).

It has been mentioned in section 2.1.1.2 that CaO and MgO can react with ferrosilicon to produce calcium and magnesium silicides at atmospheric pressure. They would be relevant reactions for the processes of smelting Fe-Si-Ca-Mg alloys. The distribution of calcium and magnesium among phases present during smelting is given in Table 2.9 [21]. More magnesium is lost as a vapour, because magnesium silicide dissociates to produce $Mg_{(g)}$. At the temperature at which the smelting of these alloys is carried out (1800 C), the pressure of magnesium in equilibrium with liquid Mg_2Si is about 640 mm Hg [23]. The pressure of calcium vapour in equilibrium with liquid CaSi at the same temperature is 0.04 mm Hg [13]. This explains why alloys richer in calcium were produced and why comparatively small losses of calcium vapour were found.

Reactions of reduction of alumina with ferrosilicon and the respective equilibrium constants at 1800 K, are given below:

$$(Al_2O_3) + 3/2\,[Si] \rightarrow 2\,Al + 3/2\,(SiO_2) \;;\; K_{(2.34)} = 2.6 \times 10^{-6} \qquad (2.34)$$

$$(Al_2O_3) + [Si] \rightarrow Al_2O_{2(g)} + SiO_{(g)} \;;\; K_{(2.35)} = 2.7 \times 10^{-14} \qquad (2.35)$$

$$(Al_2O_3) + 2\,[Si] \rightarrow Al_2O_{(g)} + 2\,SiO_{(g)} \;;\; K_{(2.36)} = 4.4 \times 10^{-10} \qquad (2.36)$$

$$(Al_2O_3) + [Si] \rightarrow 2AlO_{(g)} + SiO_{(g)} \;;\; K_{(2.37)} = 4.8 \times 10^{-32} \qquad (2.37)$$

The ΔG°_{T} changes for reactions (2.34)-(2.37) are positive. Therefore, the reduction of alumina with silicon is unlikely to occur at 1800 K. As the equilibrium constants for reactions (2.35) - (2.37)

Table 2.9

Distribution of calcium and magnesium among phases in the smelting of Fe-Si-Ca-Mg alloys, after 60 minutes, at 1600-1800°C at atmospheric pressure. (Ref. 21)

	Percentage			
Element	Slag	Metal	Vapour	Total
Calcium	65	30	5	100
Magnesium	32	30	38	100

are very small, the evolution of the vapours of aluminium and silicon sub-oxides would occur only if extremely low values of the partial pressures existed at the slag/metal interface.

2.1.2.6 - Reactions of $Mg_{(g)}$ with SiO_2 present in the slag phase and the solution of magnesium in ferrosilicon

Magnesium vapour may react with SiO_2 to produce $SiO_{(g)}$ according to

$$Mg_{(g)} + (SiO_2) \rightarrow (MgO) + SiO_{(g)} \; ; \; K_{(2.38)} = 2.37 \qquad (2.38)$$

At 1800 K the standard free energy change for this reaction is negative. Reoxidation of magnesium vapour may occur depending on the actual values of p_{Mg}, p_{SiO}, a_{SiO_2} and a_{MgO}. For example, assuming p_{Mg} = 0.092 atm (70 mm Hg), a_{MgO} = 0.17 and a_{SiO} = 0.3, the resulting equilibrium value for p_{SiO} is 293 mm Hg. For any set of values which makes the ratio $a_{MgO} \cdot p_{SiO} / p_{Mg} \cdot a_{SiO_2} < K_{(2.38)}$ the reaction will occur.

At atmospheric pressure and above 1430 C magnesium and silicon are miscible, as the phase diagram for the Si-Mg system shows [51]. The presence of iron, however, decreases the solubility of magnesium in the alloy because magnesium is practically insoluble in iron [78]. At 1500 - 1600 C and 5-30 mm Hg pressure, the tendency is for magnesium to leave the metal phase. For instance, at 1600 C and for a_{Mg} = 0.1 in the metal phase, the vapour pressure of magnesium in equilibrium with the molten alloy would be p_{Mg} = 398 mm Hg. Therefore, there is a large driving force for distillation.

2.1.2.7 - Reactions of MgO, CaO and Al_2O_3 with carbon

Hearth lining and electrodes used in industrial furnaces are made of graphite. It is relevant, therefore, to know the extent to which carbothermic reactions occur. These reactions produce carbon monoxide

which reoxidizes magnesium vapour according to

$$Mg_{(g)} + CO \rightarrow \langle MgO \rangle + \langle C \rangle \qquad (2.39)$$

The products of reaction (2.39) also contaminate the magnesium with magnesia and carbon.

The various possible reactions of oxides in the slag with carbon and the associated equilibrium constants at 1800 K are given below:

$$(MgO) + \langle C \rangle \rightarrow Mg_{(g)} + CO \quad ; \quad K_{(2.40)} = 3.4 \times 10^{-3} \qquad (2.40)$$

$$(MgO) + 3\langle C \rangle \rightarrow \langle MgC_2 \rangle + CO \quad ; \quad K_{(2.41)} = 3.8 \times 10^{-6} \qquad (2.41)$$

$$(MgO) + 5/2\langle C \rangle \rightarrow \tfrac{1}{2}\langle Mg_2C_3 \rangle + CO \quad ; \quad K_{(2.42)} = 5.3 \times 10^{-5} \qquad (2.42)$$

$$(SiO_2) + 2\langle C \rangle \rightarrow [Si] + 2\,CO \quad ; \quad K_{(2.43)} = 3.4 \times 10^{-2} \qquad (2.43)$$

$$(SiO_2) + 3\langle C \rangle \rightarrow \langle Si \rangle + 2\,CO \quad ; \quad K_{(2.44)} = 1.44 \qquad (2.44)$$

$$(SiO_2) + \langle C \rangle \rightarrow SiO_{(g)} + CO \quad ; \quad K_{(2.45)} = 7.9 \times 10^{-3} \qquad (2.45)$$

$$(CaO) + \langle C \rangle \rightarrow Ca_{(g)} + CO \quad ; \quad K_{(2.46)} = 4.5 \times 10^{-5} \qquad (2.46)$$

$$(CaO) + 3\langle C \rangle \rightarrow \langle CaC_2 \rangle + CO \quad ; \quad K_{(2.47)} = 4.5 \times 10^{-2} \qquad (2.47)$$

$$(Al_2O_3) + 3\langle C \rangle \rightarrow 2[Al] + 3\,CO \quad ; \quad K_{(2.48)} = 1.6 \times 10^{-8} \qquad (2.48)$$

$$(Al_2O_3) + 9/2\langle C \rangle \rightarrow \tfrac{1}{2}\langle Al_4C_3 \rangle + 3\,CO \quad ; \quad K_{(2.49)} = 3.8 \times 10^{-7} \qquad (2.49)$$

$$(Al_2O_3) + 2\langle C \rangle \rightarrow Al_2O_{(g)} + 2\,CO \quad ; \quad K_{(2.50)} = 8.1 \times 10^{-9} \qquad (2.50)$$

$$(Al_2O_3) + \langle C \rangle \rightarrow Al_2O_{2(g)} + CO \quad ; \quad K_{(2.51)} = 1.2 \times 10^{-3} \qquad (2.51)$$

$$(Al_2O_3) + \langle C \rangle \rightarrow 2\,AlO_{(g)} + CO \quad ; \quad K_{(2.52)} = 2.2 \times 10^{-21} \qquad (2.52)$$

Carbothermic reduction of magnesia is unlikely to occur at 1800 K. In fact, industrial processes based on reaction (2.40) are operated at 2000 C under vacuum [2,3,48]. Production of magnesium carbides also

cannot occur. Formation of silicon carbide (2.44) is bound to take place even at atmospheric pressure, whereas reactions (2.43) and (2.45) would occur if p_{CO} is less than 140 mm Hg and p_{CO} less than $0.008/p_{SiO}$, respectively. Production of calcium carbide (2.47) is favoured to that of calcium vapour (2.46) and may occur at reduced pressures (p_{CO} less than 161 mm Hg). Reduction of alumina to aluminium (2.48) and production of aluminium carbide (2.49) cannot take place. Reactions (2.50) and (2.52) are also unlikely. Reaction (2.51), however, could occur under reduced pressures if $p_{Al_2O_2}$ is less than $0.001/p_{CO}$.

2.1.2.8 - Formation of carbides

For reasons outlined in the section 2.1.2.7 the reactions of aluminium, silicon, iron and magnesium with carbon must also be considered. Curves of standard free energy of formation of the respective carbides are plotted in Fig. 2.6. [15], from which it is clear that aluminium, silicon and iron may react with carbon to produce Al_4C_3, SiC and Fe_3C. Magnesium does not react with carbon at the high temperatures at which reduction of slags is carried out. This is very convenient as graphite can be used for making retorts and ducts for confining and transporting magnesium vapour.

2.1.2.9 - Evaporation of metals, oxides and carbides

Curves of vapour pressure of magnesium, aluminium, silicon and iron as function of temperature are given in Fig. 2.7 [13]. It is evident that at 1700 K and 30-70 mm Hg pressure, which is relevant to the experiments reported in this work, boiling of magnesium actually occurs when it is reduced from slags. Contamination of magnesium condensates with aluminium due to distillation of aluminium from the ferroalloy would become pronounced only at temperatures above 2200 K. Much higher temperatures would be required for the vaporization of silicon and iron.

Figure 2.6 - Standard free energy of formation of carbides (Ref. 15)

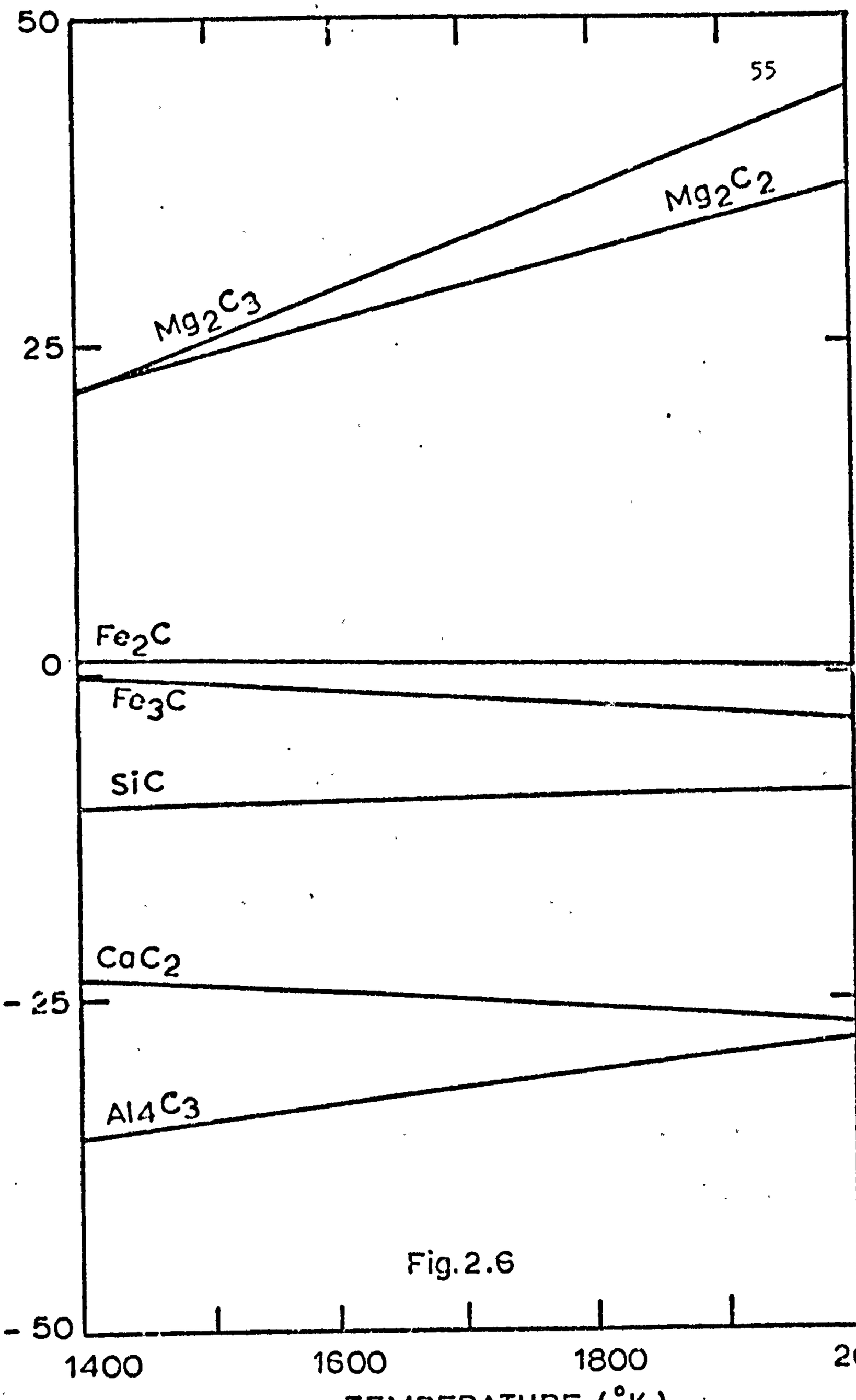

50
25
0
- 25
- 50
55
Mg_2C_2
Mg_2C_3
Fe_2C
Fe_3C
SiC
CaC_2
Al_4C_3
ΔG°_T (kcal/mole)
1400
1600
1800
2000
TEMPERATURE (°K)

Fig. 2.6

Vapour pressures of oxides and carbides are given in Table 2.10 [49,50]. Contamination by volatilization of oxides is unlikely. Calcium carbide has the highest vapour pressure among the carbides considered. However, it would be necessary to reach more than 1800 K for p_{CaC_2} to be greater than 1 mm Hg.

2.1.2.10 Conclusions from the thermodynamic assessment of reduction of molten MgO-bearing slags with ferroalloys

a) An accurate thermodynamic assessment of the reduction of MgO-bearing slags in the liquid state is not possible as all the relevant scientific information required is not available at present. However, the equilibrium vapour pressure of magnesium may be estimated from equations (2.20) and (2.21), for reduction with ferroaluminium and ferrosilicon described by overall reactions (2.18) and (2.19) respectively.

b) Calculated values of $K_{(2.18)}$ and $K_{(2.19)}$ vary within a wide range when the uncertainties in the values of ΔG^0_T for reactions (2.18) and (2.19) are taken into consideration.

c) If a great excess of ferroalloy is present, the equilibrium vapour pressure will decrease linearly with the yield of magnesium.

d) Ferroaluminium selectively reduces MgO from $MgO-Al_2O_3-CaO$ molten slags. For the slag composition considered (5.6% MgO - 48.1% Al_2O_3 - 46.3% CaO), reduction at 1700 K would take place for $p_{Mg} \simeq 117$ mm Hg with the 80% - Al alloy and $p_{Mg} \simeq 56$ mm Hg with the Al - 35% alloy. These figures were estimated assuming activity coefficients of MgO and Al_2O_3 equal to unity, $a_{Al} = 0.87$ and $a_{Al} = 0.29$ for the 80% - and 35% - Al alloys respectively and ΔG^0_T value of reaction (2.18) derived from the average values of $\Delta G^0_{T,f}$ for hypothetical liquid Al_2O_3 and MgO.

e) Reduction with ferroaluminium is endothermic. For the size

Figure 2.7 - Curves of vapour pressure of pure magnesium, aluminium, calcium, silicon and iron (Ref. 13)

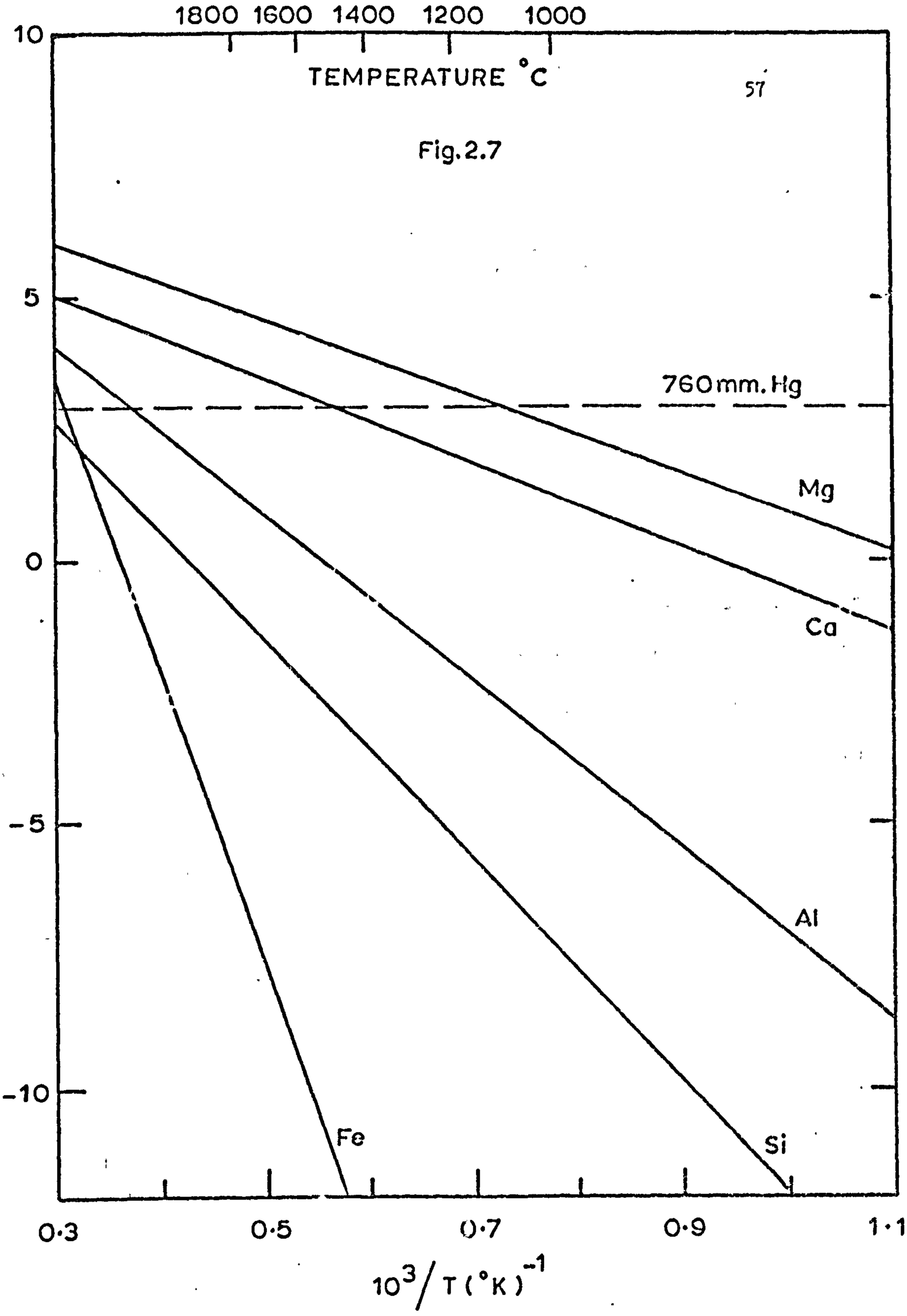

1800 1600 1400 1200 1000
TEMPERATURE °C
10
5
0
-5
-10
LOG P_{Mg} (mm.Hg)
760mm.Hg
Mg
Ca
Al
Fe
Si
0·3
0·5
0·7
0·9
1·1
$10^3/T(°K)^{-1}$

Fig. 2.7

Table 2.10

Vapour pressures of oxides and carbides (Ref. 49)

Oxides:	Temperatures (^{o}K) for vapour pressures (mm Hg)						
	10^{-6}	10^{-5}	10^{-4}	10^{-3}	10^{-2}	10^{-1}	10^{0}
MgO	1600	1714	1841	1968	2128	2330	2535
CaO	1728	1858	2000	2148	2323	2553	2795
Al_2O_3	1910	2037	2178	2339	2518	2735	3000
SiO_2(*)							2545
Carbides:							
CaC_2	920	1007	1102	1222	1359	1567	1811
Al_4C_3	1151	1236	1337	1442	1570	1730	1858
SiC	1570	1670	1820	1959	2190	2270	2443
F_3C	1303	1396	1496	1607	1736	1892	2061

(*) Ref. (50)

of samples used in the experiments reported in this work, temperature drops of about 10 C/gram of magnesium produced would be expected, if the reaction was carried out under adiabatic conditions.

f) Magnesium vapour does not reoxidize when it is brought into contact with the bulk of slag phase in the absence of silica. Very little, if any, pick up of magnesium by the metal phase would be expected.

g) Reduction of MgO from slags with ferrosilicon could be accompanied by side reactions which produce $SiO_{(g)}$ and $CO_{(g)}$. Slags in which a_{SiO_2} is low favour reduction of MgO and inhibit that of $SiO_{(g)}$. In industrial furnaces where a pile of solids containing CaO exists on top of the slag layer, $SiO_{(g)}$ may react with lime according to reaction (2.33).

h) Crucibles made of graphite are suitable for containing melts of ferroaluminium and $MgO-Al_2O_3-CaO$ slags. Formation of calcium carbide may take place if p_{CO} is less than 161 mm Hg, but no carbothermic reduction of MgO and Al_2O_3 would be expected under the conditions relevant to the experimental programme. For silica-bearing slags, formation of SiC could occur even at atmospheric pressure with evolution of carbon monoxide.

i) Retorts and ducts for confining and transporting magnesium vapour at high temperatures may be made of graphite, as magnesium carbides are unlikely to be formed.

j) At 1700 K and 30-70 mm Hg pressure, magnesium is reduced directly to vapour and boils off the melt. Evaporation of other metals as well as that of oxides and carbides are unlikely.

2.2 KINETICS OF REDUCTION OF MgO-BEARING SOLID MATERIALS WITH METALS

The literature on the kinetics of metallothermic reduction of solid MgO-bearing materials is, in fact, restricted to reactions of magnesia and calcined dolomite with silicon alloys [10,18,24-26]. Results from previous investigations aimed at obtaining rate data for these reactions are mainly given in the form of yield vs. time curves. Experimental factors such as mineralogical differences between raw materials, oxides/alloy weight ratios, particles size, density and porosity of briquettes makes it impossible to adequately compare even results obtained at the same temperature-pressure conditions with similar alloys. Therefore, it is advisable not to use rate data for design purposes without a critical assessment of the experimental conditions used for their generation.

Hughes, et al. [26] concluded that the Pidgeon process is controlled by the rate of heat transfer to the pile of briquettes in the retorts They also postulated three reaction mechanisms to explain the reduction of calcined dolomite with ferrosilicon in individual briquettes, i.e.,

a) "prehardening reaction";

b) "permeation control";

c) "trailing reaction".

The first step is the "prehardening reaction" which is that of CaO with silicon (equation 2.17). In the presence of iron and at 1000 C a liquid Fe-Si-Ca alloy is formed very rapidly. It establishes a metallic network which increases the strength of the briquette. The Fe-Si-Ca alloy is the actual reducing agent for MgO. Following the first step, reduction of magnesia takes place (equation 2.15). This reaction produces a sharp front which moves into the briquette. It was found that the rate at which this front moves depends on the porosity of the briquette. Low density and high porosity are associated with high rates of movement of the receding front. The authors concluded that diffusion of

magnesium vapour out of the briquette controls this stage. Finally, a trailing reaction (equation 2.16) takes place in the depleted layers of the briquette. The rate of this reaction was found to be directly proportional to the residual concentration of MgO in the depleted zone. At 1000 - 1100 C the overall process, however, was found to be controlled by the second step discussed above.

The influence of several experimental factors on the rate of evolution and yield of magnesium may be summarized as follows:

a) Initial rates and yields increase with temperature.

b) Initial rates increase as lower pressures are imposed on the reacting briquettes. Yields decrease linearly as pressure increases. Near the value of equilibrium vapour pressure of magnesium yields decrease sharply.

c) Materials with high surface areas and small grain size give high rates.

d) Briquetted mixtures of fine powders favour the extraction of magnesium.

e) Very dense briquettes do not favour diffusion of magnesium and high rates of extraction.

f) Lime and ferrosilicon contribute to the formation of liquid phases which accelerate the reduction, provided that the actual interfacial area for reaction does not decrease due to coalescence of liquids inside the briquette.

g) Initial rates are directly proportional to a_{Si} in the ferrosilicon. Yields increase with the concentration of silicon in the alloy.

h) The presence of 2-5% of calcium fluoride in the briquetted mixtures was found to increase the rate of evolution of magnesium. Calcium fluoride helps the formation of molten phase of the system CaF_2 - CaO - MgO, which creates a faster medium for diffusion of reacting species.

2.3 KINETICS OF SLAG/METAL/GAS REACTIONS

The rates of pyrometallurgical processes are very often controlled by transport phenomena, rather than by the rates of chemical reactions because, at high temperatures, chemical kinetics are very rapid.[29,77]. However, there are cases where transfer of species from one phase to another requires a number of strong bonds to be broken. Such reactions have large values of the activation energies, consequently, they may be chemcially controlled. At present, very little is known about the interfacial nature of slag/metal reactions and the determination of the activation energy for a particular reaction taking place at the liquid/liquid interface is difficult. Nevertheless, based on the enthalpy change for a number of slag/metal reactions involving liquid iron, Richardson [29] considers those with silica and alumina, which are exceptionally endothermic, as bound to be chemically controlled.

Investigations carried out by Turkdogan et al. [52] have shown that the reduction of silica, present in silicate slags, with carbon may be controlled by chemical kinetics at the interface. Fulton and Chipman [53] had earlier suggested that the controlling mechanism for this reaction is associated with the breaking of Si - O bonds. The results of a more recent work on the reduction of silica from silicate melts with CO [54] support the hypothesis that the reaction is controlled by a chemical step which occurs at the interface (reaction 2.53):

$$\square + (SiO_2) \rightarrow SiO_{(g)} + \boxed{O}_{(absorbed)} \qquad (2.53)$$

Pomfret and Grieveson [54] also found that the rate of transfer of silicon to the metal phase is increased by the introduction of CaF_2 into the slag, by deep melts and by carrying out the reaction under an ambient atmosphere of argon.

In any slag/metal/gas system the rate of reaction could be controlled by one or more of the following steps:

a) Transport of reacting species from the bulk of the slag (or metal) phase to the reaction interface.

b) Chemical reactions taking place at the interface (adsorption and desorption of ionic species and electrochemical reactions).

c) Transport of products of reaction away from the interface into the liquid or gaseous phases.

Many slag/metal reactions which occur in pyrometallurgical processes of extraction and refining of metals produce carbon monoxide. For example, when metal oxides - dissolved in slags - are reduced with carbon saturated iron, the overall reaction may be described as follows:

$$(M_xO_y) + y\,[C] \rightarrow x\,[M] + y\,CO \qquad (2.54)$$

In such a case, transport of "M_xO_y" in the slag and that of M and C in the metal phase must be considered. If reaction (2.54) is split into

$$(M_xO_y) \rightarrow x\,[M] + y\,[O] \qquad (2.55)$$

plus

$$y\,[C] + y\,[O] \rightarrow y\,CO \qquad (2.56)$$

then the transport of O in the metal phase must be considered, as well as that of the other reacting species. Reaction (2.55) occurs at the slag/metal interface, whereas reaction (2.56) will occur where a suitable site for nucleation of CO bubbles exists. Nucleation of the product gas may then be considered as a potential controlling mechanism, at least in principle.

The rate equation for reaction (2.54) may be derived under the assumption that no oxygen accumulates in the metal phase, i.e., the flux of oxygen entering the metal as "M_xO_y" is equal to that of oxygen leaving it as CO. The rate equation for the flux of oxygen may be derived as follows.

For the concentration gradients shown in Fig. 2.8, solute is transferred from the slag to the metal phase. If the concentrations of oxygen in the slag and metal at the interface are in equilibrium with one another, then the rate may be described by

$$\dot{n} = A_s\, k_{sl}\, (C_{sl}-C_{sl,i}) = A_s\, k_M\, (C_{M,i}-C_M) \qquad (2.57)$$

Putting $m = C_{sl,i}/C_{M,i}$ = the partition coefficient or equilibrium constant, then equation (2.57) becomes

$$\dot{n}/A_s = k_{sl}\, (C_{sl}-m\, C_{M,i}) = (k_M/m)(m\, C_{M,i}-m\, C_M) \qquad (2.58)$$

From equation (2.58) the following equations may be derived:

$$(\dot{n}/A_s)(1/k_{sl}) = C_{sl} - m\, C_{M,i} \qquad (2.59)$$

$$(\dot{n}/A_s)(m/k_M) = m\, C_{M,i} - m\, C_M \qquad (2.60)$$

By adding up equations (2.59) plus (2.60) the following flux equation results:

$$(\dot{n}/A_s)(1/k_{sl} + m/k_M) = C_{sl} - m\, C_M \qquad (2.61)$$

In equation (2.61) $\dot{n}/A_s$ is the flux of the species being transferred from slag to metal, $(C_{sl}-mC_M)$ is the driving force in terms of concentration because mC_M is the concentration in the slag that would be in equilibrium with C_M and the term consisting of the reciprocals of the two mass transfer coefficients represent the overall resistance to the transport of solute from the slag to the metal. At equilibrium the driving force term becomes zero.

For the case where the chemical rate is so low that equilibrium is not obtained at the interface, i.e. $C_{sl,i}/C_{M,i} \neq m$, it is still possible to derive a simple rate equation, provided the chemical rates are first

Figure 2.8 - Generalised representation of concentration gradients across a slag/metal system

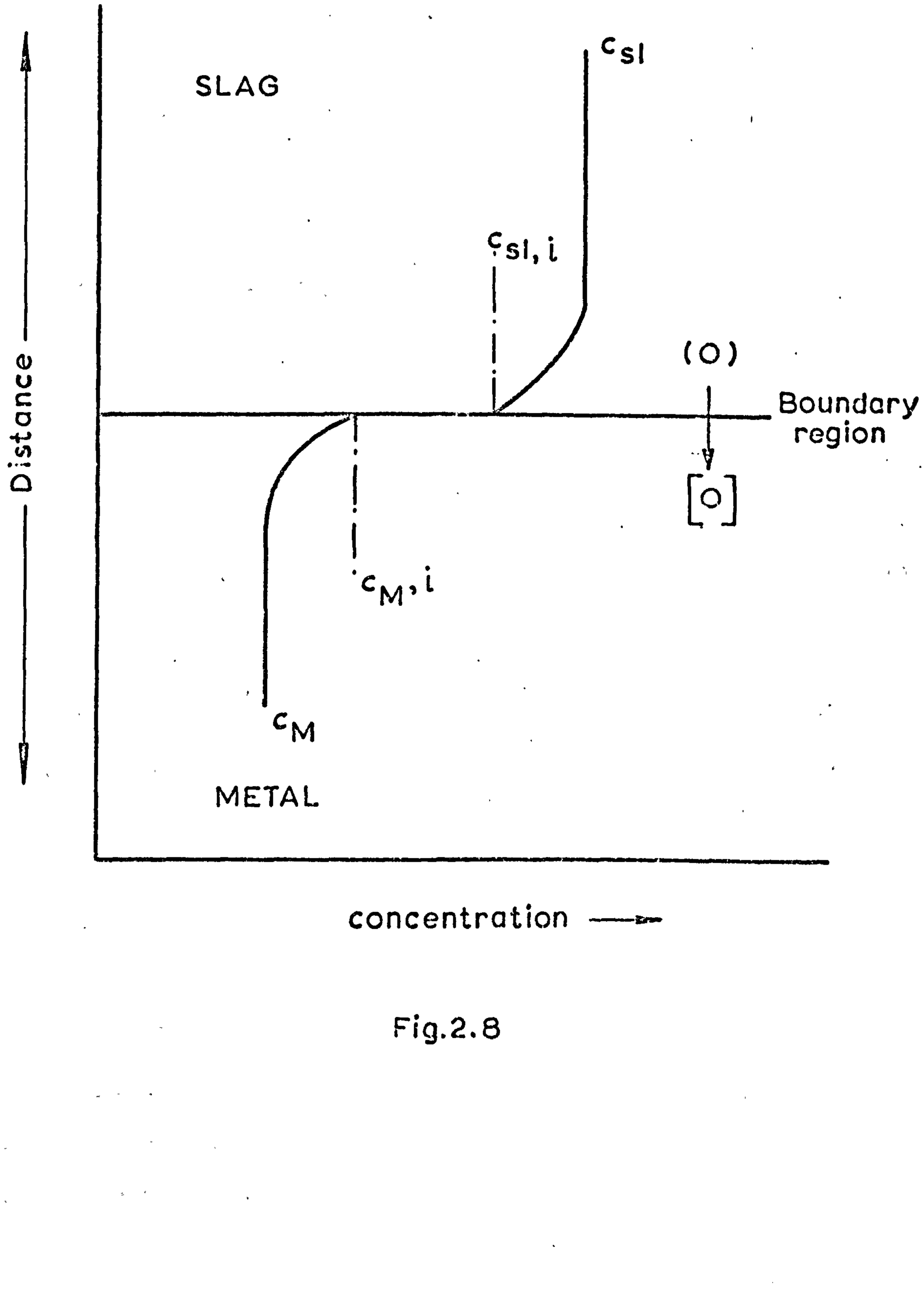

SLAG
c_{sl}
$c_{sl,i}$
(O)
Boundary region
[O]
Distance
$c_{M,i}$
c_M
METAL
concentration

Fig.2.8

order with respect to the solute transferred in both directions. If K_1 and K_2 are the two chemical rate constants then

$$\dot{n}/A_s = K_1 C_{M,i} - K_2 C_{sl,i} \tag{2.62}$$

At equilibrium between slag and metal, the chemical rates in both directions would be equal. Therefore, from equation (2.62) we get

$$K_1 C_M = K_2 C_{sl} \quad \text{or} \quad K_1/K_2 = C_{sl}/C_M = m \tag{2.63}$$

and equation (2.62) becomes

$$\dot{n}/A_s = mK_2 C_{M,i} - K_2 C_{sl,i} \quad \text{or} \quad (\dot{n}/A_s)(1/K_2) = mC_{M,i} - C_{sl,i} = 0 \tag{2.64}$$

From equations (2.61) and (2.64) the equation for the flux of solute across the slag/metal interface may be rewritten as

$$(\dot{n}/A_s)(1/k_{sl} + 1/K_2 + m/k_M) = C_{sl} - mC_M \tag{2.65}$$

If the reaction was not of the first order, it would not have been possible to eliminate the interfacial concentrations and one or other of these concentrations would have to appear in the resistance term associated with the chemical rate constant.

Transfer of solute from the metal phase to the gas bubbles is described by the equation

$$\dot{n}/A_g\ (1/k'_M + m_g/k_g) = C_M - m_g C_g \tag{2.66}$$

where the terms in the parentheses are the reciprocals of the mass transfer coefficients in the metal around the gas bubbles and in the gas. The driving force for the flux across the metal/gas interface is given by $C_M - m_g C_g$. In deriving the equation (2.66) it has been assumed that equilibrium is achieved at the interface. In the case of bubbles

of pure gas, there is no resistance in the gas phase and equation (2.66) becomes

$$(\dot{n}/A_g)(1/k'_M) = C_M - m_g C_g \qquad (2.67)$$

By combining equations (2.65) and (2.67), the equation for the overall flux of oxygen from the slag to the bubbles of CO under mixed control becomes

$$(n/A_s)\,[1/k_{sl} + 1/K_2 + m/k_M + (A_s/A_g)(m/k'_M)\,] = C_{sl} - m\, m_g C_g \qquad (2.68)$$

The application of this equation to real conditions is not simple. Complications arise when, for example, more than one species are transferred from one phase to another simultaneously. Moreover, conducting experiments under real conditions is often impossible, due to the experimental difficulties involved.

The chemical reaction given by equation (2.54) may be split into three steps which describe the adsorption of "M_xO_y" on the slag side of the interface (reaction 2.69), followed by desorption of M and O on the metal side (reaction 2.70) and, finally, by the production of CO, according to reaction (2.56).

$$(M_xO_y) + \square \rightarrow \boxed{M_xO_y} \qquad (2.69)$$

and

$$\boxed{M_xO_y} \rightarrow x\,[M] + y\,[O] + \square \qquad (2.70)$$

If θ is the fraction of occupied and $(1 - \theta)$ that of unoccupied sites of the adsorption layer, then the equilibrium constant of the adsorption reaction (2.69) is

$$K_{(2.69)} = K_a = \theta / a_{M_xO_y,i}\,(1 - \theta) \qquad (2.71)$$

Assuming that the oxygen entering the metal phase is removed immediately by reaction with carbon (reaction 2.56), then the rate of transfer of M from slag to metal may be described by the following equation:

$$\dot{n} = A_s K_1' - K_2' a_{M,i}^x (1-\theta) \qquad (2.72)$$

K_1' and K_2' are the rate constants for the forward and backward reactions, respectively. When the activity of M at the interface is low and/or the fraction of occupied sites is high ($\theta \to 1$), then the reverse reaction term in equation (2.72) may be neglected and it becomes

$$\dot{n} = A_s K_1' \theta \qquad (2.73)$$

By substituting θ from equation (2.71) into equation (2.73), the rate may be written as

$$\dot{n} = A_s K_1' \left[1/(a_{M_xO_y} K_a)^{-1} + 1\right] \qquad (2.74)$$

In equation (2.74), the activity of M_xO_y at the interface is assumed to be the same as that in the bulk of the slag, which may be true for well-stirred systems. According to equation (2.74), the rate of reduction of the oxide is directly proportional to its activity and to the slag/metal interfacial area. Where large amounts of slag are present and small amounts of metal are transferred across the liquid/liquid boundary, then the rate would be expected to be constant throughout the reaction time. This was observed by Turkdogan et al.[52] for the case of reduction of SiO_2 with Fe-C, in the presence of CO bubbles at the slag/metal interface. A constant rate may also be associated with high values of the equilibrium constant for the adsorption reaction. In fact, if $K_a \gg 1$, then $(a_{M_xO_y} K_a)^{-1} \ll 1$ and the rate results to be virtually equal to $A_s K_1'$ for a long period of reaction time. Eventually the rate will drop, as M_xO_y will become scarce in the

slag and its activity will fall.

Resistance to mass transfer in slag/metal reactions decreases by stirring the reacting phases. For instance, gas bubbles rising in the melt help mixing of the bulk phases and the disturbances they cause at the interface assist liquid/liquid mass transfer. Bubbles also create dispersion of metal droplets in the slag, which contributes to enlarge the actual interfacial area for reaction. When a gas is produced, bubbles provide extra sites for nucleation and may drive the reaction to new equilibrium points by lowering the local partial pressure of the generated gas.

Model studies [55-59] on mass transfer across slag/metal interfaces stirred by bubbles have been made using either room temperature systems, with amalgams and aqueous solutions or low melting point alloys and molten salts to simulate metal and slag respectively. From recent work by Robertson and Staples [60] it is clear that the results of various investigations on transport controlled reactions show that

$$k^2 \alpha D\, Q/d^2_{vessel} \qquad (2.75)$$

where k is the mass transfer coefficient, D the diffusion coefficient and d_{vessel} the diameter of the reaction vessel. In all model systems considered, however, no gas was generated at the liquid/liquid interface.

In summary, the kinetics of reduction of MgO in molten slags with ferroalloys, which is the subject of this thesis, are far from clear. No systematic study has been reported which would allow the prediction of the rate of reaction under various conditions. In particular it would be important to study the influence of reduced pressure on the rate of reduction and the yield of magnesium. This would allow a useful analysis of the chemical and transport phenomena involved. The survey has shown that existing processes rely exclusively on the application of reduced pressure to recover magnesium by batch operations.

It is felt that in principle, magnesium could be recovered also by bubbling an inert gas at atmospheric pressure through the slag/metal melt. Apart from a comparison between the two methods in relation to rates of recovery and yield of magnesium the research would also provide a useful scientific basis for the assessment of further developments in this field.

CHAPTER 3

EXPERIMENTAL WORK

A special apparatus was designed and constructed to obtain continuous measurements of the weight of magnesium recovered from a molten $MgO-Al_2O_3-CaO$ slag reacted with ferroaluminium. The apparatus had provision for varying the total pressure, below atmospheric, above the melt as well as for bubbling inert gas through the melt at atmospheric pressure.

A second apparatus, which allowed visual observation of the surface of the melt, was set up to determine the pressure below which the evolution of magnesium bubbles commenced at reduced pressures. A series of experiments in which slags containing silica and magnesia were reacted with ferrosilicon, at reduced pressures, was also carried out in a modified version of the second apparatus. Preliminary experiments of an exploratory nature were conducted in this apparatus before commissioning the furnaces in which experiments aimed at measuring rates of reduction of MgO from molten slags were carried out.

3.1 APPARATUS AND TECHNIQUE USED FOR MEASURING RATES OF EVOLUTION OF MAGNESIUM

Rates of reduction of MgO from molten $MgO-Al_2O_3-CaO$ slags with ferroaluminium were determined by continuously weighing the deposit of solid magnesium which was collected in a condenser. Figure 3.1 shows a schematic diagram of the apparatus. The magnesium vapour was generated when slag and metal reacted in the crucible [1], placed inside the retort [2]. For the reaction to occur it was necessary to reduce the partial pressure of magnesium at the slag/metal interface to below its equilibrium value, either by lowering the total

Figure 3.1 - Schematic diagram of the apparatus used for measuring rates of evolution of magnesium

[1] crucible; [2] retort; [3] retort chamber; [4] condenser vessel; [5] duct; [6] nozzle; [7] load cell; [8] surge tank; [9]reaction tube; [10] hot chamber of the furnace; [11] gas cylinder; [12] needle valve; [13] rotameter; [14] pressure transducer; [15] probe; [16] graphite supports; [17] platform; [18] water-cooled jacket; [19] lid; [20] plugs; [21] graphite tubes; [22] cover; [23] thermocouple; [24] vacuum valve; [25] vacuum pumps; [26] mercury manometer

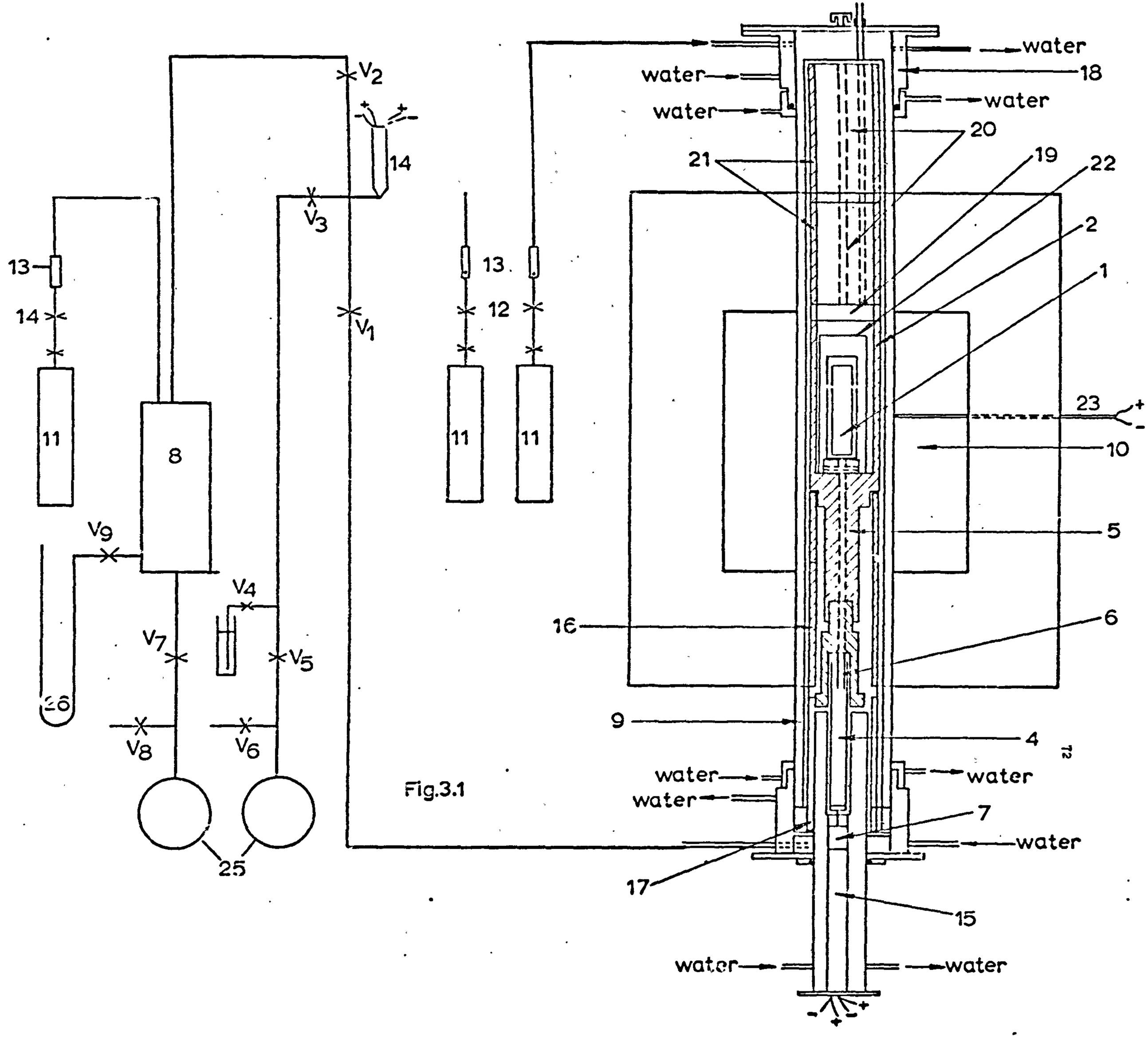

V2
14
V3
V1
13
14
11
8
V9
26
V4
V7
V5
V8
V6
25
13
12
11
11
water
water
water
water
18
20
21
19
22
2
1
23
10
5
16
6
9
4
water
water
water
water
7
17
15
water
water

Fig.3.1

pressure above the melt, or by bubbling argon through the melt at atmospheric pressure. The magnesium vapour which evolved from the melt and was transported from the retort chamber [3] to the condenser vessel [4] via the duct [5] and the nozzle [6]. The weight gain of the condenser, due to the formation of a solid deposit of magnesium, was continuously monitored by means of the load cell [7]. In the experiments carried out at reduced pressures the surge tank [8] was connected to reaction tube [9] and this allowed accurate pressure control above the melt. In these experiments the weight gain of the condenser, the temperature in the hot chamber of the furnace [10] and the pressure in the reaction tube were simultaneously recorded. When the reaction was carried out at atmospheric pressure with bubbling of argon through the melt, a lance was introduced into the crucible and the gaseous mixture of Ar and $Mg_{(g)}$ was transported to the condenser. The argon[1] was supplied directly from the gas cyclinder [11] and the flow was adjusted by means of the needle valve [12] and the rotameter [13]. The temperature of the melt was not directly measured in each experiment; however, it was inferred from calibration curve against the temperature in the hot chamber of the furnace. The pressurc in the furnace was measured by means of the pressure transducer [14]. Well-fitted joints prevented the escape of magnesium vapour from the retort assembly. The efficient cooling system and the accurate location of the probe [15] in the tube of the furnace enabled the collection of all the magnesium vapour inside the condenser vessel.

---

1 HP Argon supplied by British Oxygen Corporation; typical analysis: O_2 < 2 vpm, H_2 < 0.1 vpm, N_2 < 10 vpm, hydrocarbons < 1 vpm, CO_2 < 1 vpm, CO < 1 vpm, moisture < 2 vpm.

Figure 3.2 - Layout of the furnace; (a) elevation; (b) plan

Scale: 1/6.4

[1] ceramic tube; [2] hot chamber; [3] heating elements; [4] 64 mm layer of MPK 30 bricks; [5] 76 mm layer of MPK 28 bricks; [6] 38 layer of slabs of Kipsulate 1850; [7] 13 mm Sindanyo boards (19 mm board at the bottom); [8] angle-iron frame

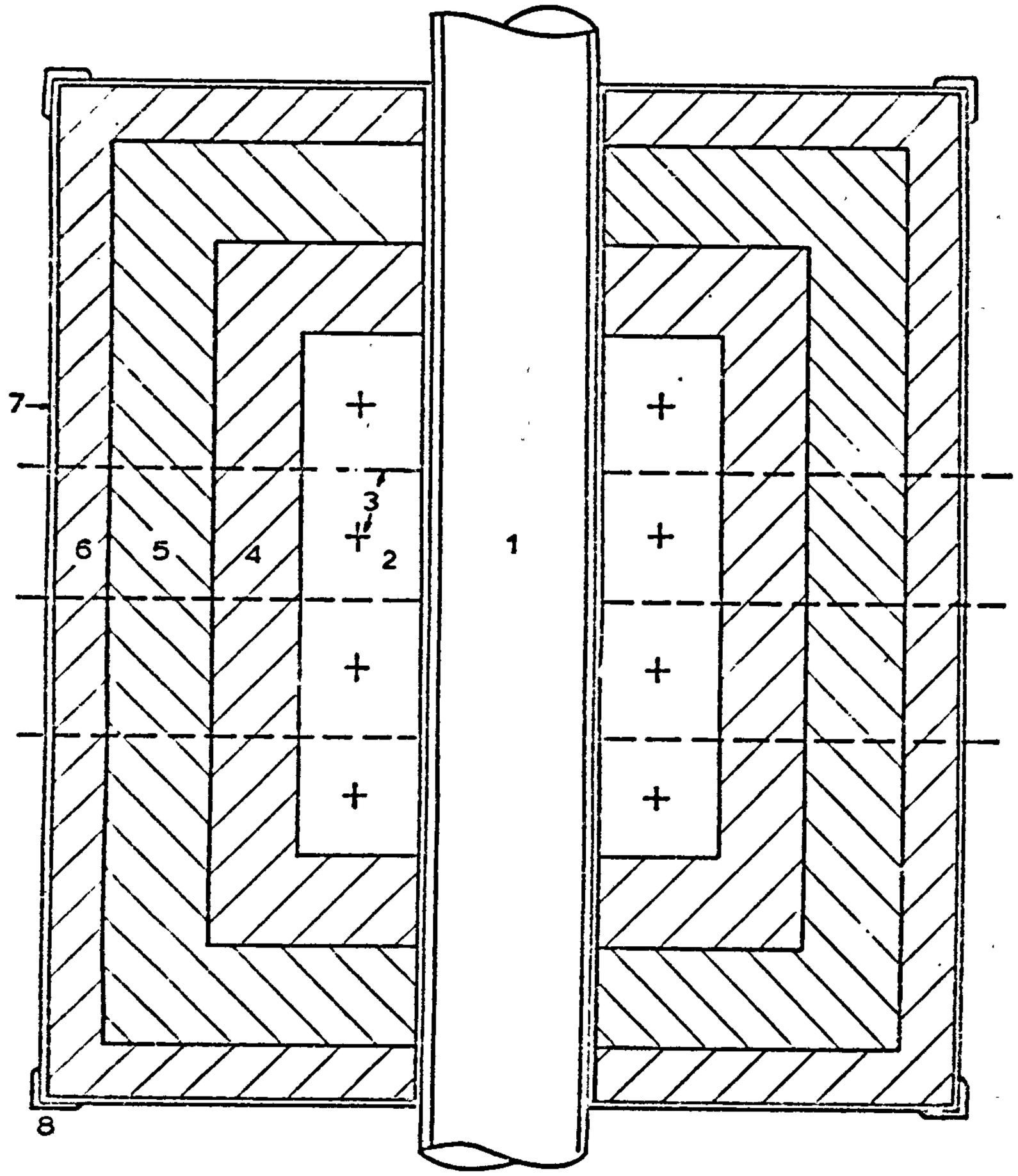


Fig.3.2.a

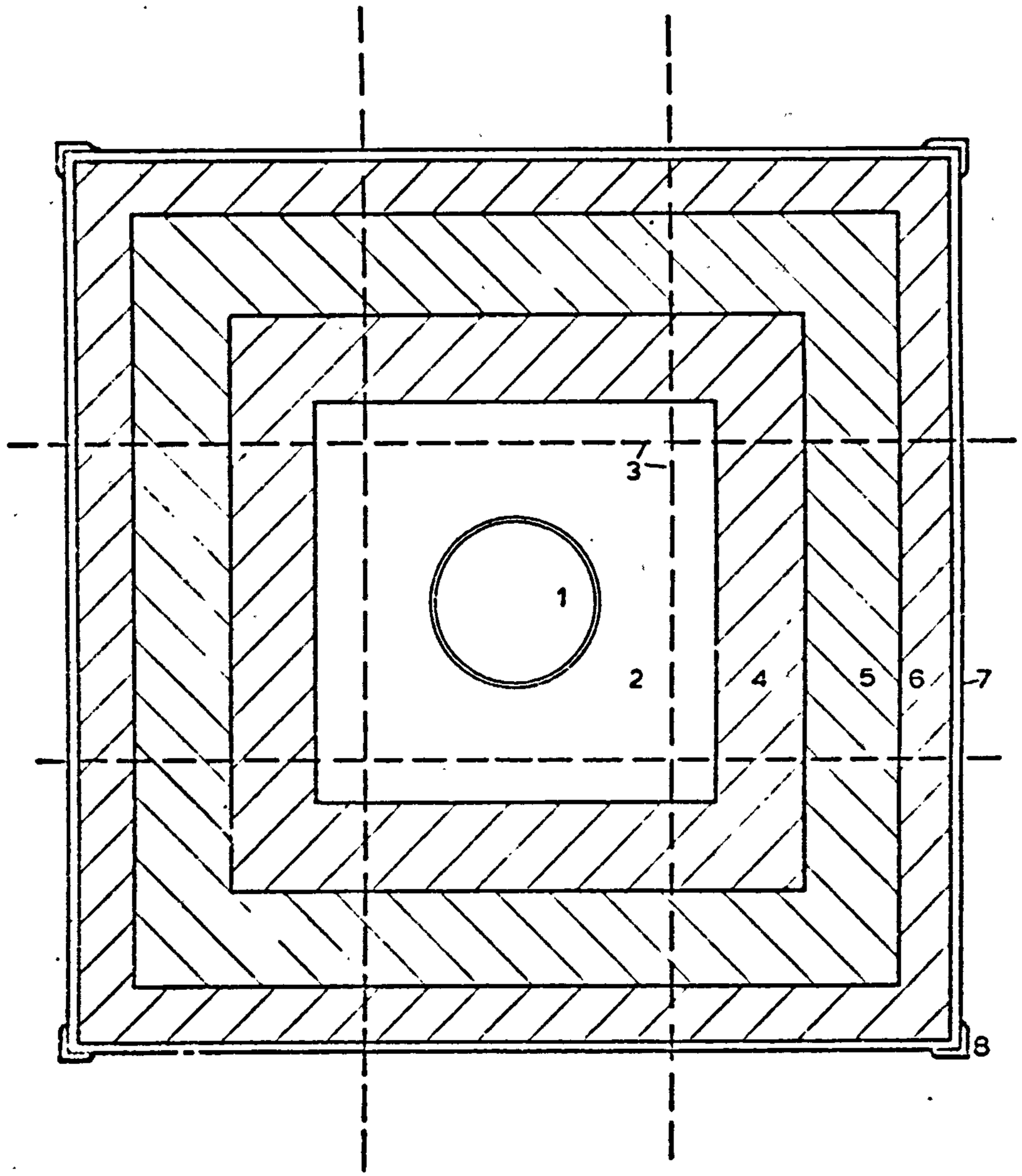


Fig.3.2.b

3.1.1 Furnace

The thermal insulation for the tube furnace (140 mm OD × 120 mm ID × 1100 mm long) consisted of two layers of refractory bricks backed by a third layer of insulation material as shown in Figure 3.2. The outer casing of the furnace was made of hard asbestos boards which were fixed within an angle iron frame. The furnace, designed for operation up to 1500 C, was provided with 14 silicon carbide elements mounted horizontally. The heating elements were connected in 7 branches of 2 elements in series. The heating elements were connected with aluminium braids which were fixed on the ends of the rods by steel clips. Electrical contacts to the network were provided by copper bars fixed on the outer casing of the furnace. Heavy cables (200 A) connected the furnace to a transformer (10 kW). Calculations for the specification of the transformer are presented in Appendix 3. The electrical circuit diagram is given in Figure 3.3. Temperature control was achieved using a proportional controller (type MK IV, Smiths & Sons Ltd.) coupled with a mercury relay rated at 30 A, 250 V a.c. .

The temperature of the hot chamber of the furnace was measured at two points using Pt/Pt - 13% Rh thermocouples sheathed with re-crystallised alumina tubes. Provision was made for measurements of the temperature of the surface of one of the heating elements using an optical pyrometer. Temperatures in the range 1500 - 1550 C were obtained in the hot chamber of the furnace when the corresponding surface temperatures of the elements were in the range 1520 - 1570 C. The recommended maximum temperature for the elements was 1575 C. Figure 3.4 shows that there is a maximum permissible surface loading which decreases with temperature.

An impervious sintered mullite tube (supplied by Anderman & Company Ltd., 140 mm OD × 120 mm ID × 1100 mm long) was vertically

Figure 3.3 - Circuit diagram of the furance

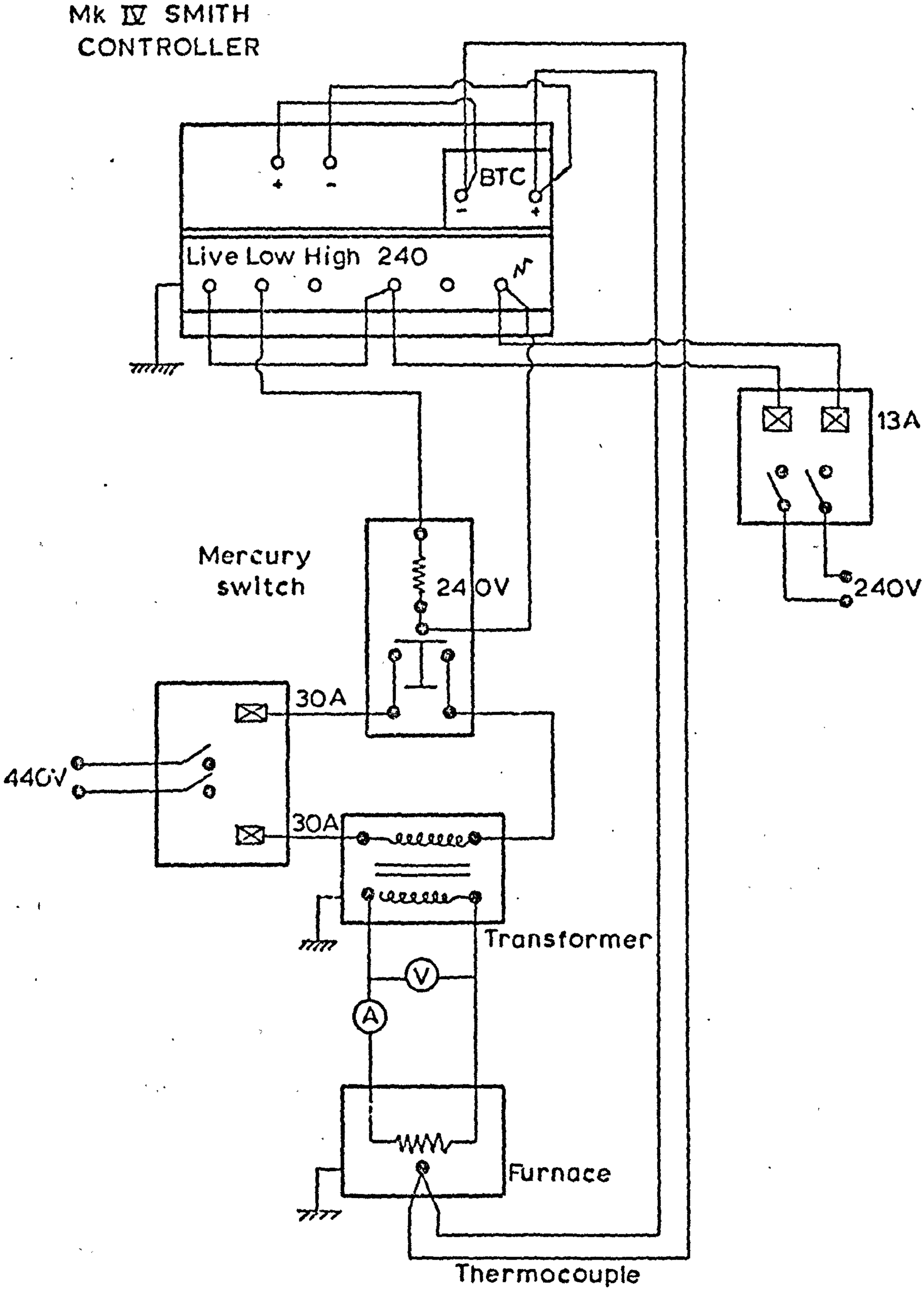

Mk IV SMITH
CONTROLLER
+
-
BTC
-
+
Live Low High 240
N
13A
240V
Mercury
switch
240V
30A
440V
30A
Transformer
V
A
Furnace
Thermocouple

Fig.3.3

mounted in the furnace. The tube could withstand the high temperatures at reduced pressures, but due to the severity of the operating conditions, its life was limited to 7 - 10 heats, especially at reduced pressures. The tube which was fixed on a platform underneath the furnace (Figure 3.5) was free to expand upward when heated. Water-cooled "O"-ring seals were provided at both ends of the tube. The water-cooled jacket for the top seal was supported by four springs so that its weight was not fully transmitted to the tube (Figure 3.6). A view of the furnace appears on the right in Figure 3.7.

3.1.2 Retort assembly

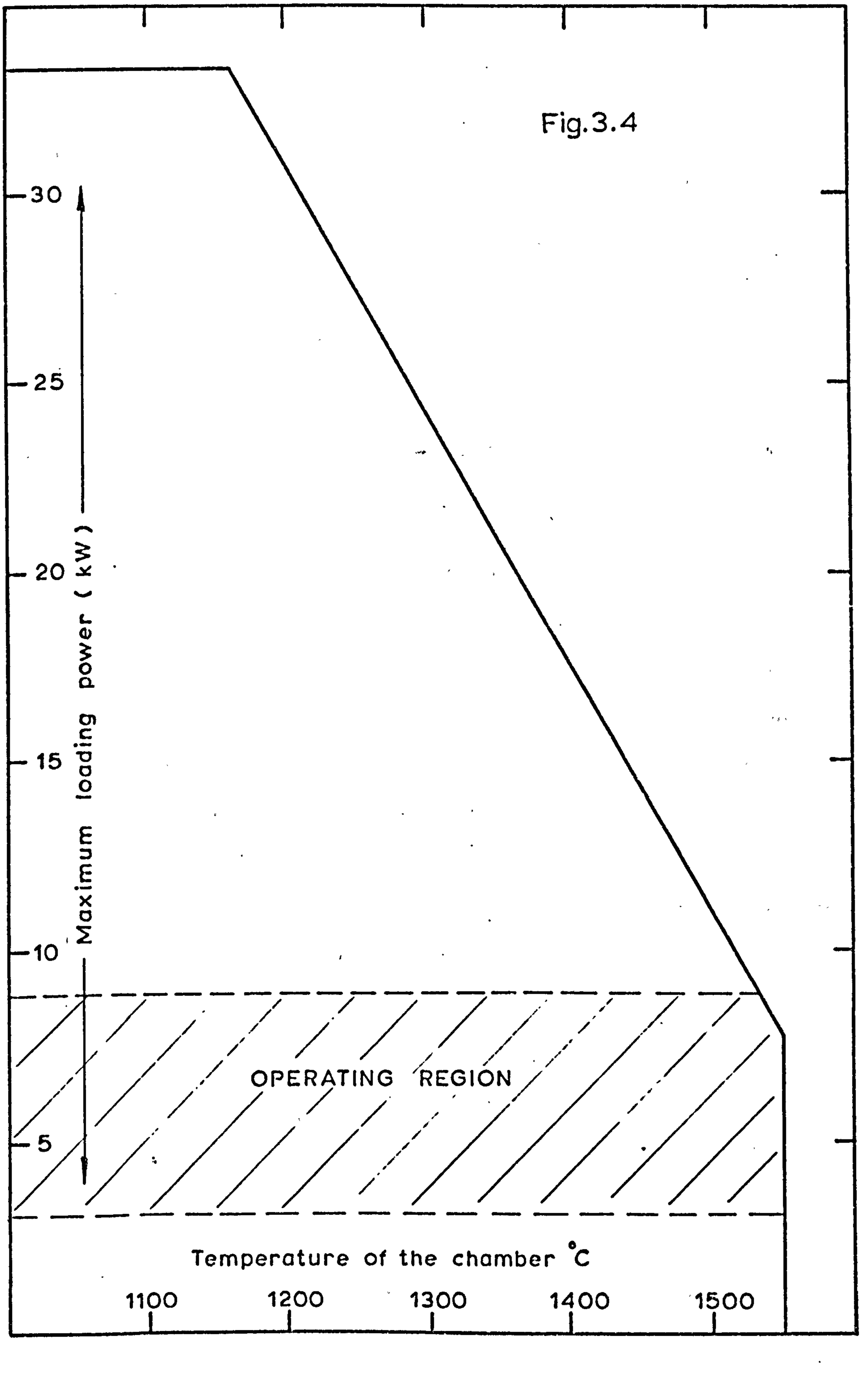
The retort assembly shown in Figure 3.8a consisted of the retort chamber [1] in which the crucible [2] rested on a pedestal [3]. Magnesium vapour could reach the nozzle [4] via the duct [5] and the six holes (10 mm) in the pedestal. The dead space around the crucible was decreased by placing the cover [9].

The above described arrangement was used only for the experiments at reduced pressures. For experiments in which argon was bubbled through the melt a graphite lance [13] was introduced into the crucible. The clearance between the lance and the opening in the lid of the retort was small enough to prevent the escape of magnesium. The lance, 12 mm OD × 3 mm ID × 1000 mm long, is shown in Figure 3.8b.

As shown in Figure 3.1 the retort assembly was supported on graphite tubes [16] which rested on a platform [17] built in the water-cooled jacket [18] for the bottom seal of the furnace tube [9]. On the top of the retort lid [19] plugs of refractory material clad in graphite tubes [20] provided thermal insulation.

Figure 3.4 - Variation of maximum permissible loading of the heating elements with temperature in the hot chamber

Fig.3.4


30
25
20
15
10
5
Maximum loading power (kW)
OPERATING REGION
Temperature of the chamber °C
1100
1200
1300
1400
1500

The entire assembly was made of high purity graphite (supplied by Morganite Special Carbons Ltd.) which would not give rise to undesirable side reactions. Graphite was machineable to close tolerances and the assembly withstood the high temperature with no apparent dimensional changes after prolonged use.

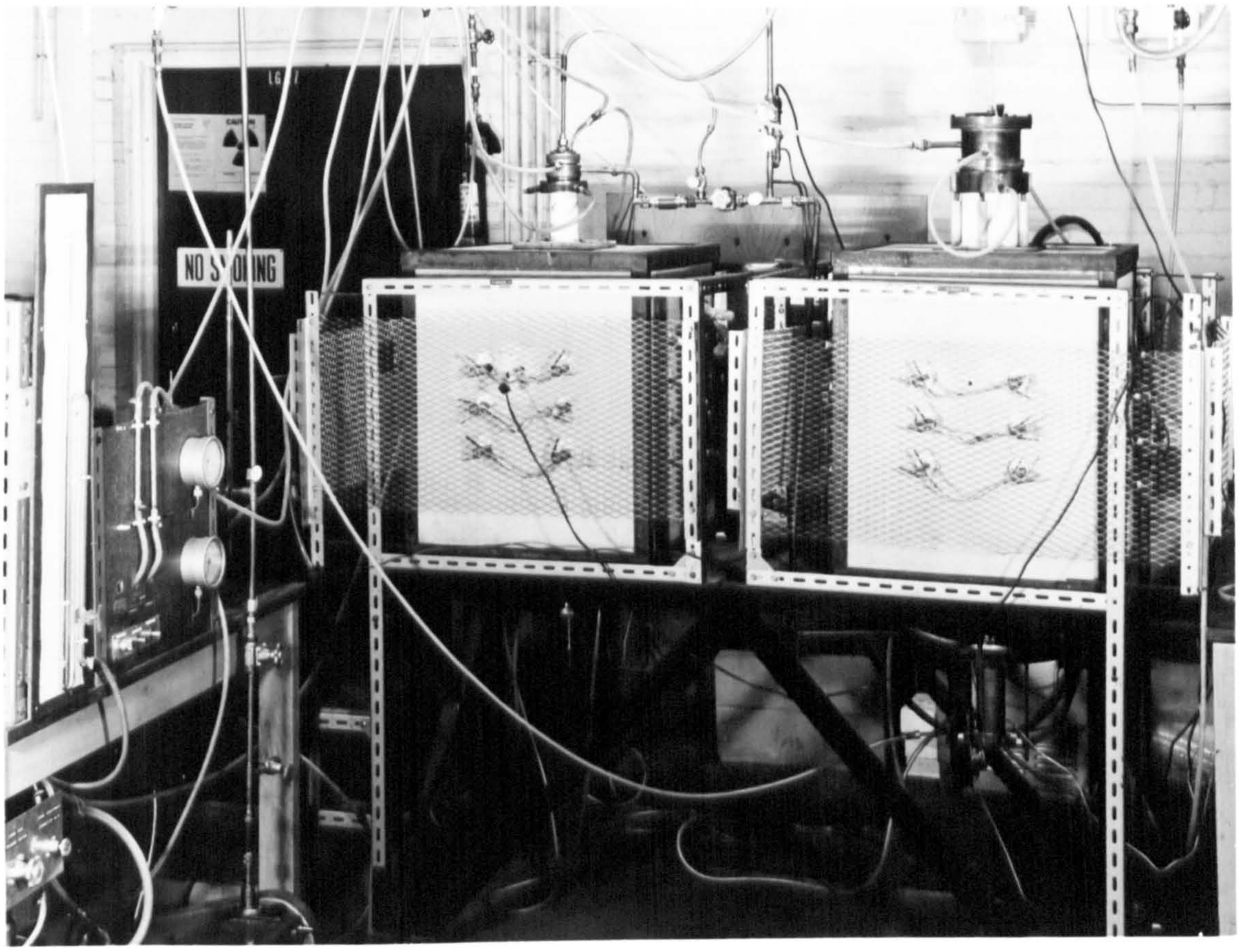
The temperature profile of the furnace and the calibration curve relating the temperature at the bottom of the crucible with that in the hot chamber are given in Figures 3.8 and 3.9 respectively. A reference thermocouple was permanently positioned on top of the lid of the retort.

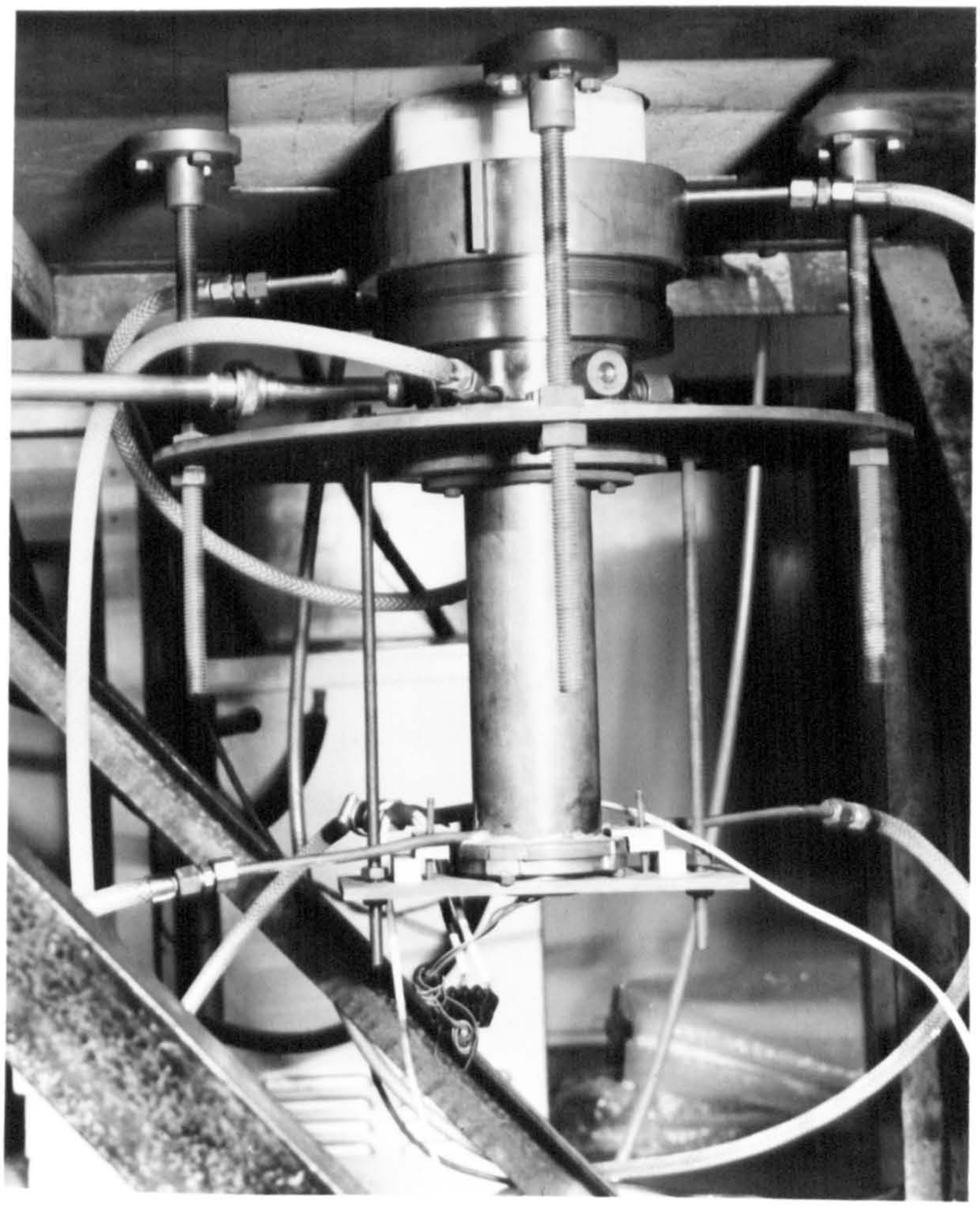
3.1.3 Probe for collecting and weighing the deposit of magnesium

From the curve of vapour pressure of magnesium plotted in Figure 2.7 the temperatures at which $Mg_{(g)}$ commences to condense, at a given pressure, may be obtained. The boiling point of magnesium is 1105 C[13], but if the pressure in the condenser zone is lower than the atmospheric then magnesium vapour will condense at lower temperatures. For instance, at 30 and 70 mm Hg pressure, the temperatures for condensation are 813 C and 873 C respectively. At the melting point (650 C)[13] the vapour pressure of magnesium is 4 mm Hg. Therefore, for the range of pressures considered above and if the temperature of the surface of condensation is below 650 C, a solid deposit of magnesium will be formed in the condenser vessel. Figure 3.10 schematically shows the two designs of condenser which were tried. In the first, a system for heat extraction from the condensation surface by radiation to a cold finger surrounded by this surface was tested (Figure 3.10a). This proved unsuccessful, however, due to the excessive thermal radiation received by the condenser in spite of the provision of radiation shields.

Figure 3.7 - Furnaces used in the experimental programme of reduction of MgO from molten slags with ferroalloys. Rate measurements were carried out in the furnace which appears on the right

Figure 3.5 - Support for the tube of the furnace and for locating the probe


NO S



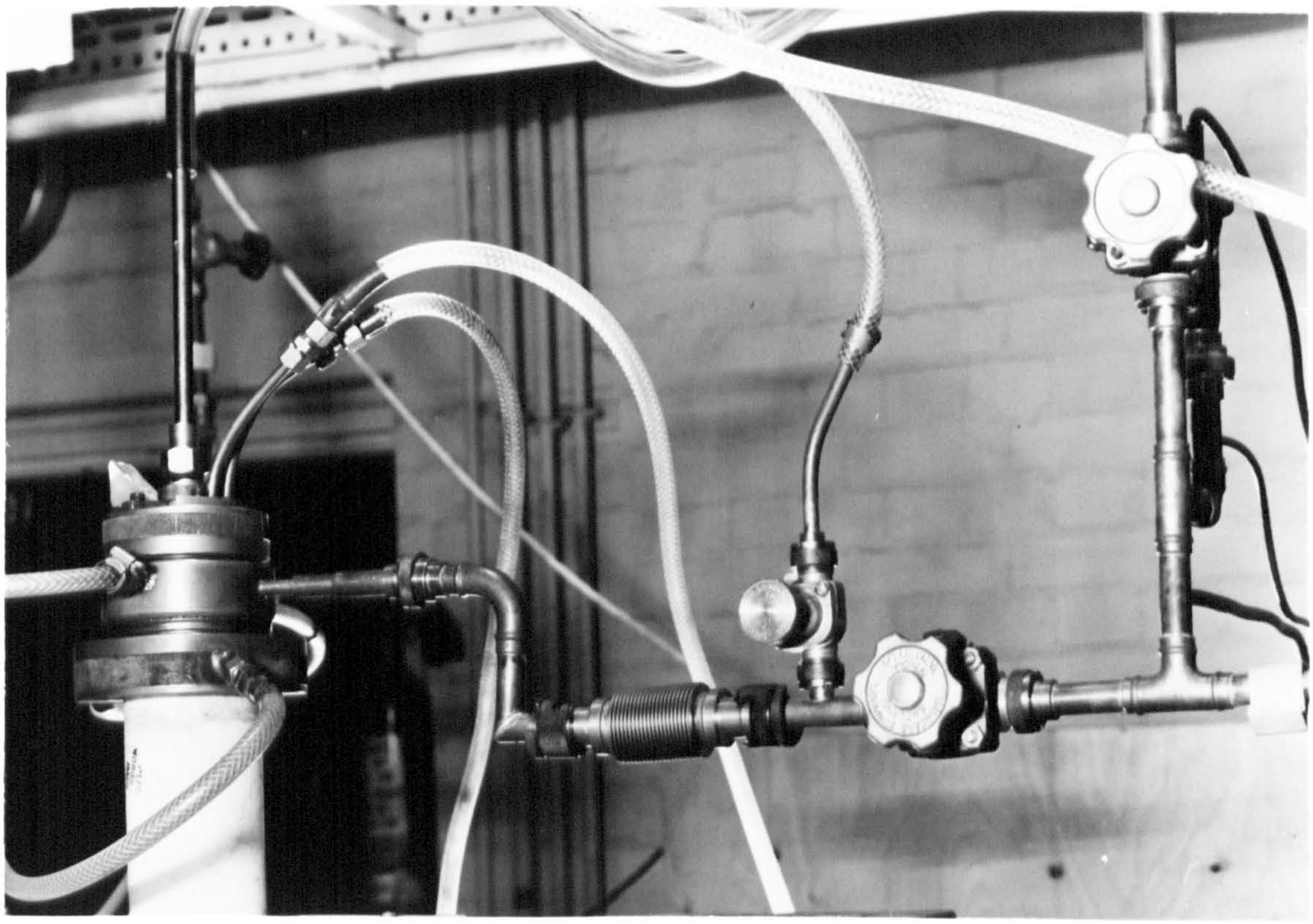
The temperature of the vapour leaving the nozzle was approximately 1150 - 1200 C and the temperature on the condensation surface was 800 - 900 C which was too high for efficient condensation of magnesium vapour. In the second design (Figure 3.10b) which was successful, the surface of condensation was protected from radiation by a water-cooled housing. This latter system was used to obtain all the rate measurements. Measurements showed that the temperature at the bottom of the condenser was as low as 160 C. A solid deposit of crystals of magnesium was formed in the middle region of the condenser vessel as shown in Figure 3.11. Deposits obtained at reduced pressures consisted of coarse crystals. In the case of condensation taking place at atmospheric pressure of argon, however, deposits of fine crystals were collected.

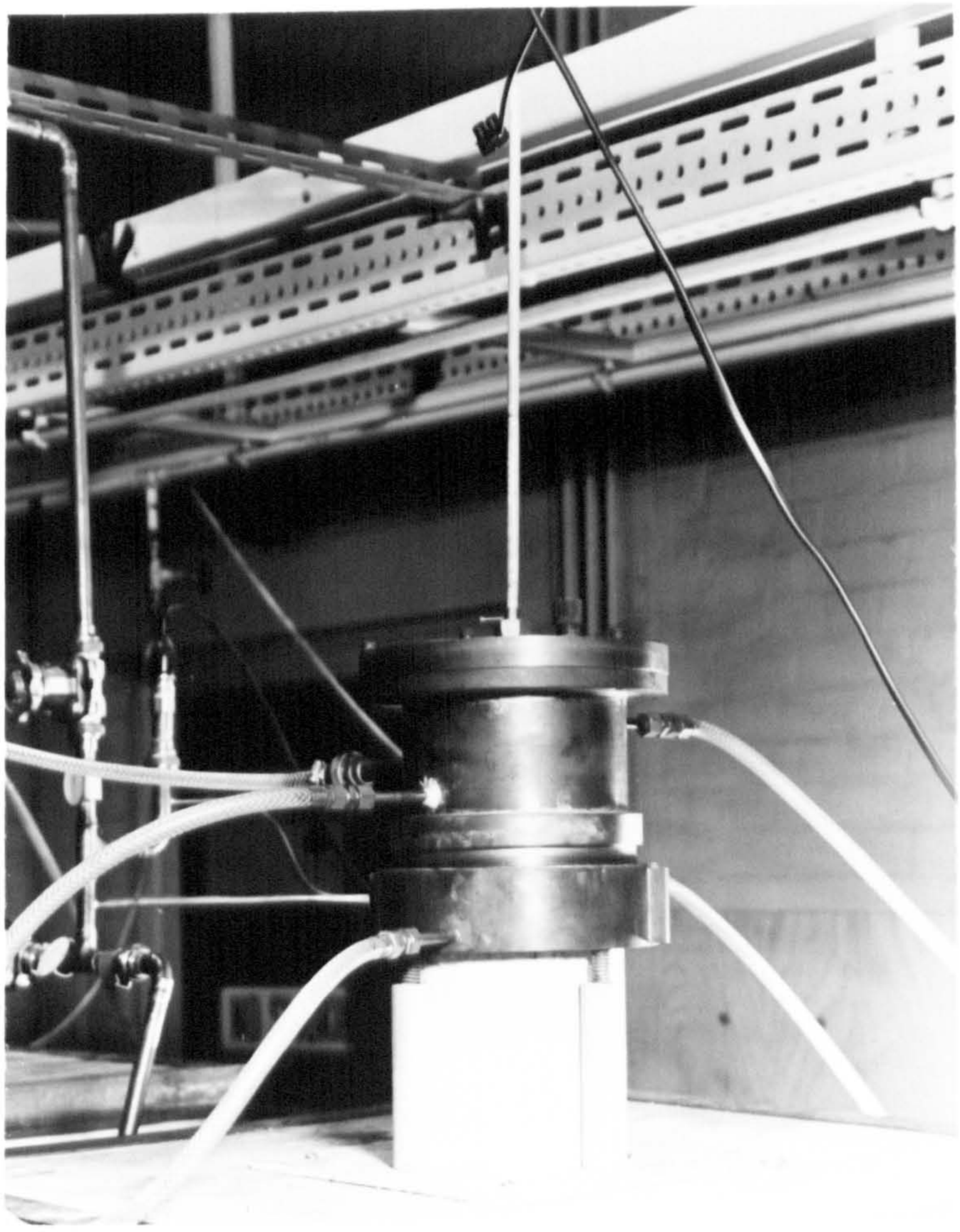
Figure 3.12 shows a schematic diagram of the probe. It consisted of the graphite condenser vessel [1] and the load cell [2]. The condenser was located in a water-cooled housing [3] and rested on a disc [4] attached to the spindle [5] of the load cell [2]. Figure 3.13 shows the probe, the load cell mounted on its pedestal and the two sections of the condenser vessel. The cooling system of the probe ensured that the load cell housing was maintained at room temperature even when the surrounding temperature was very much higher (600 - 1200 C). Preliminary experiments showed that when the hot chamber of the furnace was at 1500 C the temperatures of the disc which held the condenser vessel and of the spindle of the load cell were 160 C and 60 C respectively.

The load cell (series UF 1, Pye Ether Ltd., strain-gauge type, weight range $\pm$ 55 grams) was operated with an excitation voltage of 7.250 $\pm$ 0.005 Volts d.c. . The electrical connections to the load cell were made through vacuum-tight seals. The output signal from the cell was partially backed off using an external milivolt source

Figure 3.18 - View of the upper part of the apparatus used for visual observation of the surface of the slag/metal melt

Figure 3.6 - Water-cooled jacket for the upper part of the tube furnace used for rate measurements of reduction of MgO from molten slags with ferroaluminium. The water-cooled jacket is supported by four springs





and the net output was fed into a potentiometric recorder. The load cell was calibrated by measuring its output for a series of known weights. Figure 3.14 confirms that the calibration was linear. The voltage output of the load cell was not affected by variations in the pressure between atmospheric and 10 mm Hg. However, at lower pressures it was found that the output increased as the pressure in the furnace decreased. This behaviour did not affect the experiments because they were performed at pressures well above 10 mm Hg.

The agreement between the weight gain of the condenser detected by the load cell and the weight of magnesium determined from independent measurements of the weight of the condenser before and after each experiment was within 1 - 3%. Oxidation of the deposit was avoided by cooling them to room temperature before removing the condenser from the inert atmosphere in the furnace.

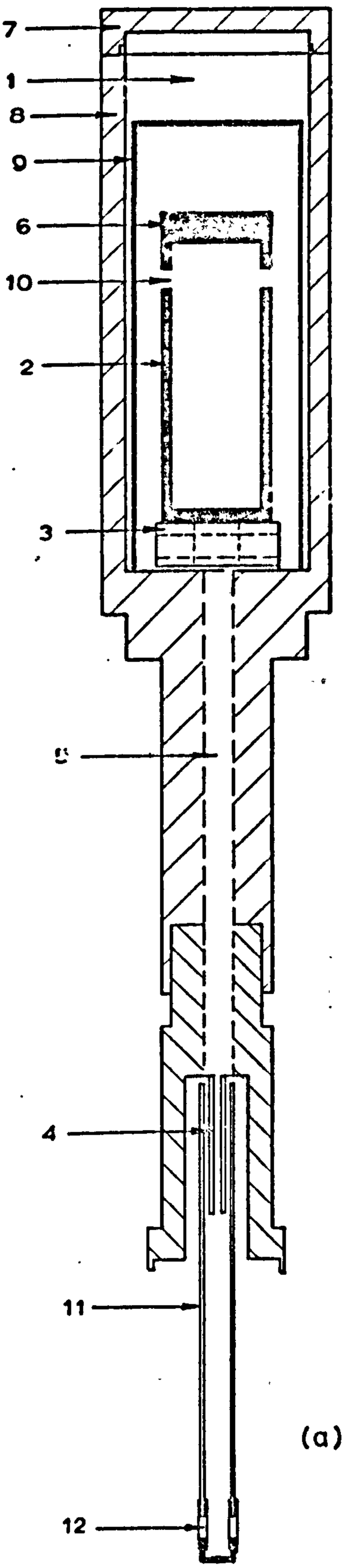
3.1.4 Pressure control for reduced pressure experiments

In the experiments at reduced pressure it was essential to determine the start of the reaction precisely. A technique was devised which enabled the precise and rapid achievement of the required pressure in the atmosphere above the slag/metal melt. A surge tank was connected to the furnace as shown in Figure 3.1. If the pressure in the furnace was p_{F1}, initially, then the tank was isolated from the rest of the system and evacuated to a pressure p_{T1} which was less than p_{F1}. The vacuum pumps [18] and [19] were then isolated and the surge tank and furnace were connected by opening valves [20] and [21]. The pressure in the furnace would then drop to a lower value $p_{F2} = p_R$, where $p_{T1} < p_R < p_{F1}$. The drop occurred within 10 seconds. By adjusting the gas flow into the system or by bleeding out argon via the vacuum pump, the level of

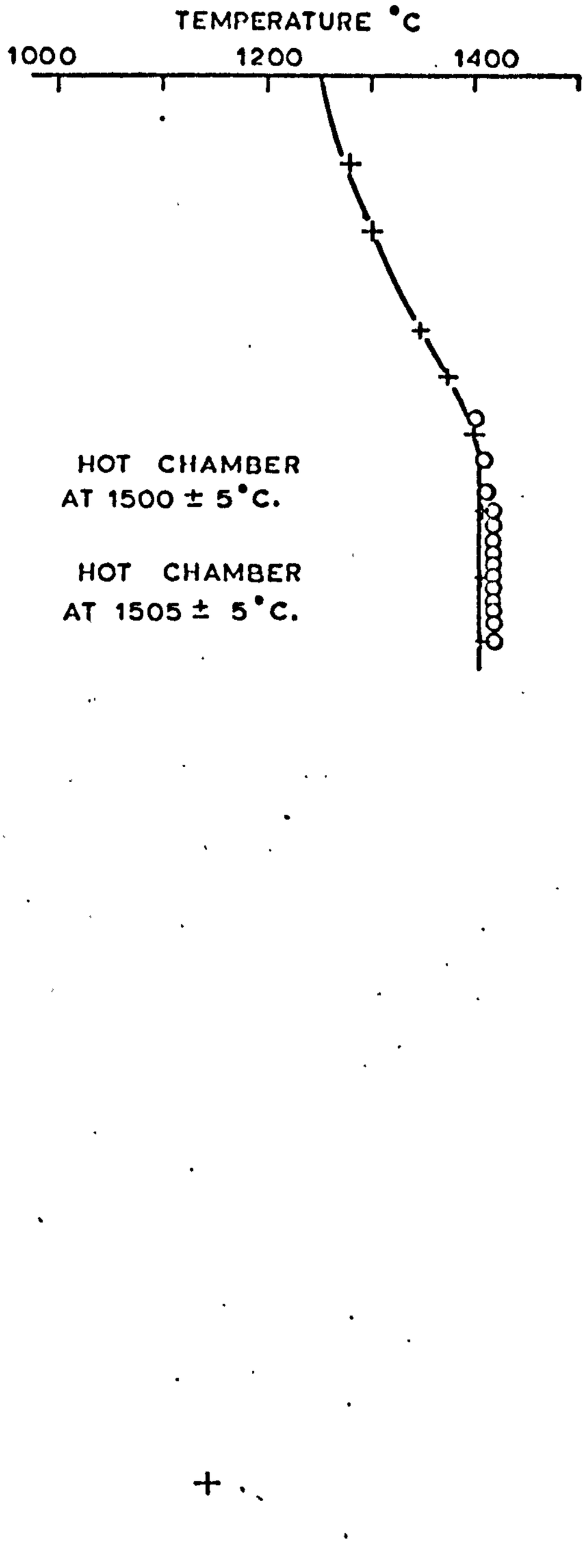
Figure 3.8 - (a) Schematic diagram of the retort assembly. Sacle: 1/3.2

(b) gas lance used for bubbling argon through the slag/metal melt at atmospheric pressure

[1] retort chamber; [2] crucible; [3] pedestal; [4] nozzle; [5] duct; [6] lid of the crucible (used for experiments at reduced pressure); [7] retort lid for experiments at reduced pressure; [8] retort; [9] cover; [10] holes for the passage of magnesium vapour (six holes); [11] condenser vessel; [12] exit holes for argon (two holes); [13] lance with two holes for bubbling argon



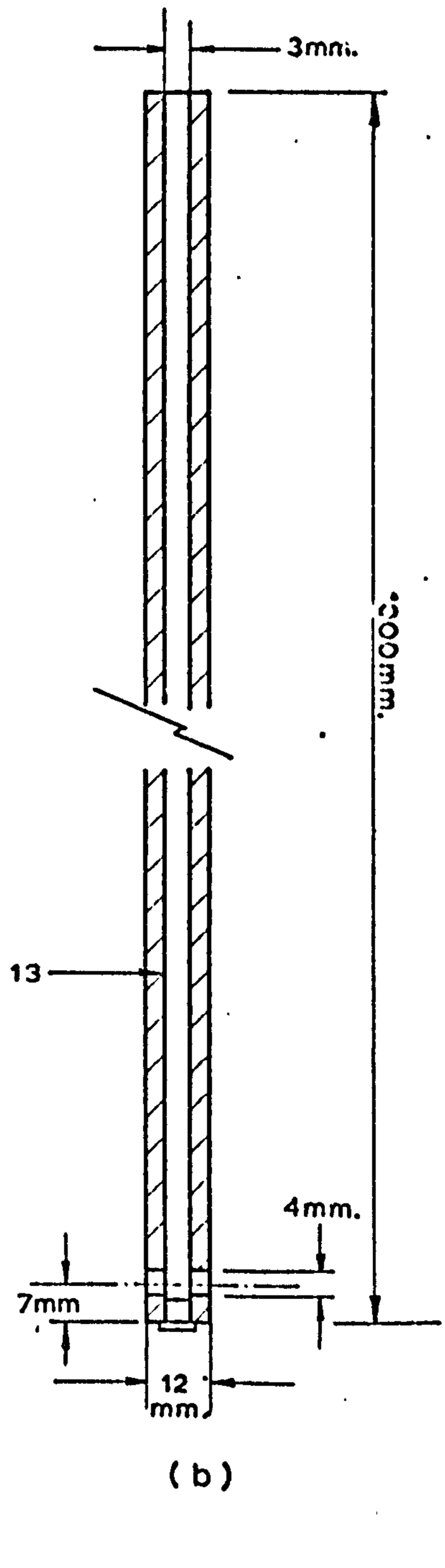
(a)



HOT CHAMBER
AT 1500 ± 5°C.

HOT CHAMBER
AT 1505 ± 5°C.

84



(b)

Fig. 3.8

pressure was maintained to within $\pm$ 1 mm Hg. The same procedure could be repeated for obtaining another value of the resulting pressure $p'_R < p_R$ from new starting values p_{F2} and p_{T2}. In a series of experiments at the operating temperature, the resultant pressure p_R was measured for various combinations of p_F and p_T. The results were satisfactorily correlated by an equation of the form

$$\hat{p}_R = 100.71 + 0.22\ (p_F - 250.04) + 0.77\ (p_T - 57.67) \qquad (3.1)$$

where pressures are expressed in mm Hg and $\hat{p}_R$ is the fitted value. The residual $|r| = |\hat{p}_R - p_R|/p_R$ was less than 0.01 - 0.05 in the range $30 \leq p_R \leq 120$ mm Hg.

A typical example is illustrated in Figure 3.15 in which the pressure in the furnace is reduced from 770 mm Hg to 45 mm Hg in two steps by setting the surge tank at 1 mm Hg (first step) and at 5mm Hg (second step).

The pressure in the furnace was measured by a pressure transducer (supplied by Bell & Howell Ltd.) mounted on the vacuum line (Figure 3.1). The calibration curve for the pressure transducer is plotted in Figure 3.16 for an excitation voltage of 18.00 $\pm$ 0.01 Volts d.c. . The pressure p (in mm Hg) was correlated with the output of the transducer E (in milivolts) by the linear equation

$$p = 18.868\ E + 96.00 \qquad (3.2)$$

The pressure in the surge tank was measured by means of a mercury manometer.

This technique was successful because the system retained low pressure adequately at high temperature. It was observed that the maximum leak rate was 0.54×10^{-7} mm Hg/sec. ml^{-1}, which corresponds to less than 1 ml/min of air at STP, for the total value of 43 liters

Figure 3.9 - Temperature at the bottom of the crucible versus temperature in the hot chamber of the furnace

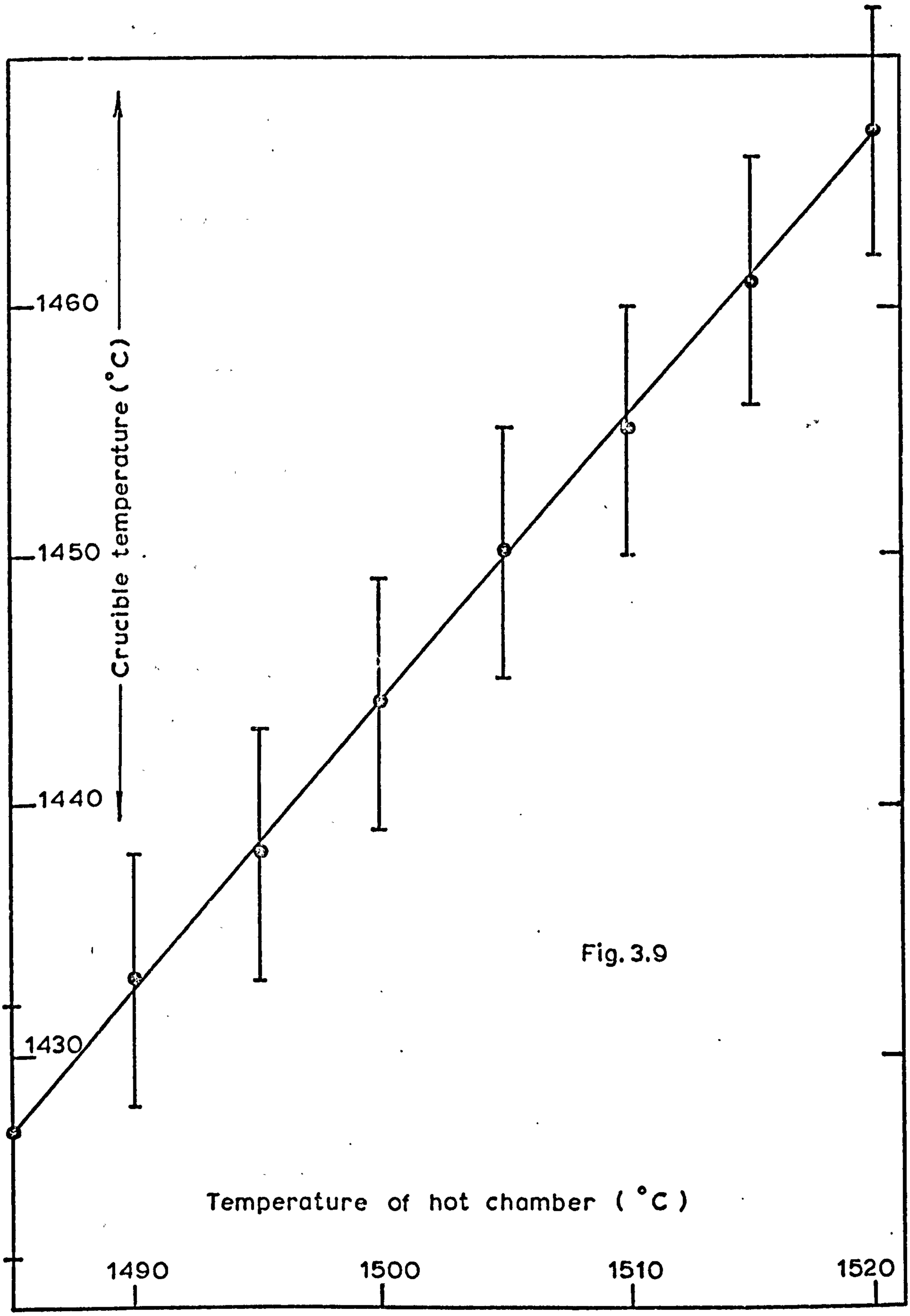

Crucible temperature (°C)
1460
1450
1440
1430
Temperature of hot chamber (°C)
1490
1500
1510
1520

Fig. 3.9

at residual pressure = 1 mm Hg. The leak rate decreased considerably at higher pressure.

3.1.5 Procedures for conducting experiments

In this section the procedures for conducting experiments on the reduction of molten slags with ferroaluminium at reduced pressures as well as at atmospheric pressure with bubbling of argon through the melt are described.

3.1.5.1 Preparation for an experiment

To start with the condenser was cleaned, weighed and positioned on its supporting disc. Then the entire probe was carefully introduced and sealed into the furnace. Pre-fused slag and metal pieces were separately weighed and charged into the crucible. A lid was fixed on the crucible for the experiments at reduced pressure. The crucible was then located on its pedestal inside the retort chamber. The lid of the retort was fixed and the insulation plugs were assembled. The top of the furnace was finally sealed. A reference thermocouple, sheathed with a recrystallised alumina tube closed at one end was introduced from the top until it touched the lid of the retort. The furnace was then evacuated and tested for leaks. It was flushed with argon twice and finally refilled with gas. The pressure of argon inside the furnace was maintained slightly above atmospheric (+ 10 cm water gauge) by bubbling the exiting gas through a column of water. This procedure prevented the leakage of air into the furnace. Argon was supplied to the furnace at 10 ml/min at STP. The apparatus was then ready for heating.

Figure 3.10 - Schematic diagram of the two types of consdenser which were tried. In design (a) the condenser surface enclosed the cold finger. In design (b) the condenser vessel was located inside a water-cooled housing.

[1] titanium cover; [2] cold finger; [3] water-cooled housing of the load cell; [4] load cell; [5] radiation schields; [6] duct for magnesium vapour; [7] heater; [8] condenser; [9] water-cooled housing; [10] load cell; [11] nozzle

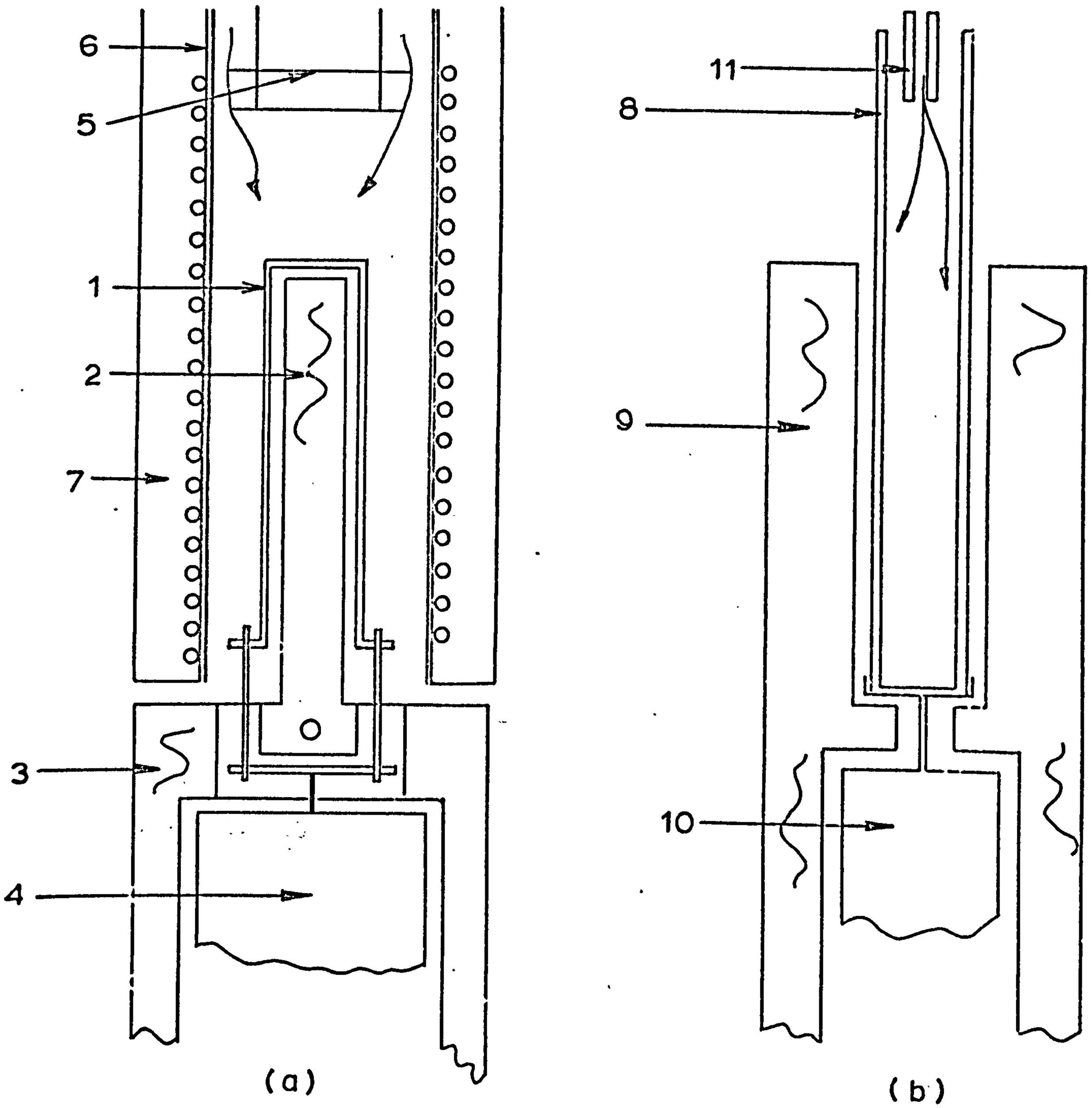


Fig.3.10

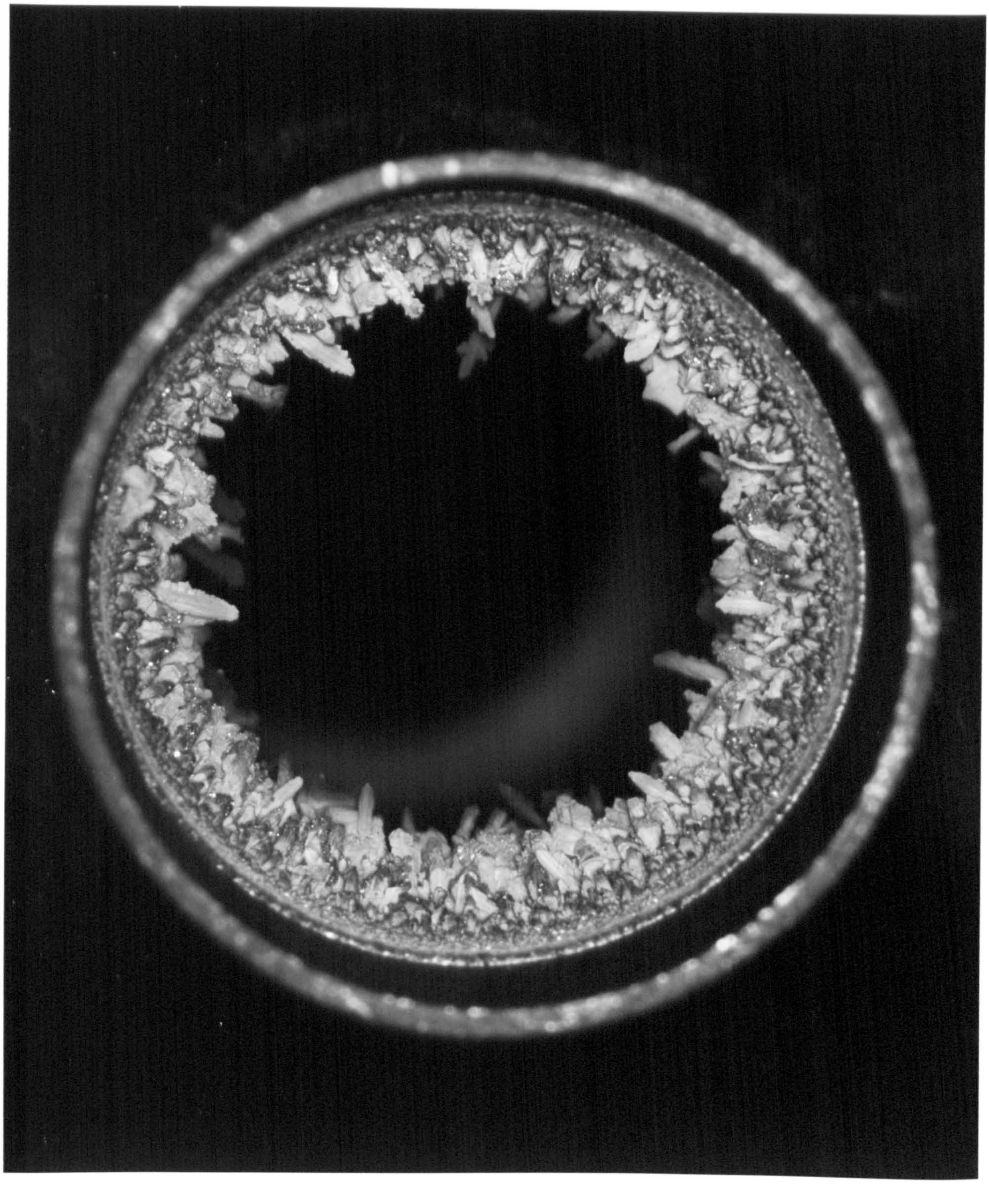
3.1.5.2 Heating cycle

The furnace was heated up from room temperature to 1510 - 1520 C (temperature of the hot chamber) in approximately 19 hours. Care was taken to limit the heating rate to less than 200 C/hour. This precaution was necessary to protect the ceramic tube from thermal shock. The selection of adequate taps on the secondary side of the transformer allowed the correct amount of energy to be supplied to the resistance network of the furnace. At 1510 - 1520 C 8.0 - 8.5 kW were required to maintain the temperature. It should be mentioned that, at this stage, the furnace was operating at its limit, as far as the surface temperature and the specific power loading of the heating elements are concerned. It could not be operated at higher temperatures without damaging the elements. The ceramic tube also was, in its hot zone, very near its recommended maximum service temperature. Once the temperature of the hot chamber had reached 1510 - 1520 C one of two procedures described below was employed.

3.1.5.3 Experiments on reduction of slags at reduced pressures

Once the temperature and the load cell signal were stable, the pressure inside the furnace was set at the required level by following the procedures described in Section 3.1.4. Temperature, pressure and weight gain of the condenser were simultaneously recorded during the experiments. The start of the reaction was precisely determined from the charts. The experiment was continued until no further weight gain of the condenser was observed. Then the system was pressurised to one atmosphere with argon and the furnace was cooled to room temperature.

Figure 3.11 - Crown of crystals of magnesium in the condenser vessel. Reduced pressure experiment. Operating pressure = = 30 mm Hg. Magnification: 10 X.



3.1.5.4 Experiments on reduction of slags at atmospheric pressure with bubbling of argon through the melt

The lance for injection of argon was kept 2-3 cm above the melt during the heating cycle. When the temperature and the signal of the load cell were both stable the flow of argon through the lance was adjusted to the required value. The load cell reading changed due to the effects of buoyancy and drag force acting on the condenser vessel. The change of the output signal of the load cell increased with the flow rate of gas. The lance with the gas flowing through it was introduced into the melt after the load cell output had stablised. Temperature and weight gain of the condenser were simultaneously recorded. At the end of the experiment the lance was removed from the melt and the furnace was cooled to room temperature. The condenser was then taken out, the magnesium deposit was removed and weighed.

3.2 PREPARATION OF SLAGS AND FERROALLOYS

The properties of slags and ferroalloys used in the experimental programme were given in Tables 2.4 and 2.7 and the relevant phase diagrams are presented in Appendix 4.

Pre-fused slags were prepared by melting mixtures of oxides in a platinum crucible. The melt was cast in a brass mould, crushed in a tungsten carbide coated mortar and re-melted for homogenization. The purity of the raw materials used was as follows:

crushed fused quartz powder - 99.99% SiO_2,

calcium carbonate - 99.50% $CaCO_3$,

magnesium oxide - 99.21% MgO. and

alumina - 99.29% Al_2O_3 .

Commercial Fe-75% Si and Fe-35% Al alloys were used. The 80% Al alloy was prepared from pure aluminium (99.9% Al) and pure

Figure 3.12 - Probe for collecting and weighing the deposit of magnesium

[1] condenser vessel; [2] load cell; [3] housing of the condenser; [4] disc; [5] spindle of the load cell; [6] load cell housing; [7] load cell pedestal; [8] water sprinkler; [9] vacuum-tight electrical connections of the load cell; [10] exit hole for argon and vacuum.

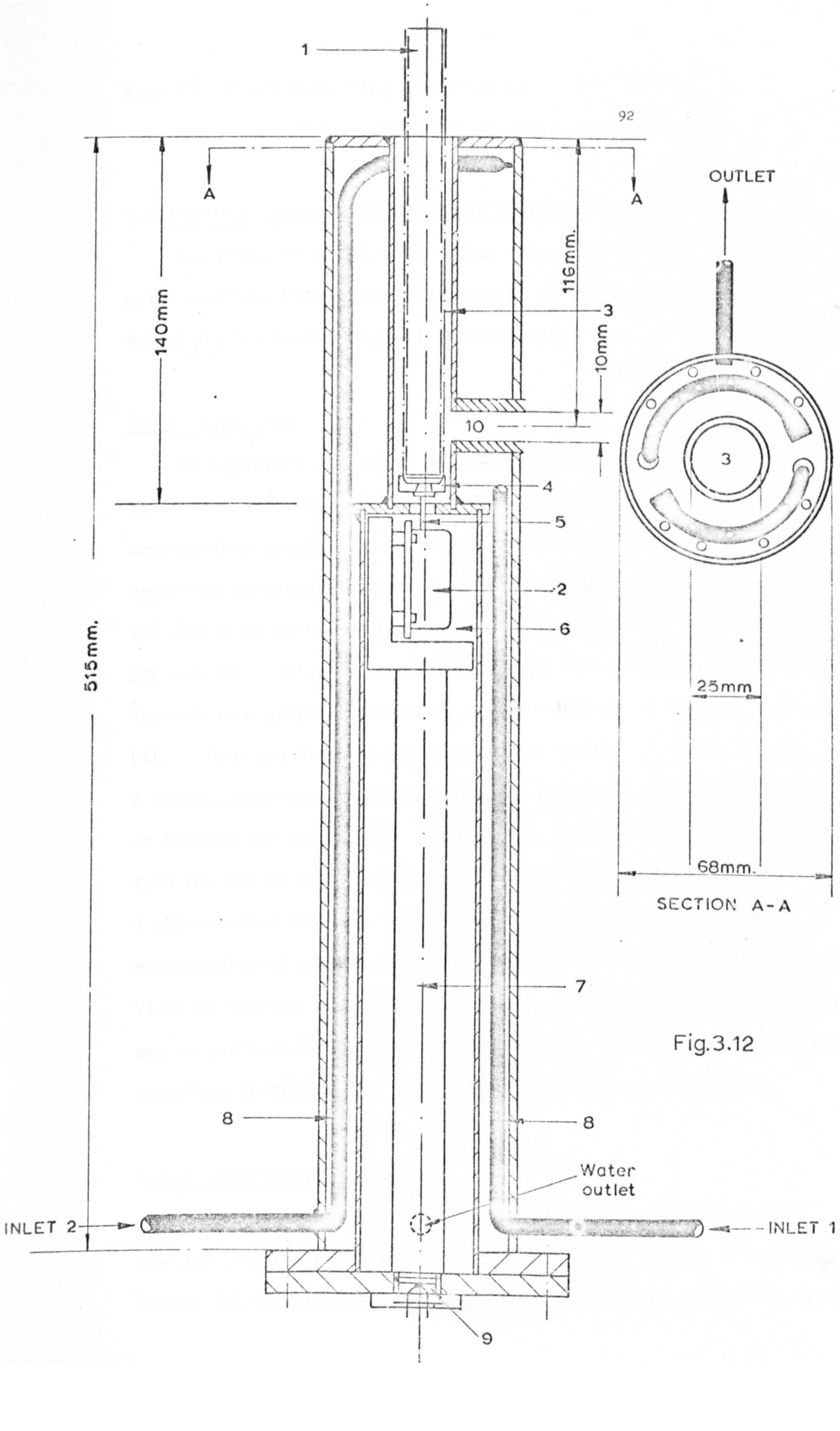

1
92
A
A
140mm.
515mm.
116mm.
10mm
3
10
4
5
2
6
7
8
8
9
INLET 2
INLET 1
Water
outlet
OUTLET
3
25mm
68mm.
SECTION A-A

Fig.3.12

iron (99.9% Fe) by melting aluminium and by adding pieces of iron rod into the crucible. The melt was cast into steel moulds.

3.3 VISUAL OBSERVATION OF THE SURFACE OF THE SLAG/METAL MELT

The pressure at which magnesium vapour boiled off the slag/metal melt was independently determined for the reaction of MgO-Al_2O_3-CaO molten slags with ferroaluminium at reduced pressures.

3.3.1 Apparatus

An apparatus was set up in a furnace similar to that described in Section 3.1.1 except for the ceramic tube, which was of re-crystallised alumina (75 mm OD × 65 mm ID × 1100 mm long). The apparatus is schematically represented in Figure 3.17. The tube [1] was sealed at both ends with water-cooled vacuum type "O"-ring seals [2] and [3]. Slag and metal were melted in a graphite crucible [4] located in a graphite vessel [5] which rested on an alumina pedestal [6]. This pedestal was cemented on the bottom lid of the furnace. A thermocouple was introduced from the bottom of the furnace until it touched the vessel [5]. The surface of the melt was observed from the top of the furnace through a transparent silica window [7]. A water-cooled coil was introduced into the furnace to prevent condensation of magnesium vapour on the inner surface of the window. Views of the top seal and of the entire furnace appear in Figure 3.18 and on the left in Figure 3.7 respectively. This apparatus and that described in Section 3.1 shared the same vacuum and gas lines.

3.3.2 Experimental procedure

Pre-fused slag and metal pieces were separately weighed and charged into the crucible which was then located inside the graphite vessel [5], (Figure 3.18). The furnace was sealed, tested for leaks

Figure 3.13a - Probe for collecting and weighing the deposit of magnesium

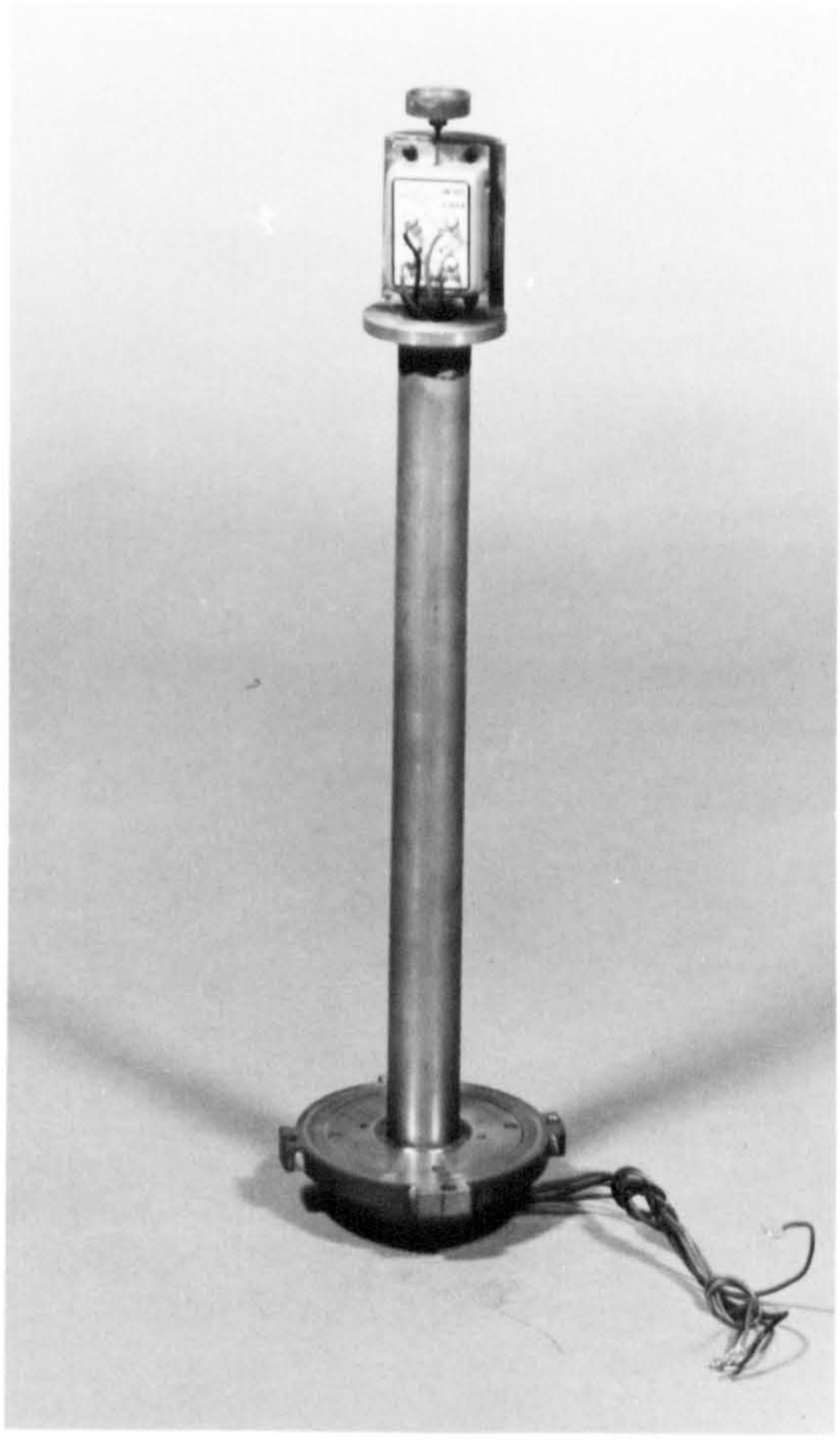
Figure 3.13b - Load cell mounted on its pedestal. The graphite disc which supports the condenser vessel is attached to the spindle of the load cell

Figure 3.13c - Two sectiosn which make up the condenser vessel

a



b



c



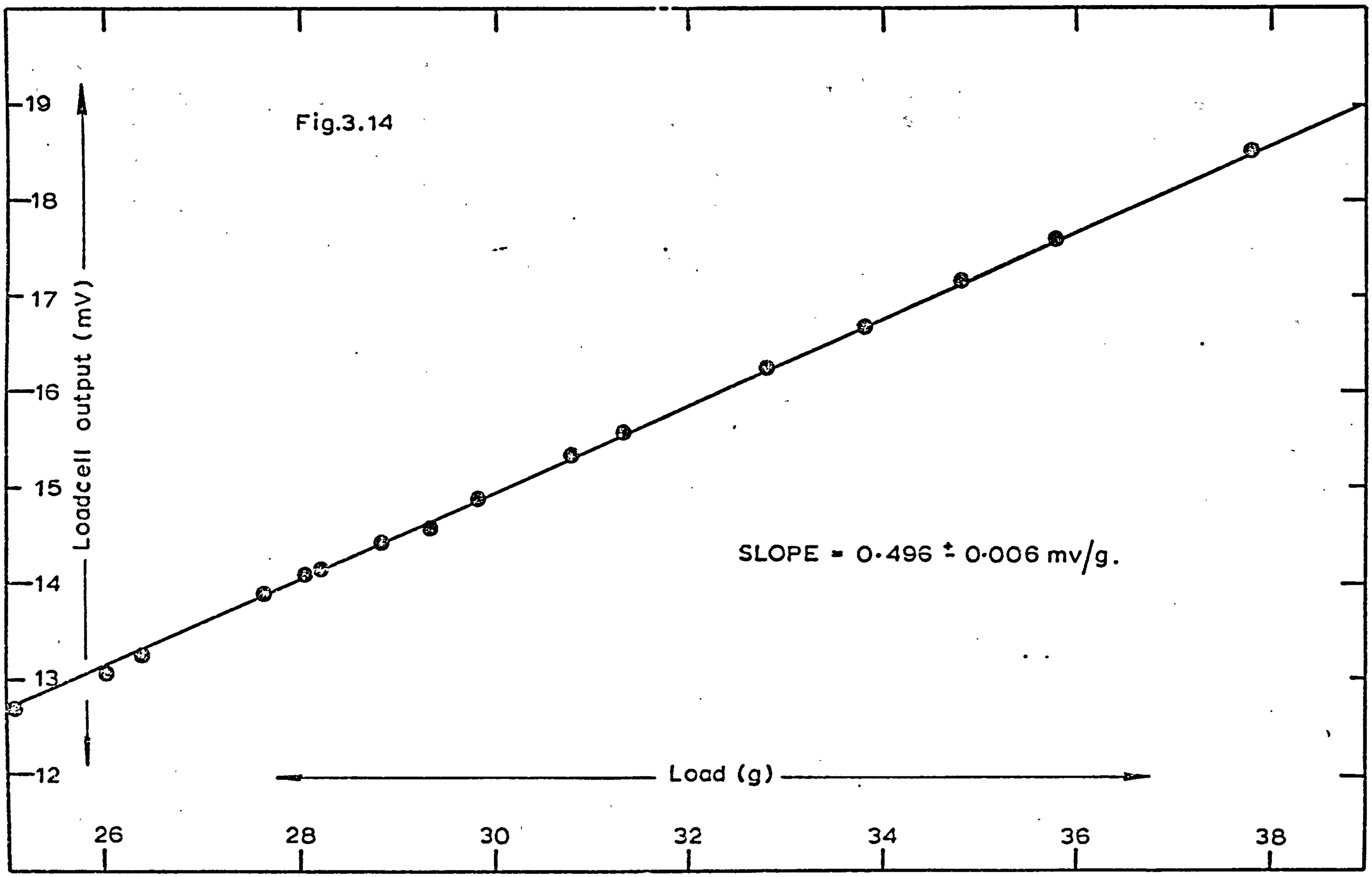
flushed and refilled with argon before starting the heating cycle. The heating cycle was similar to that described in Section 3.1.5.2 except for the power requirements which were lower due to the better thermal insulation of this furnace and the smaller size of the tube. About 6 kW were necessary at 1510 - 1520 C (temperature of the hot chamber). Once the temperature was established, the pressure in the furnace was carefully reduced by 50 mm Hg steps from atmospheric to 500 mm Hg level. From 500 mm Hg pressure downwards the pressure was reduced by 10 mm Hg steps. Each level of pressure was maintained for a certain time during which the surface of the melt was observed for the appearance of the first bubbles of magnesium vapour. If at a certain level of pressure p_B, bubbles of magnesium vapour were released from the melt, then the pressure was carefully increased to a higher value $p' > p_B$ at which the evolution ceased. For further evolution of magnesium vapour to occur the pressure had to be subsequently lowered to $p_B' < p_B$. It was possible to determine the pressure at which magnesium bubbles were first released within $\pm$ 5 mm Hg. At pressures below 50 mm Hg the evolution was very violent and it was impossible to estimate the size and frequency of bubbles. At the end of the experiment the furnace was repressurized with argon and cooled to room temperature.

3.4 REDUCTION OF SiO_2 - MgO-BEARING SLAGS WITH FERROSILICON

It was pointed out in Sections 2.1.2.5 and 2.1.2.7 that reduction of MgO from MgO-SiO_2-bearing slags with ferrosilicon in graphite crucibles at reduced pressures is bound to be accompanied by side reactions which produce silicon monoxide and carbon monoxide and the interpretation of results of measurements of rate of reaction is very difficult for such a complicated system. Moreover, the evolution of magnesium vapour will occur only at temperature-

Figure 3.14 - Calibration curve of the load cell. Excitation voltage = 7.250 $\pm$ 0.005 Volts d.c.

Fig.3.14


Loadcell output (mV)
19
18
17
16
15
14
13
12
Load (g)
26
28
30
32
34
36
38
SLOPE = 0·496 ± 0·006 mv/g.

pressure conditions even more severe than those required for the reduction of MgO with ferroaluminium. Reduction of MgO from molten slags with ferrosilicon will occur at operating pressures below 4 mm Hg at 1800 K (Figure 2.5). This would not be possible to achieve with the apparatus described in Section 3.1 for two reasons: the silicon carbide heating elements would be over-heated and overloaded and the ceramic tube of the furnace would deteriorate very rapidly and eventually collapse. Therefore it was decided not to use the system $MgO-SiO_2$-slags/ferrosilicon for experiments aimed at measuring the rates of evolution of $Mg_{(g)}$. However, a series of experiments to investigate the effect of the activity of silica on the level of contamination of the condensed deposits of reaction was carried out.

3.4.1 Apparatus

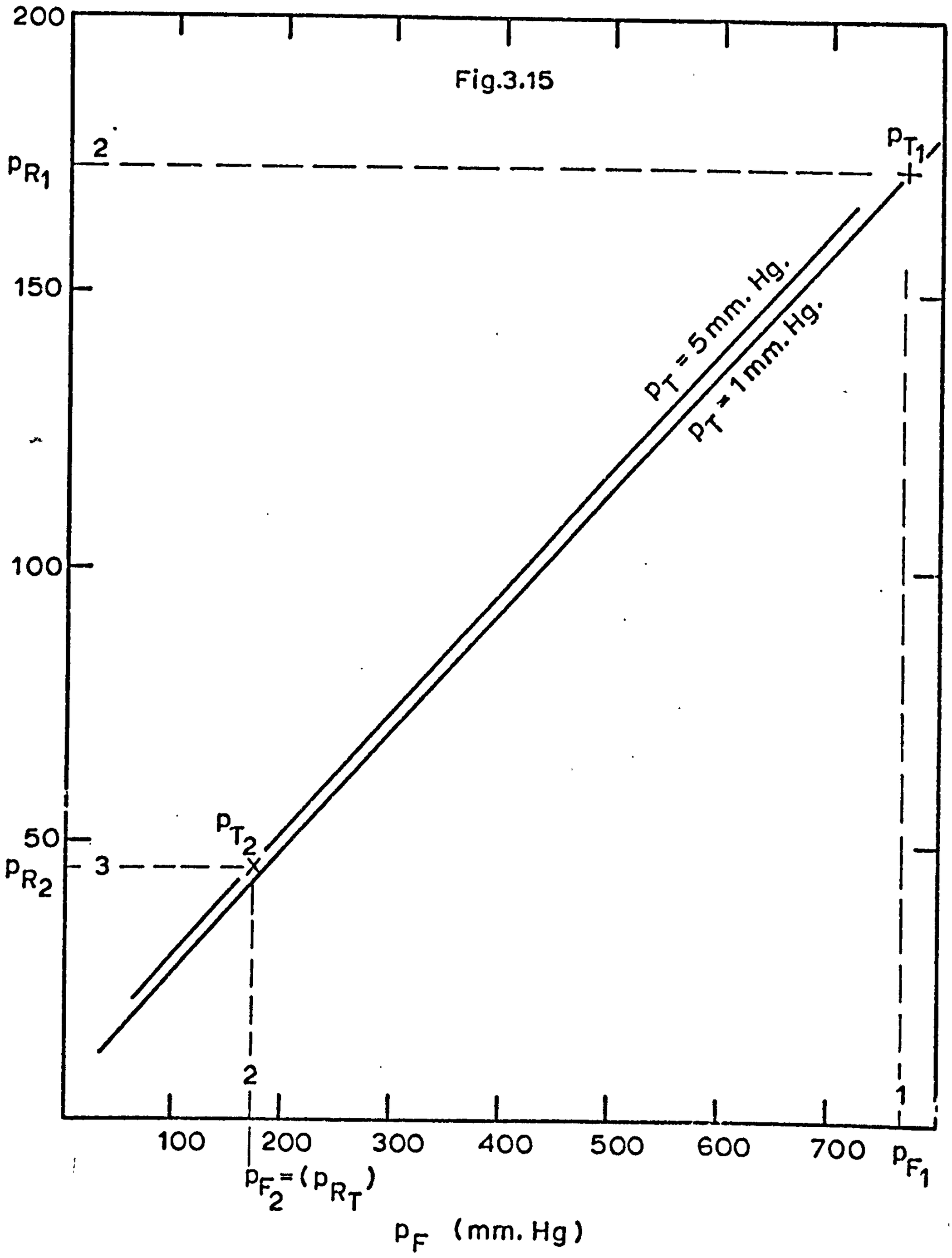
The apparatus used for the experiments on reaction of slags with ferrosilicon is schematically represented in Figure 3.19. It was a modified version of the apparatus described in Section 3.3.1 (Figure 3.17). The magnesium vapour was condensed on a water-cooled copper finger which was introduced into the furnace tube. A constant temperature zone 18 cm long was obtained as shown in Figure 3.19.

3.4.2 Experimental procedure

The preparation and the heating cycle were similar to those described in Section 3.3.2. The furnace was heated under slightly positive pressure of argon up to 1510 - 1520 C (temperature of the hot chamber). The pressure in the furnace was reduced to the required level after the temperature had become stable. The set value of pressure was maintained for a certain period of time after which the pressure of argon was restored. The furnace was cooled

Figure 3.15 - Typical example of procedure for obtaining a required pressure, p_{R2} = 45 mm Hg, in the furnace, starting from p_{F1} = 770 mm Hg

Fig.3.15


200
150
100
50
p_{R_1}
p_{R_2}
2
3
p_{T_1}
p_{T_2}
p_T = 5 mm. Hg.
p_T = 1 mm. Hg.
p_R (mm. Hg)
2
1
100
200
300
400
500
600
700
$p_{F_2} = (p_{R_T})$
p_{F_1}
p_F (mm. Hg)

to room temperature and the deposit was collected and analysed by mass spectrometry.

Figure 3.16 - Calibration curve of the pressure transducer.

Excitation voltage = 18.00 $\pm$ 0.01 Volts d.c..

p (mm Hg) = 18.868 E (mV) + 96.00

Fig.3.16

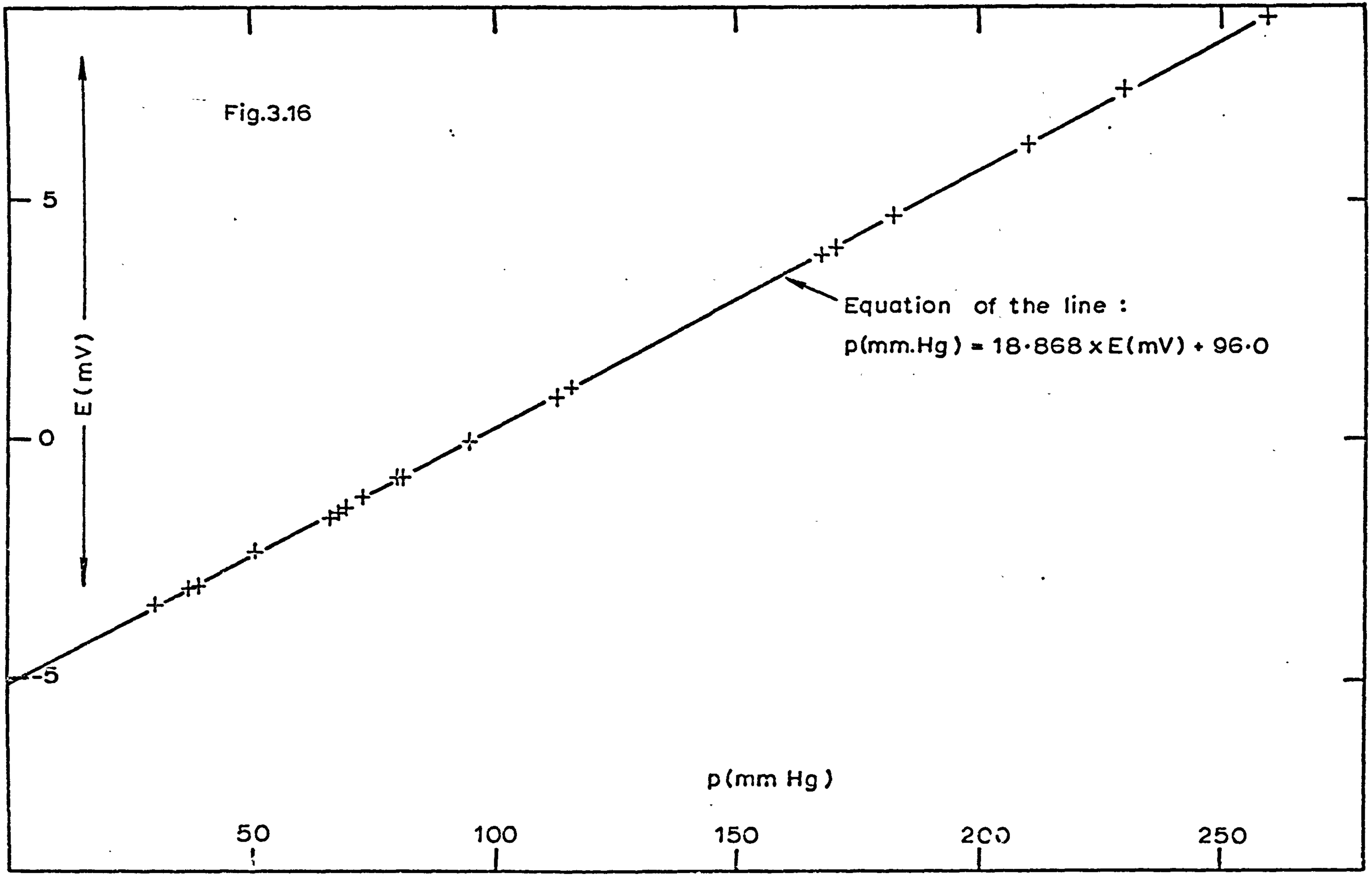

E (mV)
5
0
-5
Equation of the line :
p(mm.Hg) = 18·868 x E(mV) + 96·0
p (mm Hg)
50
100
150
200
250

Figure 3.17 - Schematic diagram of the apparatus used for visual observation of the surface of the slag/metal metl. Scale: 1/9.4

[1]furnace; [2] top seal; [3] bottom seal; [4] crucible; [5] graphite vessel; [6] alumina pedestal; [7] silica window and prism; [8] water-cooled copper coil; [9] thermocouple (Pt/Pt - 13% Rh)

(see page 102)

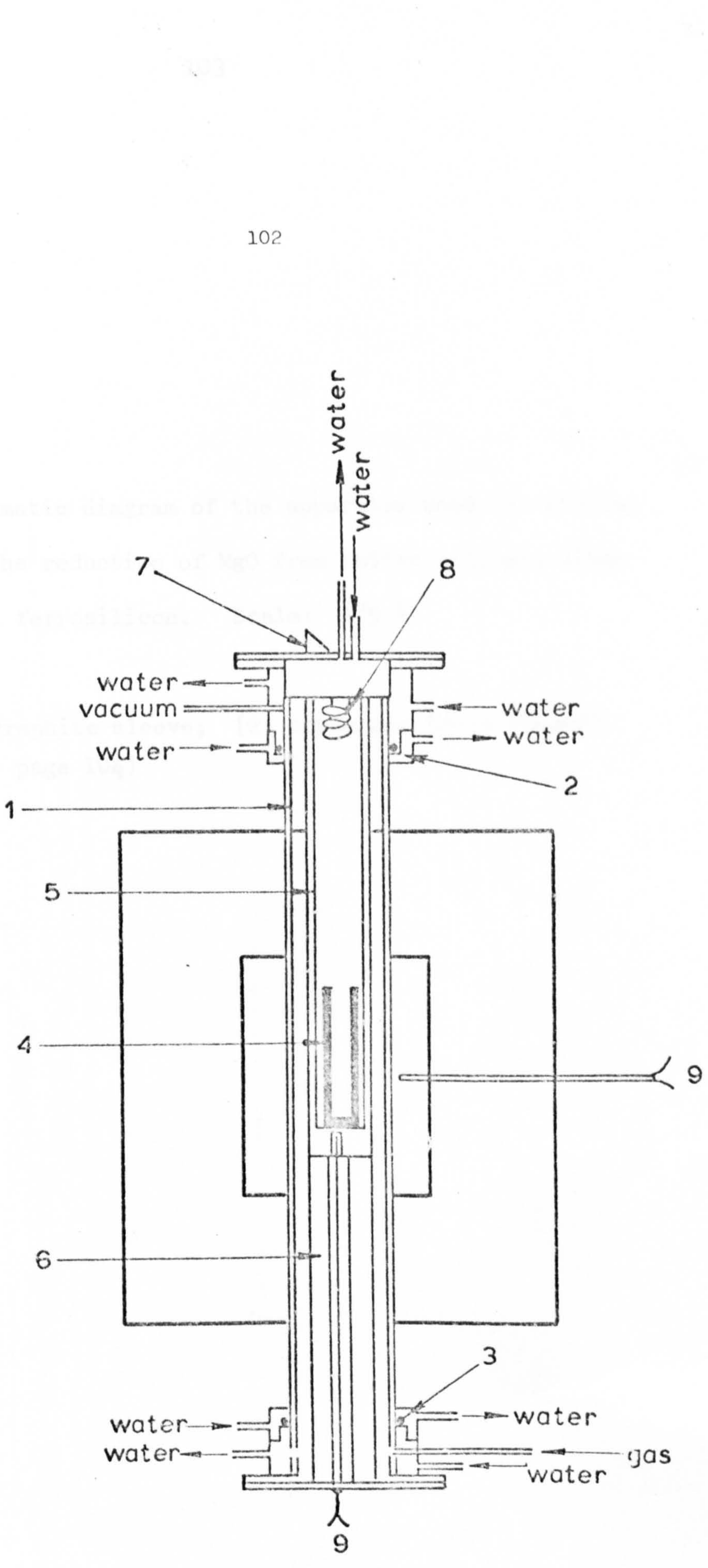

water
7
8
water
vacuum
water
water
water
2
1
5
4
9
6
3
water
water
water
gas
water
9

Fig.3.17

Figure 3.19 - Schematic diagram of the apparatus used for studies on the reduction of MgO from molten silicate slags with ferrosilicon. Scale: 1/9.4.

[1] graphite sleeve; [2] condenser (cold finger)

(see page 104)

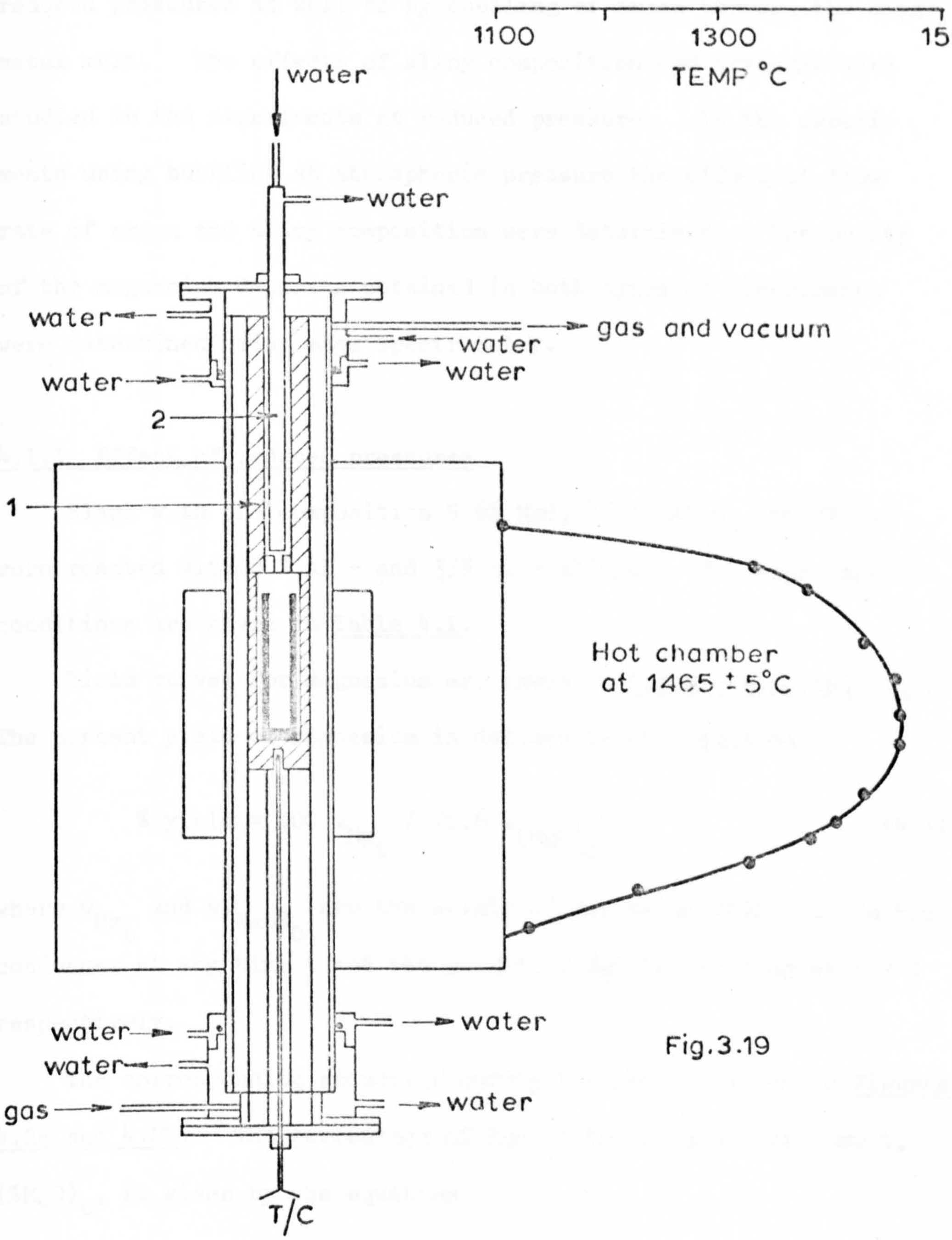

1100
1300
1500
TEMP °C
water
water
water
water
gas and vacuum
water
water
2
1
Hot chamber
at 1465 ± 5°C
water
water
gas
water
water
T/C

Fig.3.19

CHAPTER 4

RESULTS

4.1 REDUCTION OF MOLTEN $MgO-Al_2O_3-CaO$ SLAGS WITH FERROALUMINIUM

Rates of evolution and yields of magnesium were measured for the reaction of molten $MgO-Al_2O_3-CaO$ slags with ferroaluminium at reduced pressures as well as by bubbling of argon through the slag/metal melt. The effects of alloy composition and pressure were studied in the experiments at reduced pressure. In the experiments using bubbling at atmospheric pressure the effect of flow rate of argon and alloy composition were determined. The purity of the magnesium deposits obtained in both types of experiments were determined using mass spectrometry.

4.1.1 Effect of reduced pressures

Slags with the composition 5.6% MgO, 48.1% Al_2O_3, 46.3% CaO were reacted with 80% Al - and 35% Al - alloys. The experimental conditions are given in Table 4.1.

Yield curves for magnesium are shown in Figures 4.1a and 4.1b. The percent yield of magnesium is defined by the equation

$$\% \text{ yield} = 100\ w_{Mg_t} / [0.6\ w_{(MgO)_0}] \qquad (4.1)$$

where w_{Mg_t} and $w_{(MgO)_0}$ are the weight of magnesium collected in the condenser at any time t and the weight of MgO in the slag at t = 0 respectively.

The corresponding reduction curves for MgO are shown in Figures 4.2a and 4.2b. The percentage of MgO in the slag at any time t, $(\%MgO)_t$, is given by the equation

$$(\%MgO)_t = 100\ w_{(MgO)_t} / w_{(slag)_t} \qquad (4.2)$$

Table 4.1

Reduction of the 5.6% MgO - 48.1% Al_2O_3 - 46.3% CaO slag with Fe-80% Al (series A) and with Fe-35% Al (series B) at reduced pressures

Alloy (% Al)	Experiment	Temperature of the hot chamber (°C)	Temperature of the crucible (°C)	Pressure (mm Hg)	Weight of slag (g)	Weight of metal (g)	Slag/metal ratio	Diameter of the crucible (mm)
80	A-1	1495	1440	30	75.18	33.77	2.23	41.0
80	A-2	1483	1423	38	75.62	34.85	2.17	42.5
80	A-3	1495	1440	45	74.74	34.40	2.17	44.5
80	A-4	1506	1450	49	75.03	39.81	1.88	43.5
80	A-5	1470	1410	50	176.00	35.96	4.89	43.0
80	A-6	1503	1446	63	75.38	35.24	2.14	43.0
35	B-1	1510	1450	28	50.00	43.76	1.14	42.5
35	B-2	1513	1460	39	52.51	45.96	1.14	43.5

Figure 4.1a - Effect of reduced pressure on the yield of magnesium.

80% Al-alloy. 1435 C.

Experiment	Pressure (mm Hg)	Slag/metal (vol.)
A-1	30	2.8
A-2	38	2.8
A-3	45	2.8
A-4	49	2.4
A-5	50	6.2
A-6	63	2.7

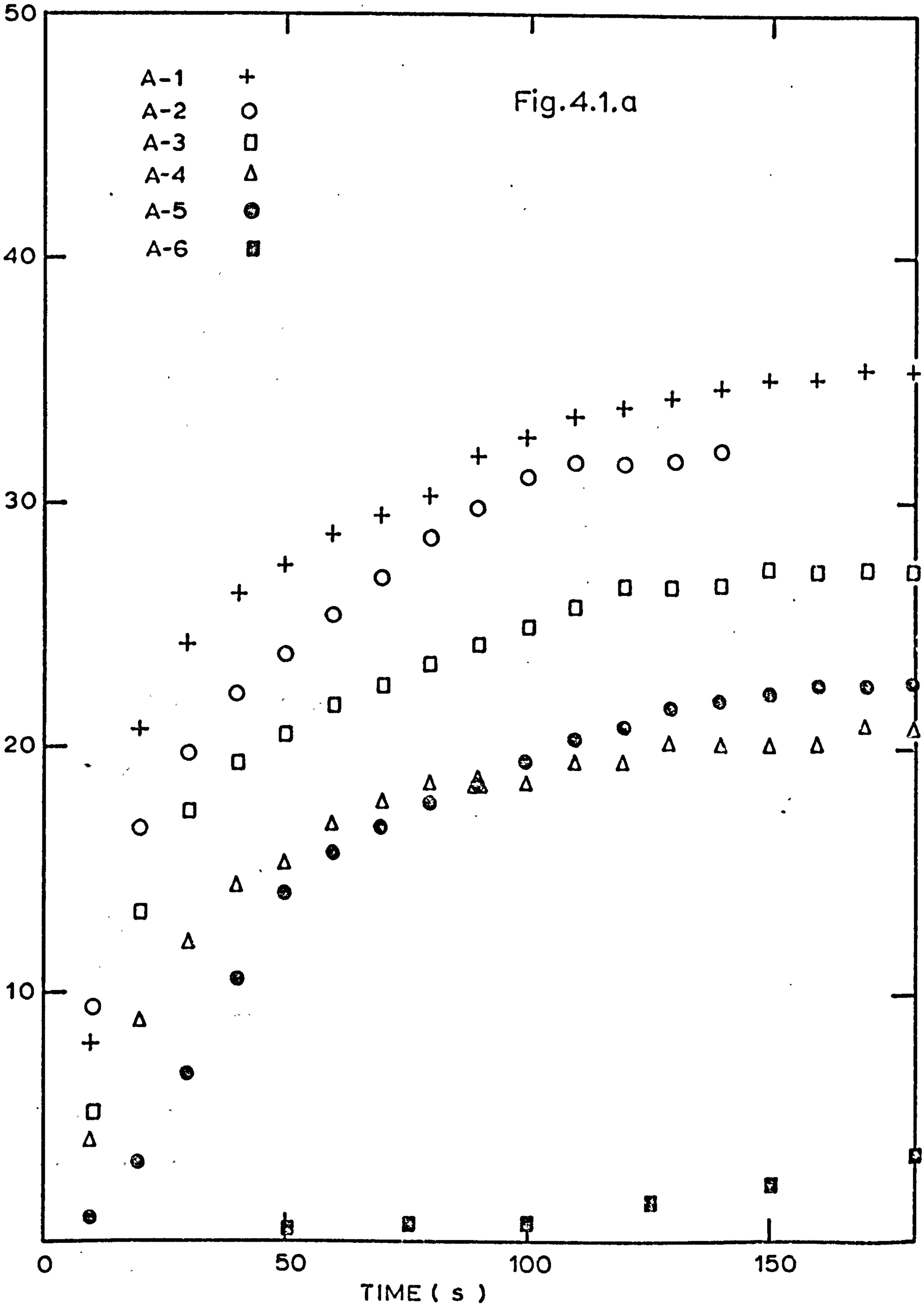

A-1 +
A-2 O
A-3 □
A-4 Δ
A-5 ●
A-6 ■
MAGNESIUM YIELD (%)
50
40
30
20
10
0
50
100
150
TIME (s)

Fig.4.1.a

The weight of MgO present in the slag is related to w_{Mg_t} by

$$w_{(MgO)_t} = w_{(MgO)_0} - 1.666\ w_{Mg_t} \qquad (4.3)$$

Equation (4.3) is based on the stoichiometry of reaction (2.18).

The weight of slag at any time t is given by

$$w_{(slag)_t} = w_{(MgO)_t} + w_{(Al_2O_3)_t} + w_{(CaO)_t} \qquad (4.4)$$

From the discussion presented in Sections 2.1.2.2, 2.1.2.3 and 2.1.2.7 it is reasonable to assume that alumina and lime did not take part in any side reaction so that, according to reaction (2.18), the weight of Al_2O_3 in the slag can be expressed as function of w_{Mg_t} by the equation

$$w_{(Al_2O_3)_t} = w_{(Al_2O_3)_0} + 1.416\ w_{Mg_t}\ . \qquad (4.5)$$

The weight of CaO at any time t is given by

$$w_{(CaO)_t} = w_{(CaO)_0} \qquad (4.6)$$

It will be evident from Figures 4.1 and 4.2 that the final yield of magnesium decreased as the operating pressure increased and that the rate of reduction of MgO increased as the pressure was reduced below the equilibrium value. The curves also show that at a given pressure the rate decreased with depletion of MgO. Comparison between results from experiments A-4 and A-5, for which the values of slag/metal volumetric ratio were 2.4 and 6.2 respectively, indicate that this experimental parameter did not affect significantly the final yield of magnesium at 49-50 mm Hg pressure. At a given operating pressure, rates of evolution of magnesium were found to be higher for reduction with 80% Al-alloy than with 35% Al-alloy.

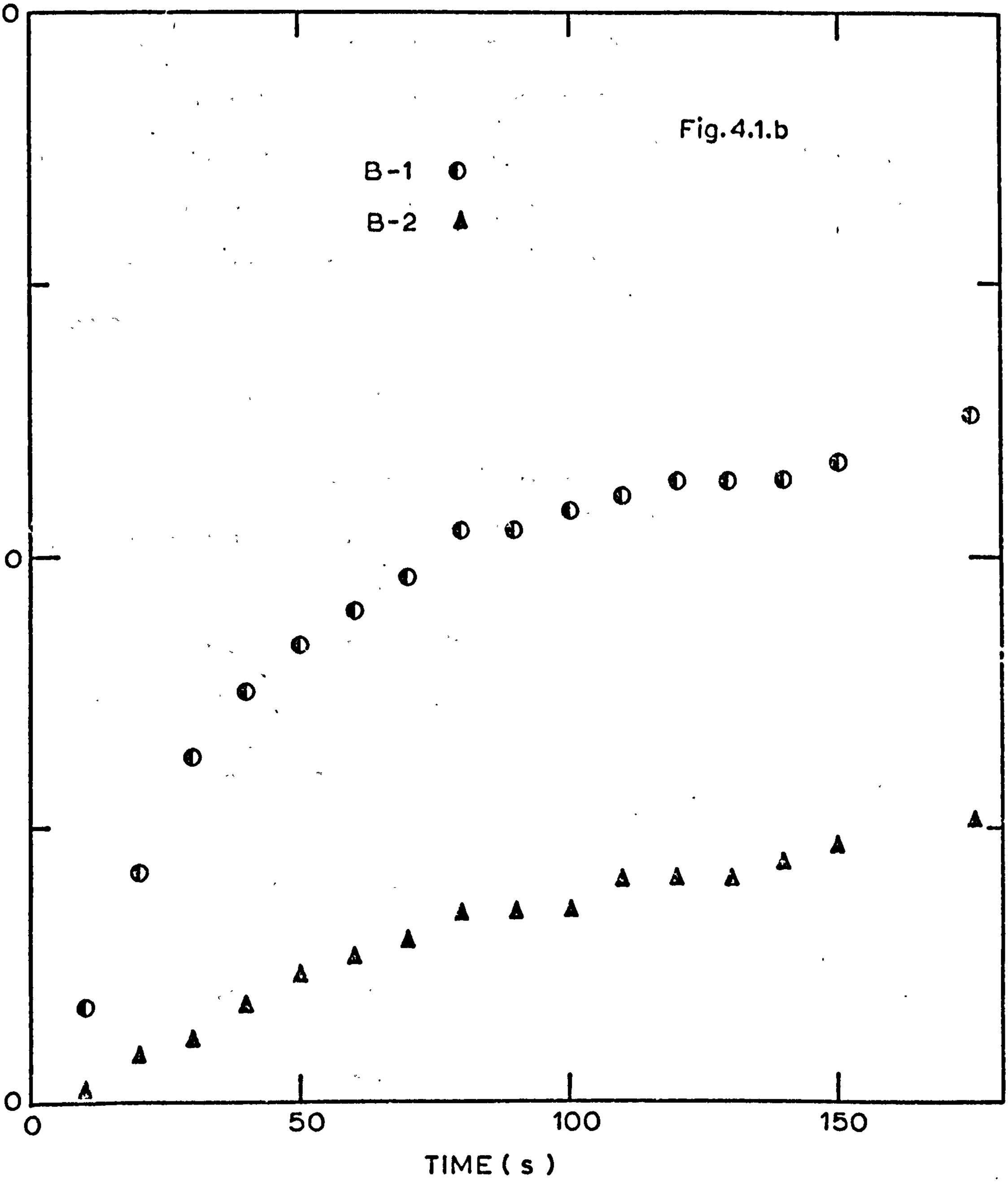
The equilibrium vapour pressure of magnesium at the slag/metal

Figure 4.1b - Effect of reduced pressure on the yield of magnesium.

35% Al-alloy. 1460 C.

Experiment	Pressure (mm Hg)	Slag/metal (vol.)
B-1	28	2.4
B-2	39	2.4

Fig. 4.1.b



interface for the reduction of MgO will vary with the concentration of MgO in the slag (see equation (2.20)). Consequently the equilibrium pressure will decrease as the yield of magnesium increases (Figure 2.4). Values for the concentration of MgO which are in equilibrium with the reducing alloy at a certain temperature and at a given value of the operating pressure correspond to points on the reduction curves (Figures 4.2a and 4.2b) at which rate equals zero. Assuming that the rate is proportional to the driving force expressed in terms of concentration differences, the rate equation becomes

$$V\, dC/dt = -k\, A\, (C - C_{eq}) \qquad (4.7)$$

where C is the concentration of the reacting species, C_{eq} is the equilibrium value for C, A is the interfacial reaction area, V is the volume of the phase in which the reacting species is present and k is the mass transfer coefficient of the reacting species.

Integration of equation (4.7) gives

$$\int_{C_0}^{C_t} dC/(C - C_{eq}) = -\int_{0}^{t} k\, (A/V)\, dt \qquad (4.8)$$

$$\ell n[(C_t - C_{eq})/(C_0 - C_{eq})] = -k\, (A/V)t \qquad (4.9)$$

or

$$\log[(C_t - C_{eq})/(C_0 - C_{eq})] = -Kt \qquad (4.10)$$

If weight percentages of MgO are used, equation (4.10) becomes

$$y = \log\{[(\%MgO)_t - (\%MgO)_{eq}]/[(\%MgO)_0 - (\%MgO)_{eq}]\} = -Kt \qquad (4.11)$$

Straight lines of the form $y = -Kt$ were satisfactorily fitted to the experimental points as shown in Figures 4.3a and 4.3b. The standard deviation σ_y was less than 0.34 in all cases. The product moment correlation coefficient r. for variables y and t, was in the

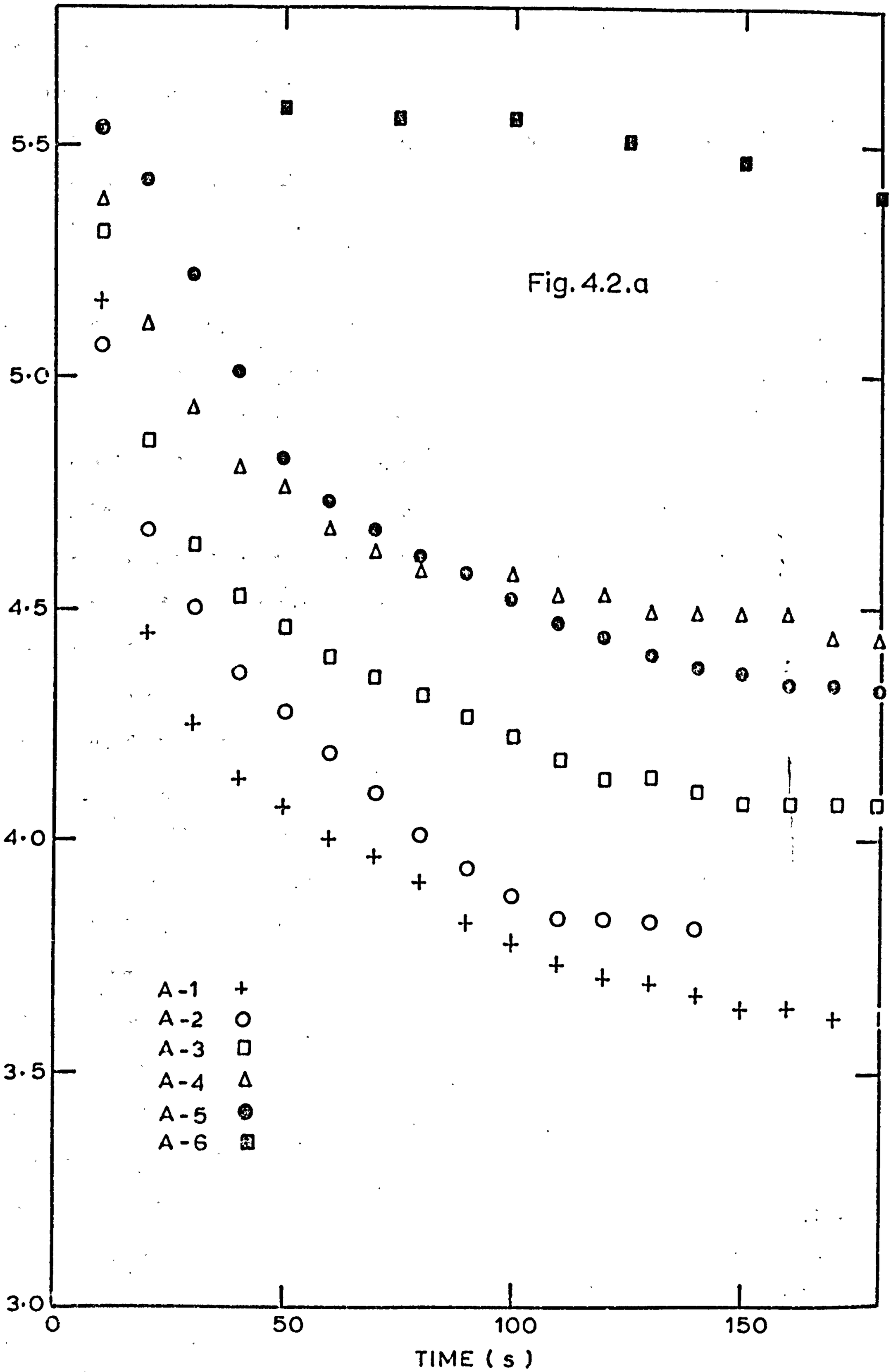

WT. % MgO IN SLAG
5·5
5·0
4·5
4·0
3·5
3·0
0
50
100
150
TIME (s)
A-1 +
A-2 O
A-3 □
A-4 Δ
A-5 ●
A-6 ■

Fig. 4.2.a

range $-1 < r < -0.97$ with an average value of -0.995 for series A and B. However, some deviation from linearity was observed particularly for times less than 10 seconds from the start, mainly due to the uncertainty regarding the exact instant at which the reaction started. In fact, the average time lag for obtaining the required pressure in the reaction chamber was 19.2 seconds (standard deviation = 5.0 seconds). During this interval the reaction could have started as soon as the pressure at the reaction interface had fallen below the equilibrium value. For example, for experiment A-2, the time required for the pressure in the reaction tube to drop from 113 mm Hg (p_{R_1}) to 38 mm Hg (p_{R_2}) was 23.5 seconds as determined from Figure 4.4. Examination of the curve of Figure 4.4 shows that the reaction would have proceeded for 20 seconds before the final operating pressure (38 mm Hg) was reached. It will be evident from Figure 4.4 that the level of operating pressure was constant and that no sudden increase of pressure due to generation of magnesium vapour was observed.

Table 4.2 gives values of the constant K (defined by equation 4.11) for the various experiments. It will be seen that in general the magnitude of K was higher for 80% Al-alloy than for 35% Al-alloy. A correlation between the constant K and operating pressure, in the range 28 - 50 mm Hg, was not evident, although the initial rates of reduction were higher at reduced pressures.

Photographs of cross-sections of crucibles containing the frozen melt after the reaction has taken place appear in Figures 4.5 - 4.8. Figures 4.5 and 4.6 show the results when the melt contained slag and the 80% Al-alloy, which reacted at 30 mm Hg and at 63 mm Hg respectively. Figures 4.7 and 4.8 are for the reaction with the 35% Al-alloy at 28 mm Hg and at 39 mm Hg respectively. It will be seen that with the 80% Al-alloy a fine dispersion of metal droplets in the slag phase was produced, whereas a continuous slag/metal interface could be distinguished

Figure 4.2b - Effect of reduced pressure on the reduction of MgO.

35% Al-alloy. 1460 C.

Experiment	Pressure (mm Hg)	Slag/metal (Vol.)
B-1	28	2.4
B-2	39	2.4

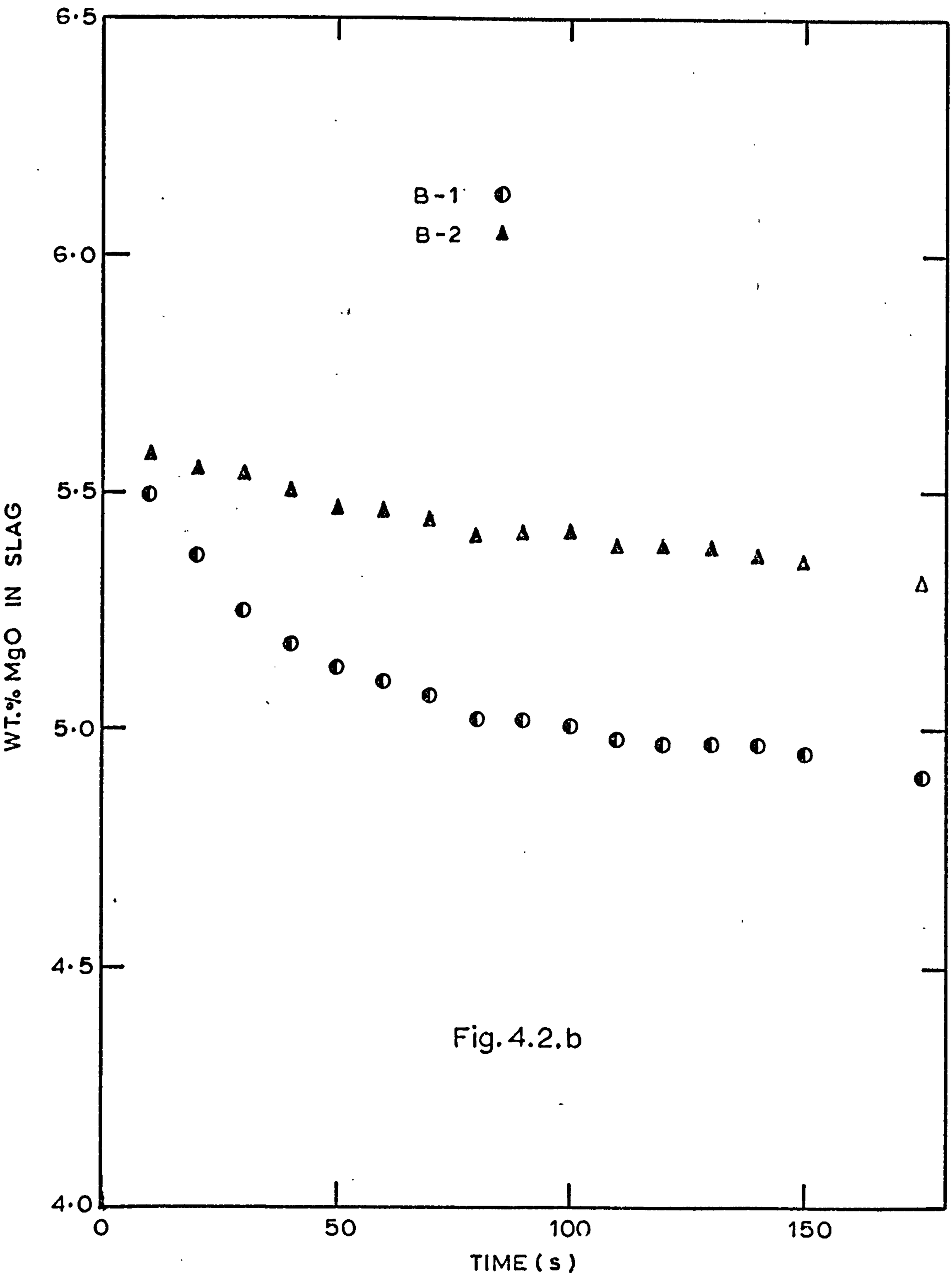


Fig. 4.2.b

Table 4.2

Values of the constant K (defined by equation 4.11) for various experiments

Experiment	Alloy (wt % Al)	Operating pressure (mm Hg)	Slag/metal volumetric ratio	V slag (cm^3)	K (s^{-1})	k A ($cm^3\ s^{-1}$)
A-1	80	30	2.8	25.9	8.28×10^{-3}	0.494
A-2	80	38	2.8	26.1	12.70×10^{-3}	0.763
A-3	80	45	2.8	25.8	8.66×10^{-3}	0.515
A-4	80	49	2.4	25.9	11.57×10^{-3}	0.690
A-5	80	50	6.2	60.7	8.83×10^{-3}	1.234
A-6	80	63	2.7	26.0	0.71×10^{-3}	0.043
B-1	35	28	2.4	17.2	3.40×10^{-3}	0.135
B-2	35	39	2.4	18.1	3.04×10^{-3}	0.127

Figure 4.3a - Semi-log plot of

$$y = \log \{[(\%MgO)_t - (\%MgO)_{eq}]/[(\%MgO)_0 - (\%MgO)_{eq}]\} = - Kt.$$

80% Al-alloy. 1435 C.

Experiment	Pressure (mm Hg)	Slag/metal (vol.)	Slope of the linear portion	r*
A-1	30	2.8	- 0.00828	-0.990
A-2	38	2.8	- 0.0127C	-0.976
A-3	45	2.8	- 0.00866t	-0.995
A-4	49	2.4	- 0.01157t	-1.000
A-5	50	6.2	- 0.00883	-0.993
A-6	63	2.7	- 0.00071t	-0.989

* r = product moment correlation coefficient =

$$= (1/n)\ \Sigma\{[(t - \bar{t})/\sigma_t]\ [(y - \bar{y})/\sigma_y]\} \quad , \text{where:}$$

n = number of experimental points (t,y)

σ_t, σ_y = standard deviation for variables t and y respectively;

$\bar{t}, \bar{y}$ = arithmetic mean of all the t values and y values respectively.

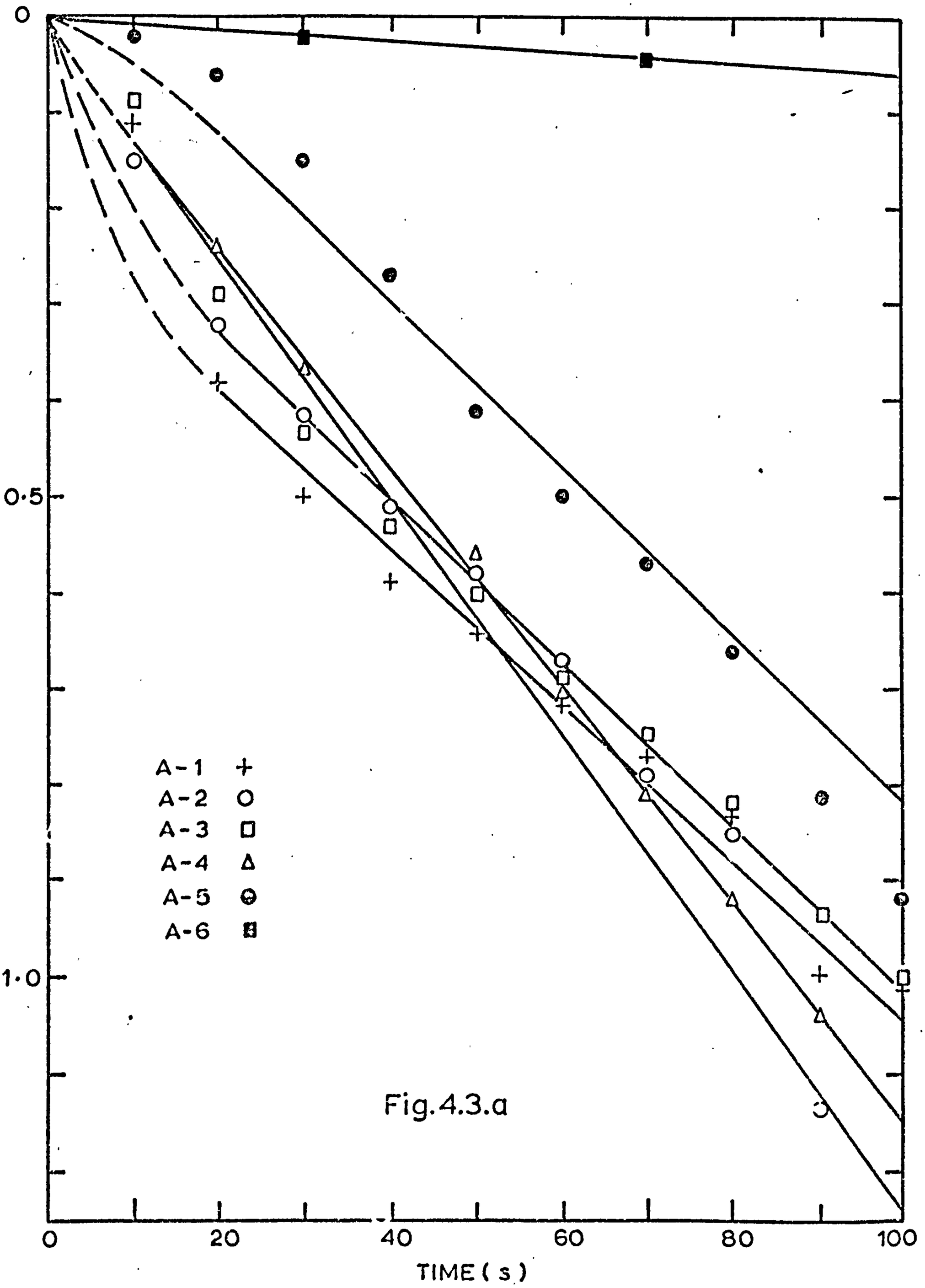


Fig.4.3.a

with the 35% Al-alloy. Droplets of the 80% Al-alloy trapped in the slag are shown in Figure 4.9. They were dense and the absence of magnesium in them was confirmed by mass spectrometry. As the operating pressure decreased the slag/metal dispersion expanded as shown in Figure 4.10.

The magnesium produced was quite pure. The composition of samples of the collected deposits determined by mass spectrometry are given as the three first results in Table 4.3. When 80% Al-alloy was used the deposits were contaminated with sodium and potassium. Chlorine, fluorine and calcium were found in all samples. Aluminium was not detected in the deposit produced with the 35% Al-alloy.

4.1.2 Pressure at which magnesium vapour boiled off the slag/metal melt

The results of the experiments on visual observation of the melt surface at reduced pressures, described in Section 3.3, are summarized in Table 4.4. It was found that, at 1480 ± 20 C, the reduction of MgO produced violent boiling. With the 80% Al-alloy evolution of magnesium bubbles was observed to commence at pressures less than 70 ± 5 mm Hg, whereas with the 35% Al-alloy bubbles were observed at less than 50 ± 5 mm Hg. In both cases the frequency of bubbles increased markedly with the decrease in pressure. Bubbles were released from the centre of the melt as well as from the regions close to the walls, at the melt/crucible line. From visual observations the bubbles appeared to be 1 - 5 mm diameter.

Figure 4.11 shows that the final yield of magnesium decreased linearly as the operating pressure increased. The values for the operating pressure below which magnesium starts to be produced, estimated by extrapolating the straight lines to zero yield, were 78 mm Hg and 47 mm Hg for the 80% Al-alloy and the 35% Al-alloy respectively. Comparison with Table 4.4 shows that these pressures

Figure 4.3b - Semi-log plot of

$$y = \log \{[(\%MgO)_t - (\%MgO)_{eq}]/[(\%MgO)_0 - (\%MgO)_{eq}]\} = - Kt.$$

35% Al-alloy. 1460 C.

Experiment	Pressure (mm Hg)	Slag/metal (vol.)	Slope of the linear portion	r*
B-1	28	2.4	- 0.00340	-0.97
B-2	39	2.4	- 0.00304	-0.970

* r = product moment correlation coefficient

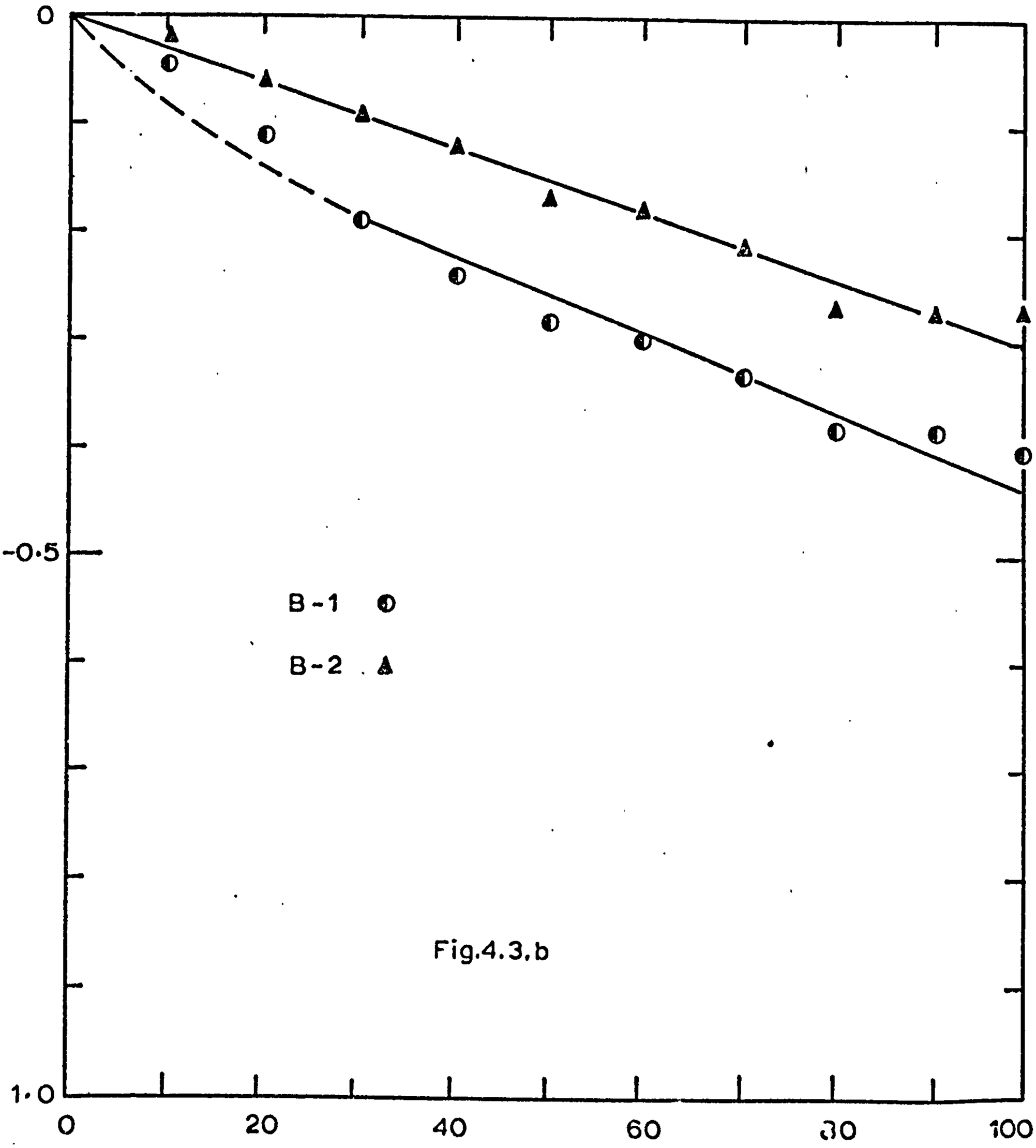


Fig.4.3.b

Table 4.3

Composition of the magnesium deposits obtained

Sample	Reducing alloy (wt % Al)	Pressure (mm Hg)	Atomic - percent						
			Mg	Ca	K	Cl	Al	Na	F
1	80	30	98.769	0.009	0.052	0.008	0.415	0.741	0.006
2	35	28	99.993	0.003	-	0.003	-	-	0.001
3	80	49	99.854	0.002	0.009	0.002	0.002	0.130	0.001
4	80	atm*	98.676	0.247	0.306	0.109	-	0.661	0.001

* argon flow rate = 1376 ml min^{-1} STP

Figure 4.4 - Pressure drop from 113 mm Hg to 38 mm Hg (experiment A-2). Speed of the chart = 120 mm min^{-1}. Voltage scale for the output of the pressure transducer = 0.1 mV per division (zero of the chart at 60 %).

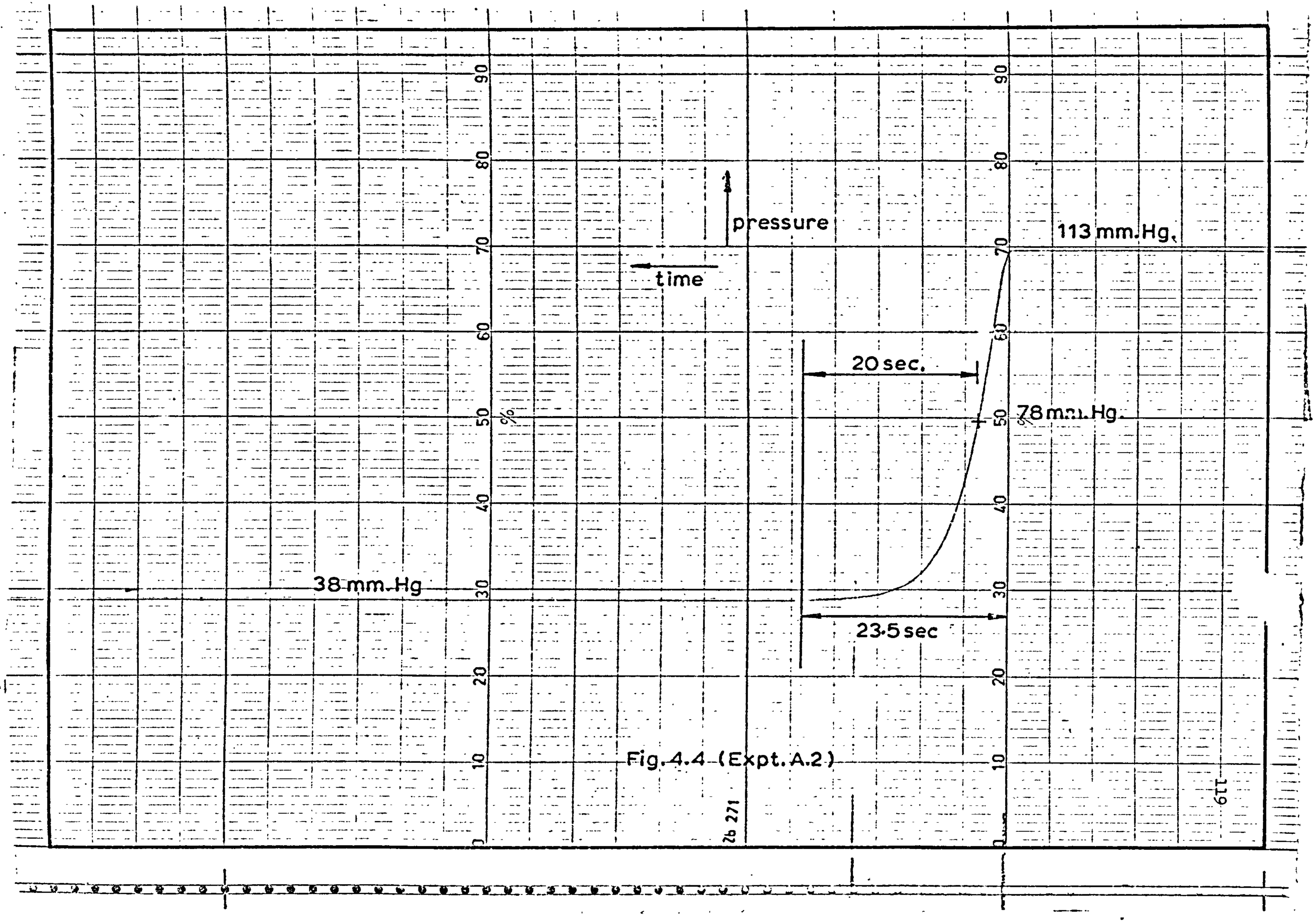


Fig. 4.4 (Expt. A.2)

are in good agreement with those at which magnesium vapour was observed to boil off the slag/metal melt.

4.1.3 The effect of argon flow rate

Experiments on the reduction of molten $MgO-Al_2O_3-CaO$ slags with Fe-80% Al and Fe-35% Al were carried out in which argon was bubbled at atmospheric pressure through the slag/metal melt at various flow rates. The experimental conditions are given in Table 4.5.

Yield curves for magnesium are shown in Figures 4.12a and 4.12b and the corresponding reduction curves for MgO are shown in Figures 4.13a and 4.13b. It will be evident from these curves that it was possible to recover magnesium from slags by bubbling argon at atmospheric pressure through the melt although the rate was much lower than that obtained at reduced pressures.

A correlation between the rate of reduction and gas flow rate, in the range 1040 - 2040 $ml.min^{-1}$ (STP), was not evident, although higher rates were obtained with the 35% Al-alloy. The reduction curves clearly show that in general the rate decreased with the depletion of MgO in the slag.

With bubbling of argon, magnesium vapour could be removed only from the sites where the partial pressure was lower than the equilibrium value, that is, at locations where slag, metal and gas meet. Figure 4.14 shows a photograph of a cross-sectioned crucible containing the frozen melt of slag and 80% Al-alloy after the reaction has taken place. The gas lance was not removed from the melt and a section of its immersed part may be seen in the photograph. In some experiments the evolution of magnesium ceased prematurely for no apparent reason. In these cases the metal phase may have been pushed away from the zone at which the gas was delivered, so that

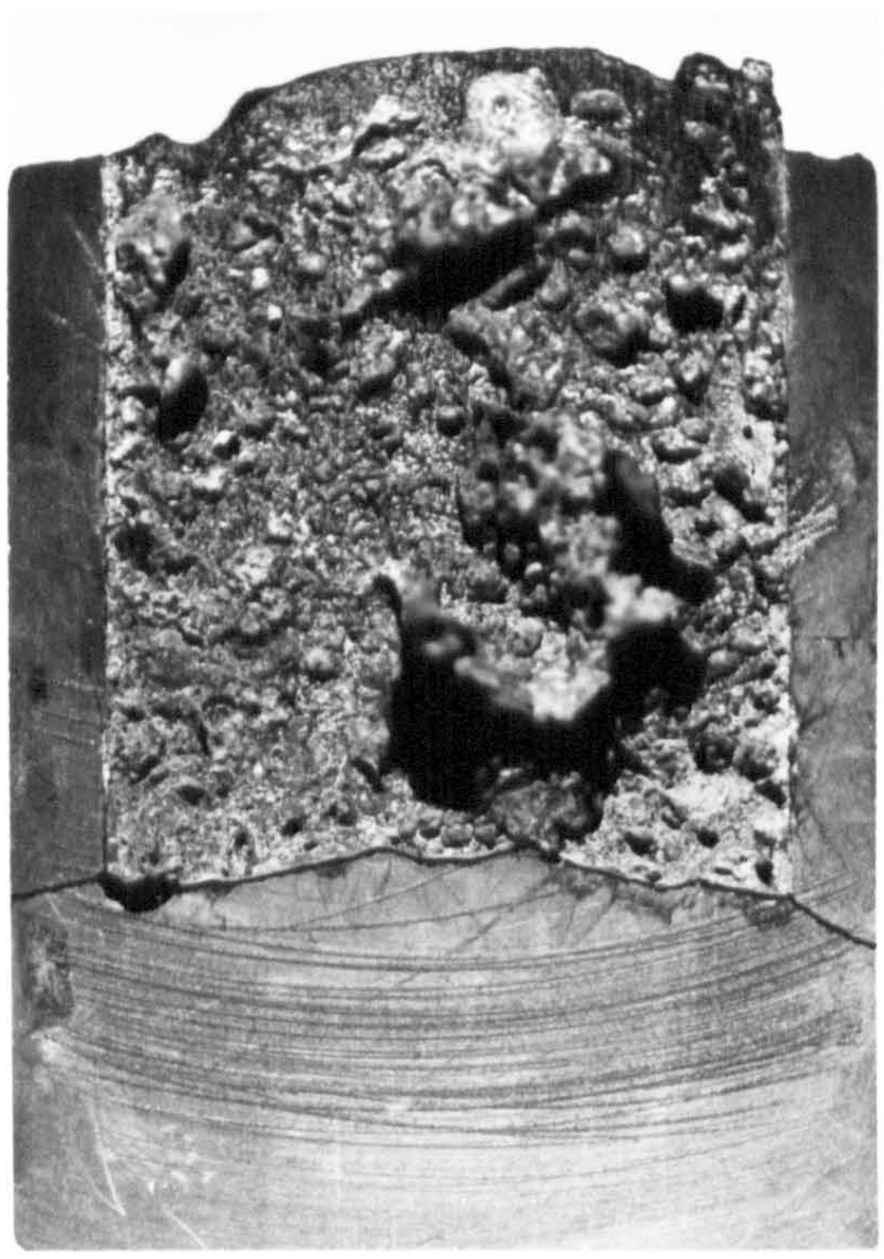
Figure 4.5 - Frozen melt (80% Al-alloy, 30 mm Hg pressure).
Fine dispersion of metal in the slag was produced.

Figure 4.6 - Frozen melt (80% Al-alloy, 63 mm Hg pressure).
The expansion of the melt, due to foaming caused by the evolution of magnesium vapour, did not occur because the operating pressure was near the pressure at which boiling of $Mg_{(g)}$ commenced.

Figure 4.7 - Frozen melt (35% Al-alloy, 28 mm Hg pressure).
The metal phase existed as a distinct layer below the slag. Gas-cavities resulted from rapid cooling of the viscous melt.

Figure 4.8 - Frozen melt (35% Al-alloy, 39 mm Hg pressure).
The flat surface of the melt resulted from the low rate of evolution of magnesium.

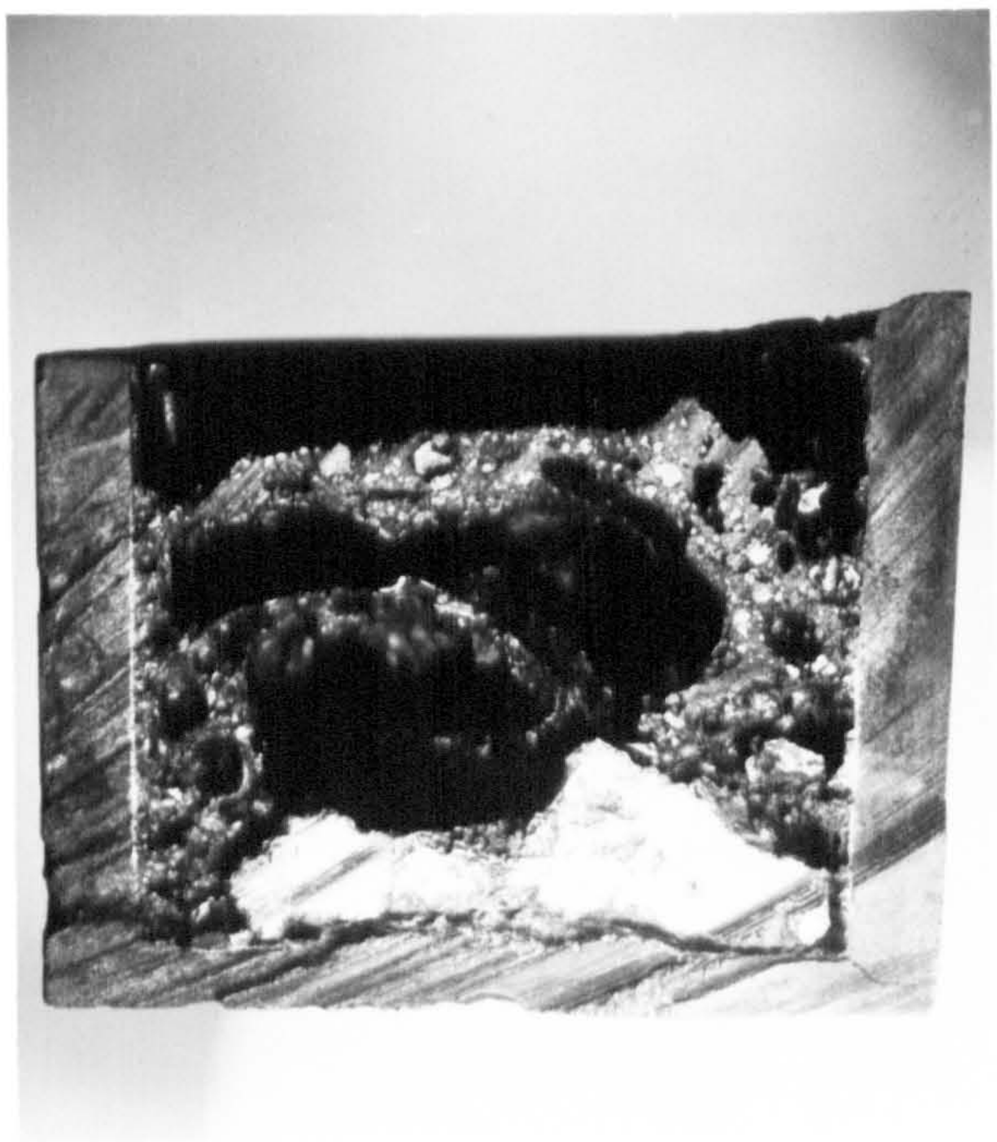
4.5



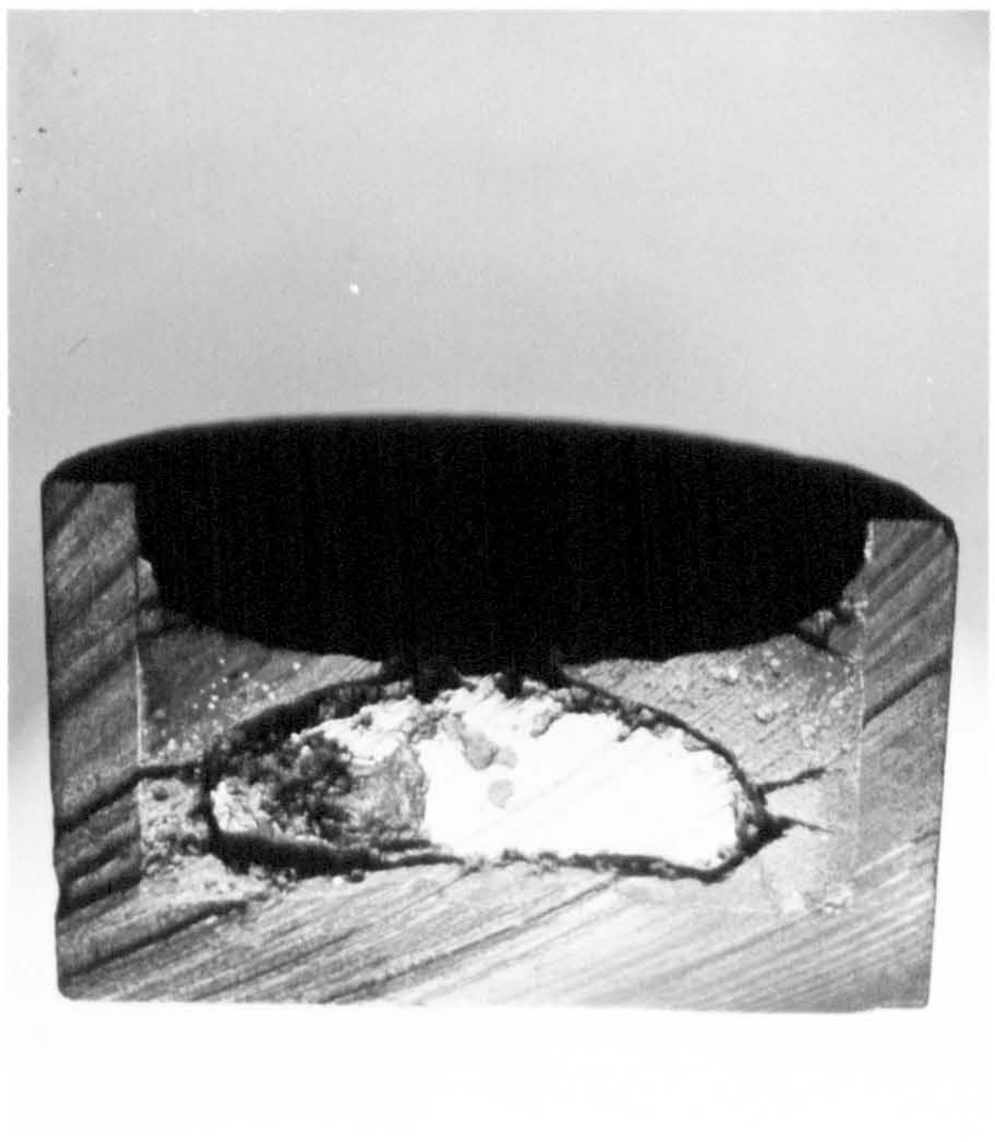
4.6



4.7



4.8



argon bubbles ascended to the surface of the melt without contacting slag/metal interfaces. In view of the uncertainty regarding the behaviour of the bubbles and the effective interfacial areas, a precise analysis of the results, which were subjected to a large amount of scatter, was not possible.

[illegible] ion with [illegible]

The composition of a sample of magnesium produced by the bubbling method is given as Sample 4 in Table 4.3. The magnesium produced was quite pure although comparatively more calcium was reduced from the slags at atmospheric pressure than at reduced pressures.

4.2 REDUCTION OF MgO FROM SILICATE SLAGS WITH FERROSILICON

Slags with the compositions

22.0% SiO_2 - 25.0% Al_2O_3 - 43.0% CaO - 10.0% MgO

and 52.0% SiO_2 - 35.3% CaO - 12.7% MgO

were reacted at 1480 ± 20 C and reduced pressures with Fe-75% Si. The recovered deposits were analysed by mass spectrometry and the results are given in Table 4.6.

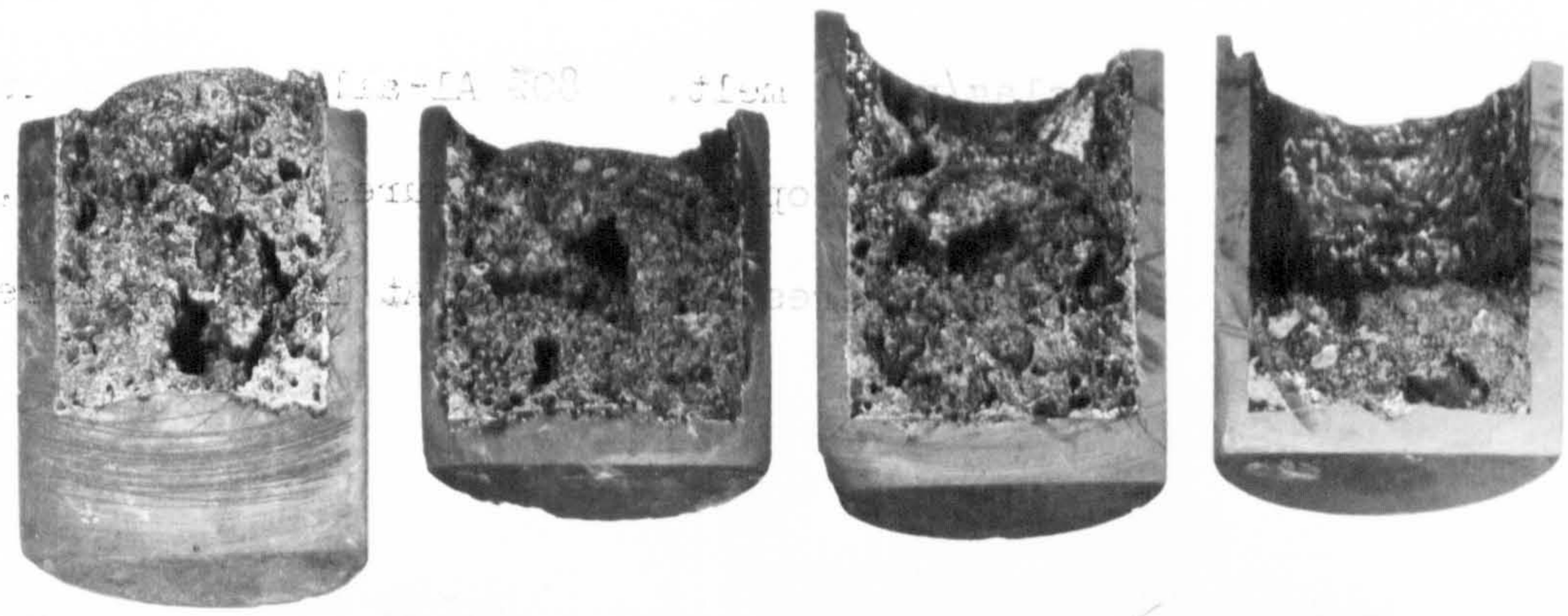
Contamination of the magnesium deposits with silicon and carbon increased with the activity of silica in the slag. Reaction with the quarternary slag (a_{SiO_2} = 0.01) produced purer deposits than with the alumina-free slag (a_{SiO_2} = 0.4). Contamination by calcium was lower for the quarternary slag, at 1 mm Hg pressure, but it was higher when the operating pressure was 11 mm Hg. The increase in pressure seemed to have depressed the evolution of $Mg_{(g)}$ more than that of $SiO_{(g)}$, as the Si/Mg ratio in the analysed deposits increased with operating pressure. The atomic-percentages of C, F, Cl, K, Al, P

Figure 4.10 - Effect of reduced pressure on the expansion of the slag/metal melt. 80% Al-alloy. From left to right the operating pressures were 30, 45, 50 and 63 mm Hg respectively. At lower pressures more expansion was observed.

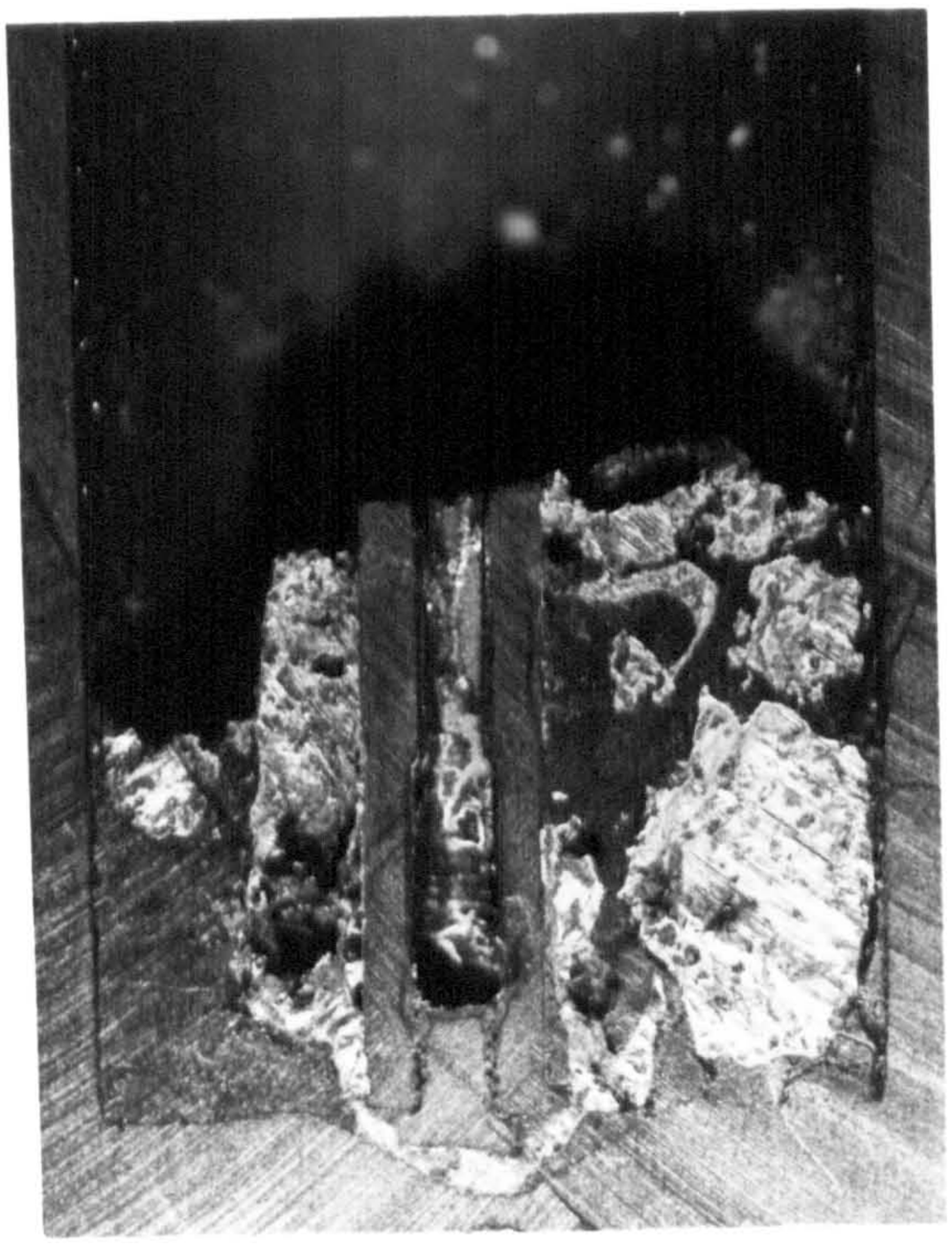
Figure 4.14 - Cross-section of crucible containing slag + metal after bubbling of argon through the melt. 80% Al-alloy. Gas flow rate - 1376 $ml.min^{-1}$ STP (experiment C-4).

Figure 4.9 - Droplets of 80% Al-alloy trapped in the slag. Analysis of the metal phase revealed that no magnesium pick up occurred. Magnification: 2X.

4.10



4.14



4.9

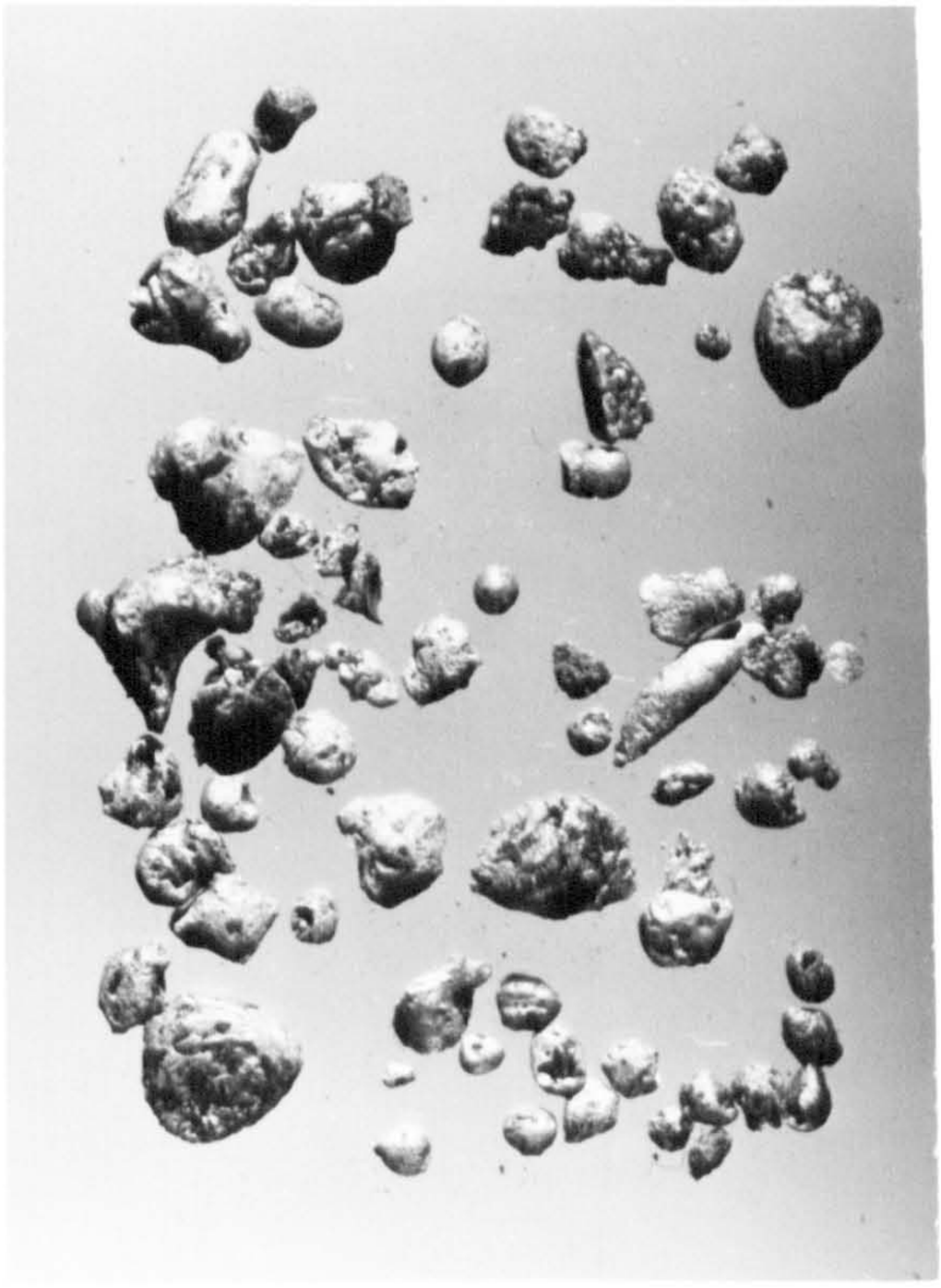


Table 4.4

Summary of observations of the surface of the melt when slag (5.6% MgO - 48.1% Al_2O_3 - 46.3% CaO) was reacted with 80% Al- and 35% Al-alloy at reduced pressures

Alloy (wt % Al)	Temperature (C)	Slag (g)	Metal (g)	Cross section of the crucible (cm^2)	Operating pressure (mm Hg)	Remarks
80	1480	39.00	22.00	18.9	atm - 500	Quiescent surface
					500 - 100	Quiescent surface
					100 - 80	Quiescent surface
					∿ 70	Small bubbles were released from the centre as well as from the edges of the melt
					< 50	Violent boiling occurred at these pressures
35	1480	40.00	36.39	18.9	atm - 50	Quiescent surface
					∿ 50	Small bubbles of magnesium vapour were observed
					< 50	The frequency of bubbles increased markedly

Figure 4.11 - Variation of the final yield of magnesium with pressure. Equation for the straight line fitted to the experimental points of series A:

$Y = - 0.815\ p_{Mg} + 61.8$ (equation 5.10)

r (= product moment correlation coefficient)

= -.0.977

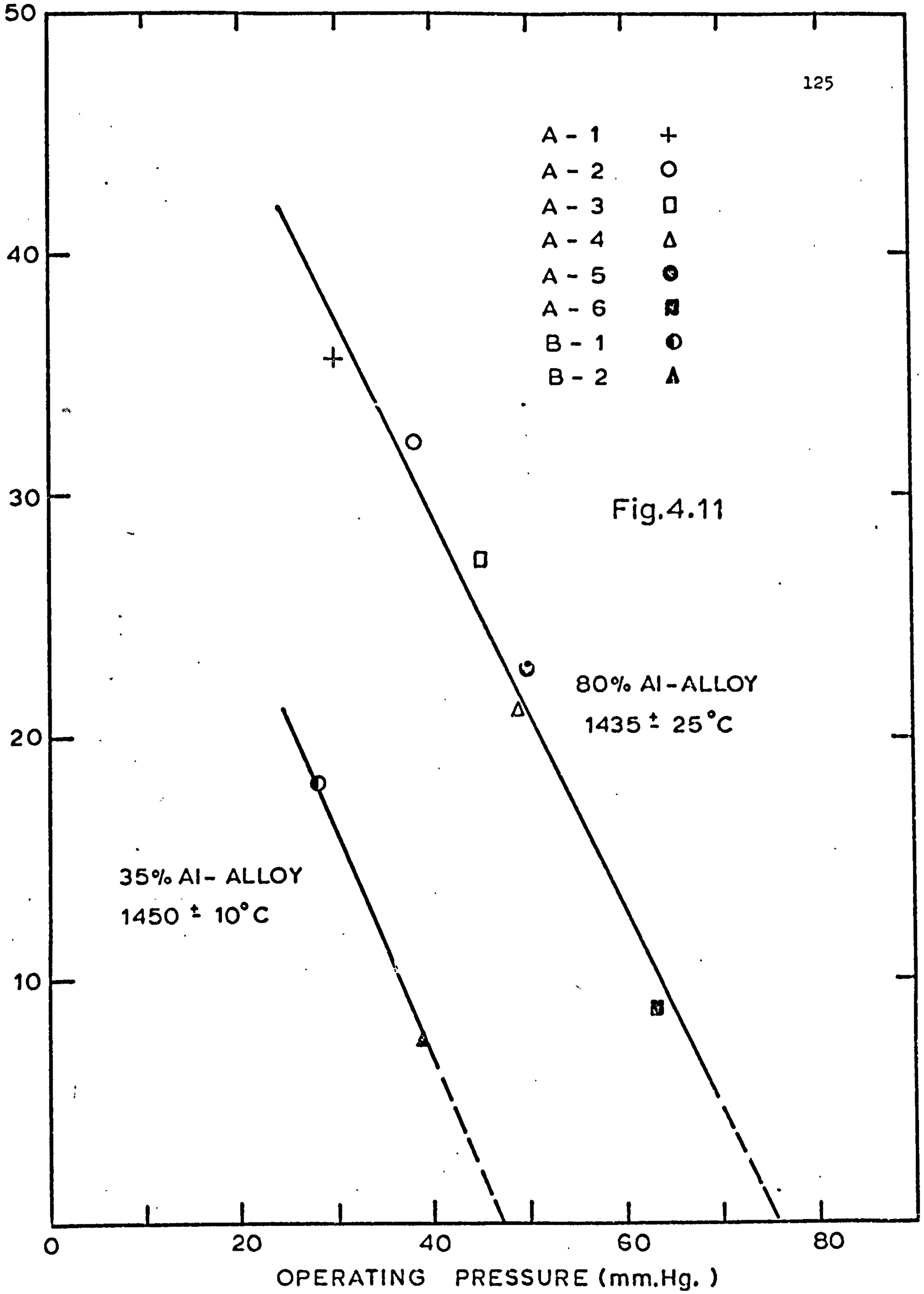

50
40
30
20
10
0
20
40
60
80
125
FINAL MAGNESIUM YIELD (%)
OPERATING PRESSURE (mm.Hg.)
A - 1 +
A - 2 O
A - 3 □
A - 4 Δ
A - 5 ●
A - 6 ■
B - 1 ◐
B - 2 ▲
80% Al-ALLOY
1435 ± 25°C
35% Al- ALLOY
1450 ± 10°C

Fig.4.11

Table 4.5

Reduction of MgO from molten slags with Fe-80% Al (series C) and with Fe-35% Al (series D) at atmospheric pressure with bubbling of argon through the slag/metal melt

	Experiments						
	C-1	C-2	C-3	C-4	C-5	D-1	D-2
Slag composition							
% MgO	5.6	5.6	5.4	5.3	5.6	5.6	5.6
% Al_2O_3	48.1	48.1	48.3	48.4	48.1	48.1	48.1
% CaO	46.3	46.3	46.3	46.3	46.3	46.3	46.3
Alloy composition							
% Al	80	80	80	80	80	35	35
Temperature of the hot chamber (C)	1486	1525	1496	1492	1525	1516	1507
Temperature of the crucible (C)	1427	1473	1440	1435	1473	1460	1453
Argon flow rate (ml min^{-1} STP)	1040	1325	1376	1376	2040	1040	1260
Diameter of the orifices (mm)	3.0	4.0	3.0	3.0	4.0	3.0	3.0
Weight of slag (g)	61.14	75.00	69.30	69.35	70.00	71.11	66.61
Weight of metal (g)	30.00	38.19	33.73	31.31	38.61	43.38	43.38
Slag/metal ratio	2.04	1.96	2.05	2.21	1.81	1.64	1.54
Diameter of the crucible (mm)	43.0	43.0	42.0	45.0	43.0	45.0	42.0

Figure 4.12a - Curves of yield of magnesium versus time for reaction at atmospheric pressure with bubbling of argon through the slag/metal melt. 80% Al-alloy. 1450 C.

Experiment	Argon flow rate ($ml.min^{-1}$. STP)	Slag/metal (vol.)
C-1	1040	2.6
C-2	1325	2.5
C-3	1376	2.6
C-4	1376	2.8
C-5	2040	2.3

Fig.4.12.a

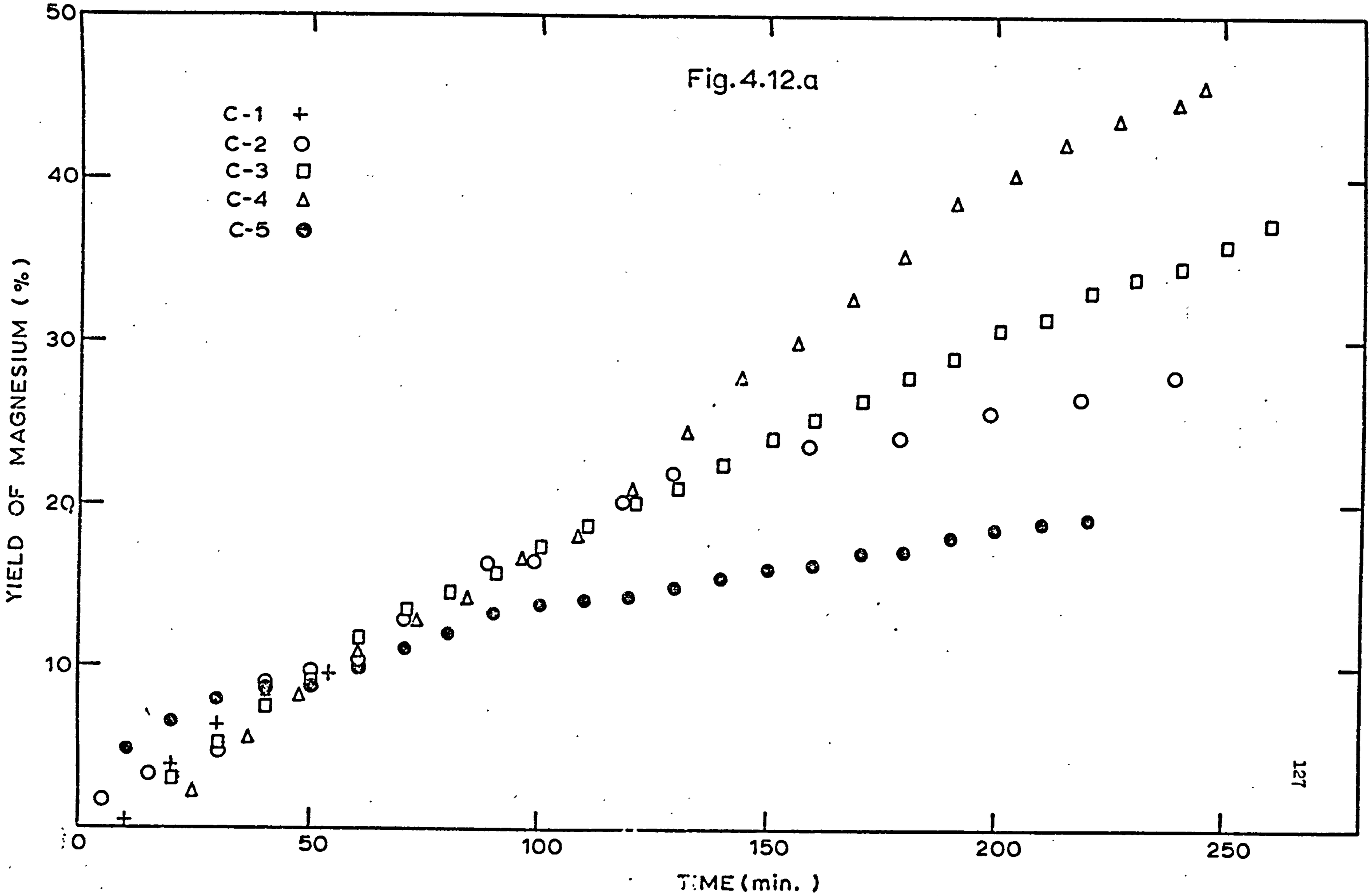

C-1 +
C-2 O
C-3 □
C-4 Δ
C-5 ◉
YIELD OF MAGNESIUM (%)
50
40
30
20
10
0
50
100
150
200
250
TIME (min.)
127

Table 4.6

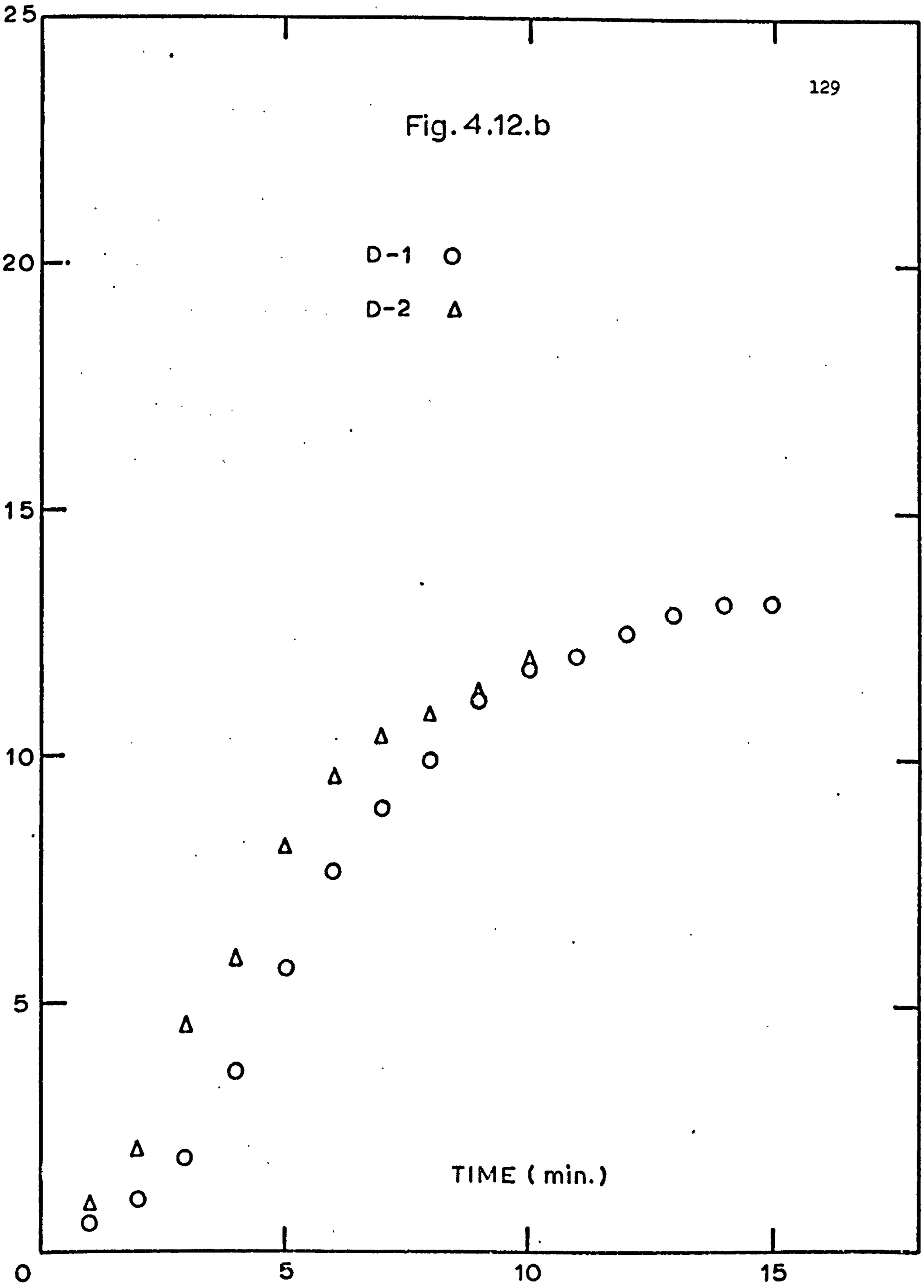
Chemical analysis of the deposits produced when silicate slags were reacted with Fe-75% Si

	Experiments: E-1	E-2	E-3	E-4
Slag composition				
% SiO2	22.0	22.0	52.0	52.0
% MgO	10.0	10.0	12.7	12.7
% Al_2O_3	25.0	25.0	-	-
% CaO	43.0	43.0	35.3	35.3
Weight of slag (g)	15.39	15.44	15.43	15.67
Weight of metal (g)	9.74	9.84	9.78	9.65
Temperature (°C)	1480	1480	1480	1480
Pressure (mm Hg)	1	11	1	11
Time (min)	10	10	10	10
Composition of the deposit (at-pct.)				
Mg	89.96	82.47	77.45	75.64
Si	1.80	9.24	4.96	12.83
C	4.68	1.90	7.75	7.55
Ca	0.18	3.30	6.90	1.29
(F,Cl,Al,K,P,S)	3.38	3.09	2.94	2.69

Figure 4.12b - Curves of yield of magnesium versus time for reaction at atmospheric pressure with bubbling of argon through the slag/metal metl. 35% Al-alloy. 1455 C.

Experiment	Argon flow rate ($ml.min^{-1}$. STP)	Slag/metal (vol.)
D-1	1040	3.4
D-2	1260	3.2

Fig. 4.12.b



and S decreased as the operating pressure increased.

In a preliminary study slags with the compositions:

41.0% SiO_2 - 15.0% Al_2O_3 - 10.0% MgO - 28.0% CaO

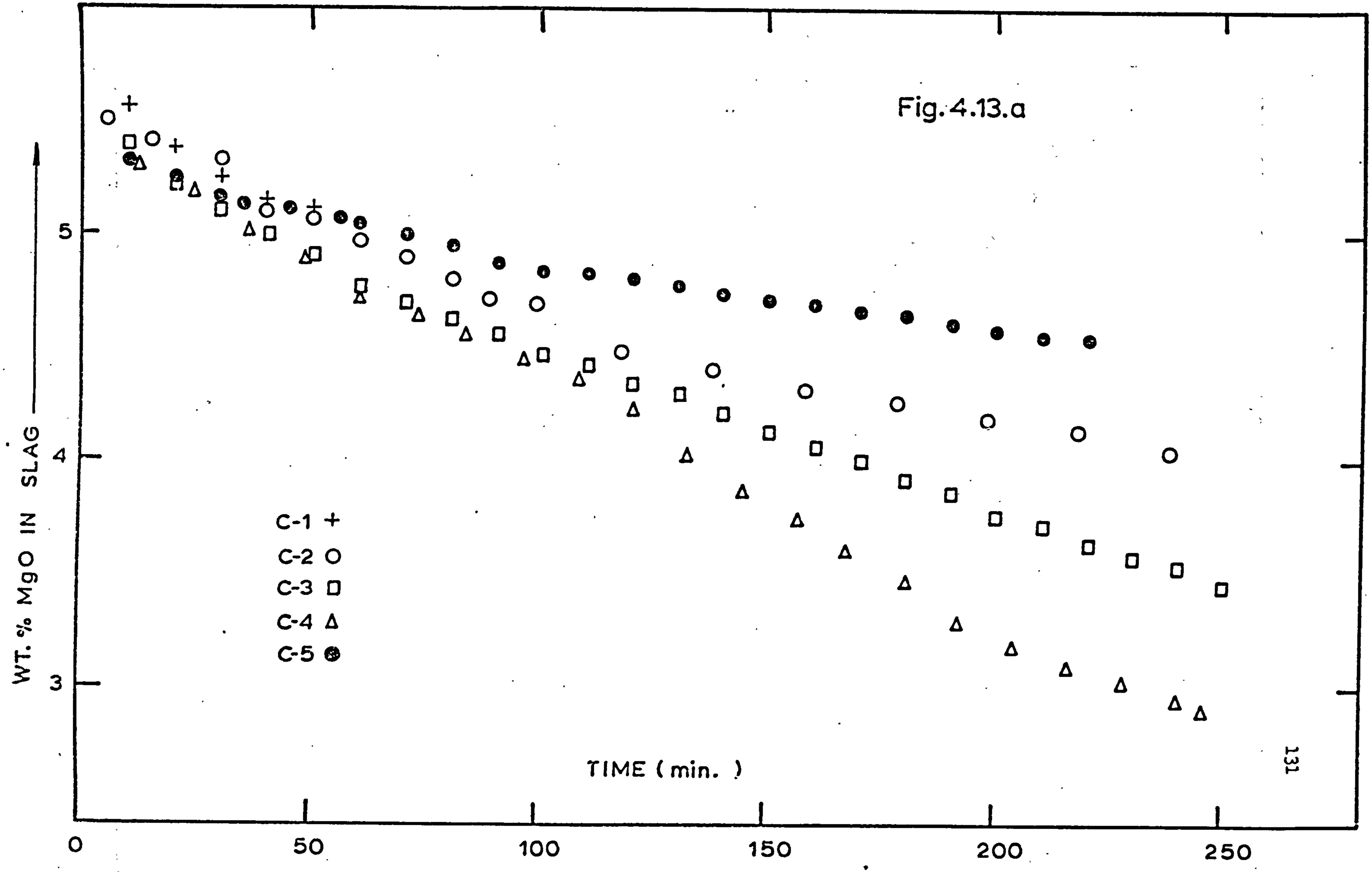
and 22.0% SiO_2 - 25.0% Al_2O_3 - 10.0% MgO - 43.0% CaO

were reacted with Fe-50% Si (at 1450 C, 10 mm Hg pressure, for 4 hours) and with Fe-65% Si (at 1450 C, 2mm Hg pressure, for 3 hours) respectively. In both cases brownish deposits were collected on the surface of the cold finger. X-ray analysis of these deposits revealed that they consisted of forsterite, silica, free silicon and magnesium. Deposits with similar qualitative composition were found by Toguri and Pidgeon[18] for the reduction of solid MgO and calcined dolomite with ferrosilicon at reduced pressures.

Figure 4.13 - Reduction of MgO at atmospheric pressure with bubbling of argon through the slag/metal melt.
(a) 80% Al-alloy. 1450 C (series C)
(b) 35% Al-alloy. 1455 C (series D)

Experiment	Argon flow rate ($ml.min^{-1}$)	Slag/metal (vol.)
C-1	1040	2.6
C-2	1325	2.5
C-3	1376	2.6
C-4	1376	2.8
C-5	2040	2.3
D-1	1040	3.4
D-2	1240	3.2

Fig. 4.13.a



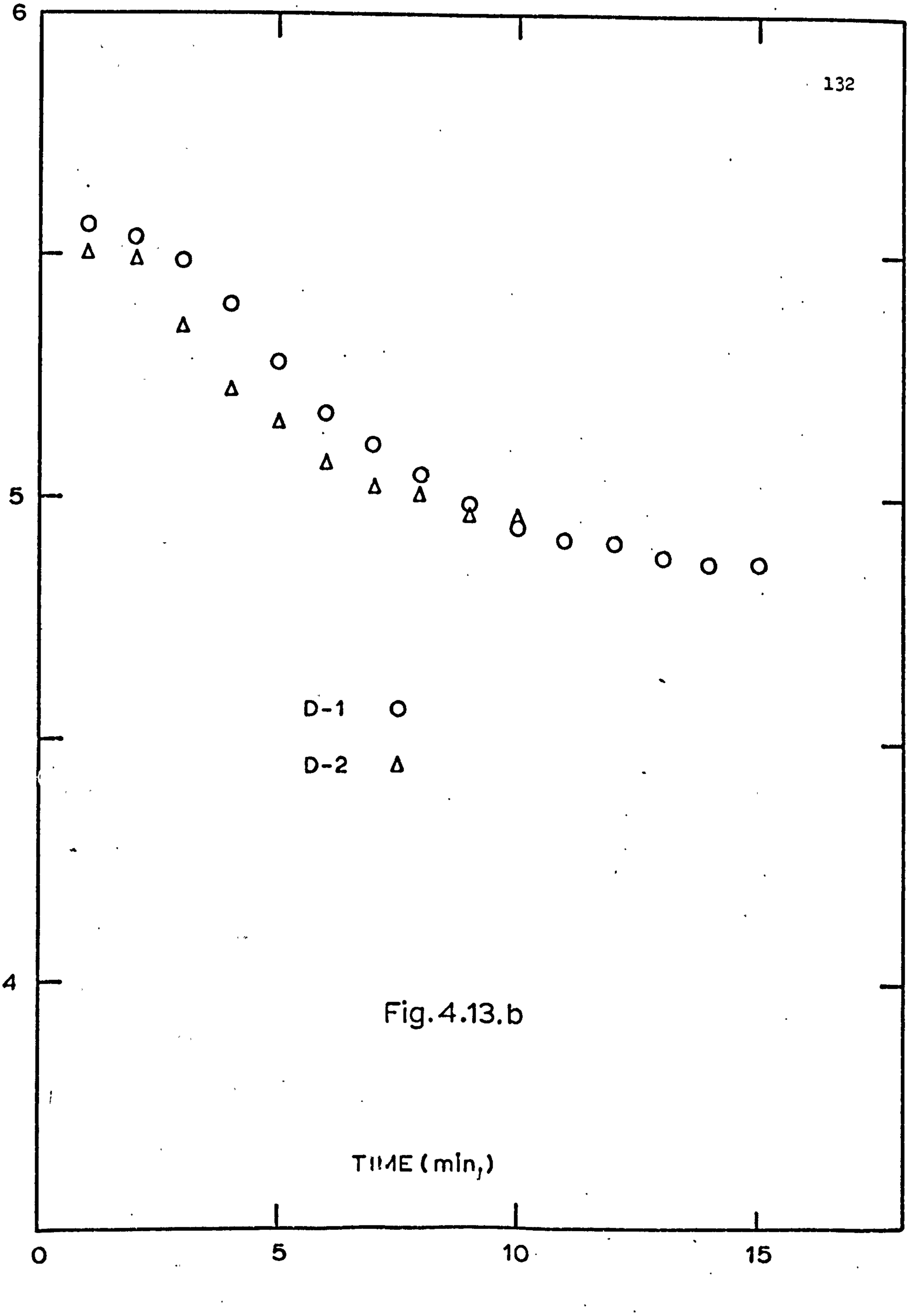


Fig. 4.13.b

CHAPTER 5

DISCUSSION

5.1 REDUCTION OF MgO FROM MOLTEN MgO - Al_2O_3 - CaO SLAGS WITH FERROALUMINIUM

5.1.1 Equilibrium between slag and alloy at reduced pressures

The equilibrium vapour pressure of magnesium for reaction (2.18) is given as function of molar fraction of MgO in the slag by the equation

$$p_{Mg}(atm) = [K(\gamma_{Al}\ x_{Al})^{\frac{2}{3}}(\gamma_{Al_2O_3}\ x_{Al_2O_3})^{-\frac{1}{3}}\gamma_{MgO}]\ x_{MgO} \qquad (5.1)$$

where K is the equilibrium constant, $\gamma_{Al_2O_3}$, γ_{MgO} and γ_{Al} are the activity coefficients of alumina, magnesia and aluminium, x_{MgO}, $x_{Al_2O_3}$ and x_{Al} are the molar fractions of magnesia and alumina in the slag and the atom fraction of aluminium in the alloy respectively.

It will be evident from equation (5.1) that, at a given temperature, a linear correlation between equilibrium vapour pressure of magnesium and molar fraction of magnesia will be valid as long as the term enclosed in square brackets remains constant during the reaction.

The concentration of aluminium in the alloy at any time will depend upon the yield of magnesium, Y,(defined by equation (4.1)) and slag/metal weight ratio, W, at zero time. For the slag and alloys used in the experiments the equations for x_{Al} are:

$$x_{Al} = (0.030 - 9.33 \times 10^{-6}YW)/(0.03357 - 9.33 \times 10^{-6}YW) \qquad (5.2)$$

for the 80% Al-alloy and

$$x_{Al} = (0.013 - 9.33 \times 10^{-6}YW)/(0.0246 - 9.33 \times 10^{-6}YW) \qquad (5.3)$$

for the 35% Al-alloy.

For the range of values of Y and W in the experiments the atom fraction of aluminium calculated from equations (5.2) and (5.3) was virtually constant during the course of reaction. Consequently, the activity of aluminium may be assumed to be constant throughout an experiment.

The concentration of Al_2O_3 in the slag increased as the reaction proceeded and its variation with yield of magnesium is expressed by the equation

$$x_{Al_2O_3} = \frac{(4.716 \times 10^{-3} + 4.66 \times 10^{-6} Y)}{(0.014384 - 9.326 \times 10^{-6} Y)} \qquad (5.4)$$

Since $9.326 \times 10^{-6} Y \ll 0.014384$, equation (5.4) becomes

$$x_{Al_2O_3} = 0.328 + 3.242 \times 10^{-4} Y \qquad (5.5)$$

From equation (5.5) it will be seen that, for the maximum recovery of magnesium achieved in the experiments at reduced pressures (Y = 35.5%), the value of $x_{Al_2O_3}$ increased only by 3.5% (from 0.328 to 0.340). Therefore, activity of alumina probably increased by a certain amount during the reaction. Unfortunately, it appears that activities for ternary melts of the system MgO - CaO - Al_2O_3 have not been determined, so that changes in $a_{Al_2O_3}$ could not be exactly evaluated. Nevertheless, considering the low value of concentration of MgO in the slag ($x_{MgO} = 0.0973$), it is reasonable to sum the concentration of MgO and CaO as a first approximation. It is then interesting to look at the variation of activity of alumina which would have occurred in the appropriate binary melt of CaO and Al_2O_3. Figure 5.1 shows activity curves for lime and alumina in CaO - Al_2O_3 melts at 1500 C relative to solid and liquid CaO and Al_2O_3. Activities relative to liquid CaO and Al_2O_3 have been derived

Figure 5.1 - Activities of Al_2O_3 and CaO in CaO - Al_2O_3 melts at 1500 C

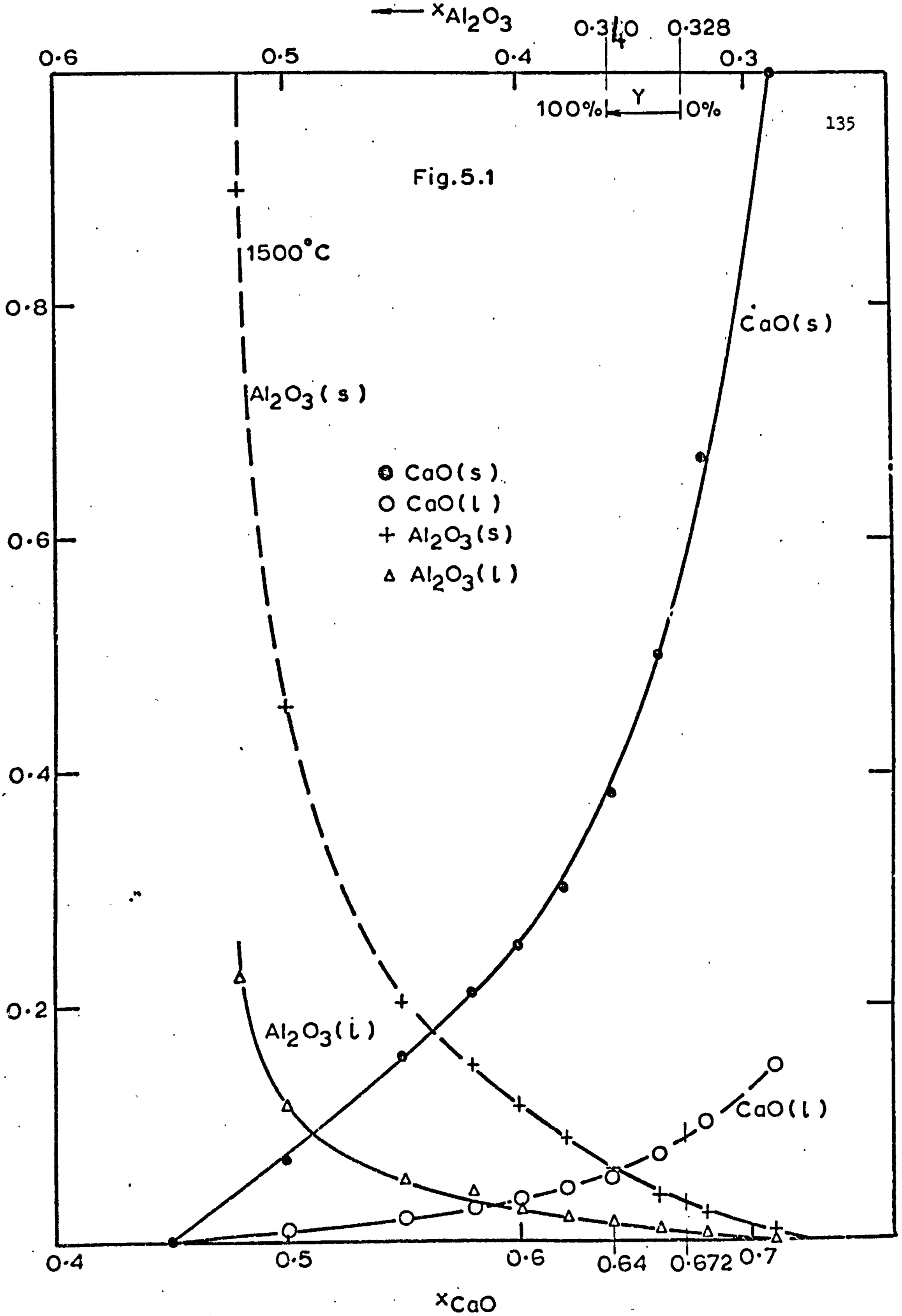

$x_{Al_2O_3}$
0·6
0·5
0·4
0·3
0·310
0·328
100%
Y
0%
1500°C
Al_2O_3(s)
Al_2O_3(l)
CaO(s)
CaO(l)
● CaO(s)
○ CaO(l)
+ Al_2O_3(s)
△ Al_2O_3(l)
activity
0·8
0·6
0·4
0·2
0·4
0·5
0·6
0·64
0·672
0·7
x_{CaO}

Fig.5.1

from equations:

$$RT \ln a_{CaO_{(l)}} = RT \ln a_{CaO_{(s)}} - \Delta G^0_{fus_{CaO}} \qquad (5.6)$$

and

$$RT \ln a_{Al_2O_{3(l)}} = RT \ln a_{Al_2O_{3(s)}} - \Delta G^0_{fus_{CaO}} \qquad (5.7)$$

where $\Delta G^0_{fus_{CaO}}$ and $\Delta G^0_{fus_{Al_2O_3}}$ denote the standard free energies of fusion cf lime and alumina respectively, determined from existing values of the standard free energy of formation of solid and hypothethical liquid CaO and Al_2O_3 at 1500 C. Values of $a_{CaO_{(s)}}$ and $a_{Al_2O_{3(s)}}$ obtained by Sharma and Richardson[61] were used in the calculations. It will be seen from the curves that the activity of alumina would have doubled as $x_{Al_2O_3}$ increased from 0.328 to 0.340.

The molar fraction of magnesia and yield of magnesium are related by the equation

$$x_{MgO} = (1.4 \times 10^{-3} - 1.399 \times 10^{-5}Y)/(0.014384 - 9.326 \times 10^{-6}Y) \qquad (5.8)$$

which may be written as

$$x_{MgO} = 0.0973 - 9.73 \times 10^{-4}Y \qquad (5.9)$$

because $9.326 \times 10^{-6}Y << 0.014384$.

Figure 4.11 shows that the yield of magnesium increased linearly as the pressure decreased. The results with the 80% Al- and the 35% Al-alloy could be correlated by the following equations:-

80% Al-alloy:-

$$Y = -0.815p_{Mg} + 61.8; \quad 30 \leq p_{Mg} \leq 76 \text{ mm Hg} \qquad (5.10)$$

35% Al-alloy:-

$$Y = -0.955p_{Mg} + 44.7; \quad 28 \leq p_{Mg} \leq 47 \text{ mm Hg} \qquad (5.11)$$

The elimination of Y between equations (5.9) and (5.10) gives

$$p_{Mg}(\text{mm Hg}) = 1261.0\, x_{MgO} - 46.9; \quad 30 \leq p_{Mg} \leq 76 \text{ mm Hg}$$

(for the 80% Al-alloy) (5.12)

Similarly, from equations (5.9) and (5.11)

$$p_{Mg}(\text{mm Hg}) = 1076.2\, x_{MgO} - 57.9; \quad 28 \leq p_{Mg} \leq 47 \text{ mm Hg}$$

(for the 35% Al-alloy) (5.13)

Figure 5.2 shows curves of p_{Mg} against x_{MgO} corresponding to equations (5.12) and (5.13). The ratio of slopes of the straight lines is 1.17 which is lower than the corresponding ratio of the activities of aluminium to the two-thirds power. This is probably an indication that $a_{Al_2O_3}$ and γ_{MgO} were not constant so that p_{Mg} is not a genuine linear function of x_{MgO} although the experimental points could be apparently fitted by a straight line in the range of concentrations of MgO considered. In fact, if the behaviour of Al_2O_3 and MgO in the ternary slag were respectively similar to those of Al_2O_3 and CaO in the binary CaO - Al_2O_3 melt, then p_{Mg} would not be a linear function of x_{MgO}. The operating temperatures for the two lines of Figure 5.2 were not the same, however the difference was small so that it would not affect significantly the values of the equilibrium constant K for the reduction reaction (see Figure 2.3).

If γ_{MgO} decreased markedly for $x_{MgO} < 0.061$ so that the activity of MgO approaches zero when x_{MgO} reaches a certain value within the range of concentrations $0 < x_{MgO} < 0.061$, then yield of magnesium equal to 100% can not be achieved. In practice the static pressure

Figure 5.2 - Variation of p_{Mg}(mm Hg) with x_{MgO}

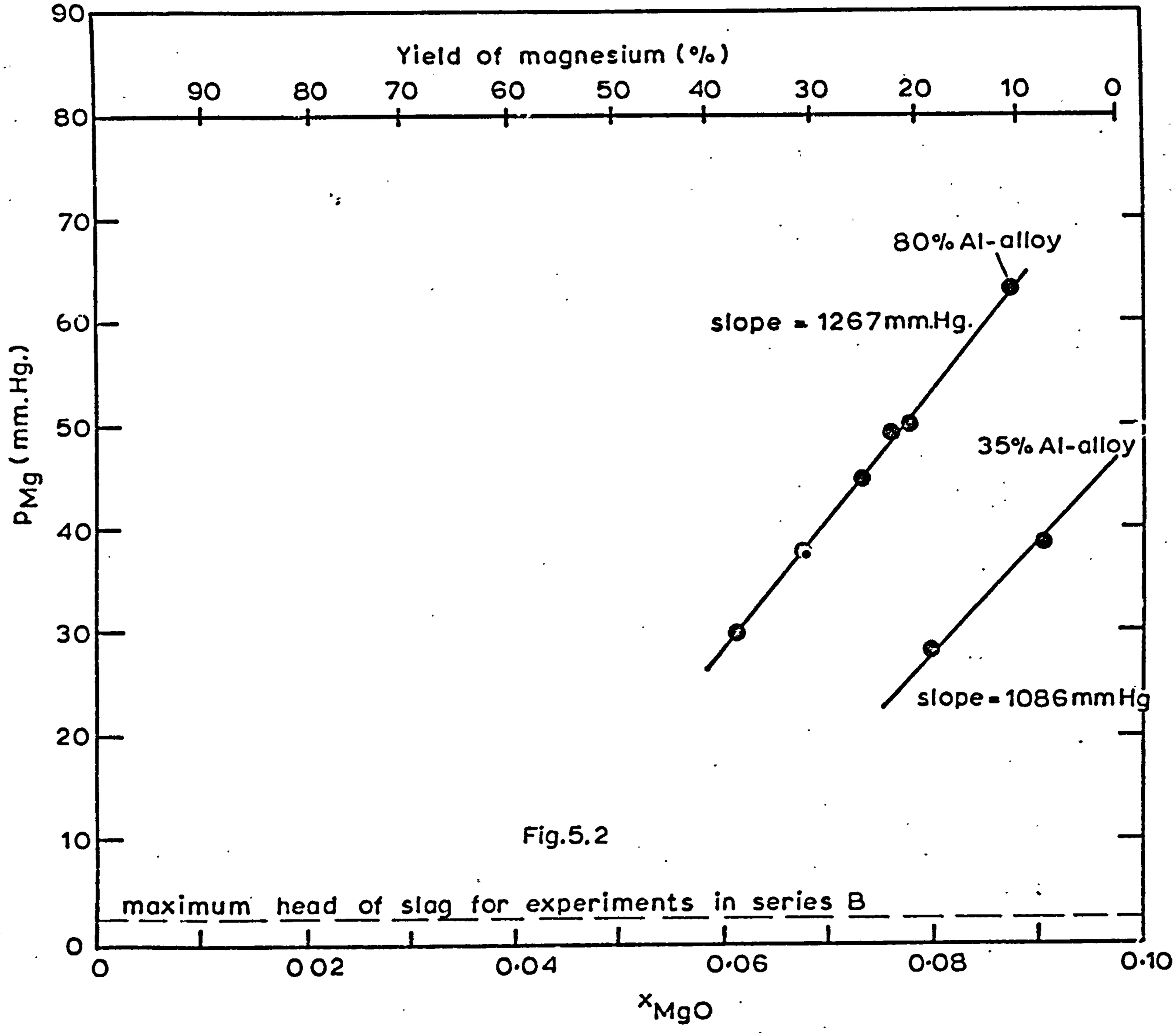

Yield of magnesium (%)
90
80
70
60
50
40
30
20
10
0
p_{Mg} (mm.Hg.)
80% Al-alloy
slope = 1267mm.Hg.
35% Al-alloy
slope = 1086mm Hg
maximum head of slag for experiments in series B
0
0 02
0·04
0·06
0·08
0·10
x_{MgO}

Fig.5.2

of the melt on any slag/metal interface could eventually limit the maximum recovery of magnesium. In experiments with the 35% Al-alloy, the height of slag on the metal phase was less than 12.2 mm which corresponded to less than 2.6 mm Hg. This value is much smaller than the operating pressure so that it is unlikely that the static pressure could have stopped the reaction in any of the experiments. The conditions were even more favourable with the 80% Al-alloy since it existed as a dispersion of drops in the slag.

The equilibrium constant and standard free energy of reaction for reduction of MgO could not be accurately calculated from the experimental results because the actual values of a_{MgO} and $a_{Al_2O_3}$ are not known for the slag used. Nevertheless, an attempt was made to estimate K and ΔG_T^0 for the purpose of comparison with values derived from existing thermodynamic data on the standard free energies of formation of hypothetical liquid Al_2O_3 and MgO. For $a_{Al_2O_3}$ in the ternary slag the value of activity in the binary CaO - Al_2O_3 melt of the same alumina concentration existing in the (CaO + MgO) - Al_2O_3 melt was used. In the temperature range 1500 - 1700 C, the effect of temperature on the activities of lime and alumina in CaO - Al_2O_3 melts depends on the composition [44]. For $x_{CaO} < 0.5$ the activity of CaO increases with temperature and for $x_{CaO} > 0.5$ a_{CaO} decreases as the temperature increases. On the other hand, for $x_{Al_2O_3} < 0.37$ the activity of alumina increases with temperature and for $x_{Al_2O_3} > 0.37$ $a_{Al_2O_3}$ decreases as the temperature increases. However, the activity of alumina is not very sensitive to temperature in the concentration range $0.328 \leq x_{Al_2O_3} \leq 0.360$. Therefore, it is reasonable to assume that values of $a_{Al_2O_3}$ at 1430 - 1450 C are equal to those at 1500 C. Two values for a_{MgO} corresponding to $\gamma_{MgO} = 1$ and $\gamma_{MgO} = 0.1$ were considered. Table 5.1 gives values of K derived by replacing p_{Mg} (atm) and T (^{0}K) in equation (5.1) by operating pressure and average operating temperature

Table 5.1

Values for the equilibrium constant of reaction (2.18) derived from experimental results

Temp (K)	Alloy (% Al)	a_{Al}	x_{MgO}	Y (%)	$x_{Al_2O_3}$	$a_{Al_2O_3}$	p_{Mg} (mm Hg)	K	
								$\gamma MgO = 1$	$\gamma MgO = 0.1$
1708	80	0.87	0.0973	0	0.328	0.0075	76	0.221	2.21
1708	80	0.87	0.087	10.6	0.331	0.008	63	0.210	2.10
1708	80	0.87	0.077	20.9	0.335	0.010	50	0.203	2.03
1708	80	0.87	0.076	21.9	0.335	0.010	49	0.199	1.99
1708	80	0.87	0.073	25.0	0.336	0.010	45	0.191	1.91
1708	80	0.87	0.067	31.1	0.338	0.015	38	0.202	2.02
1708	80	0.87	0.061	37.3	0.340	0.015	30	0.173	1.73
1723	35	0.37	0.0973	0	0.328	0.0075	47	0.242	2.42
1723	35	0.37	0.091	6.5	0.330	0.0075	39	0.213	2.13
1723	35	0.37	0.0795	18.3	0.334	0.008	28	0.181	1.81

respectively. ΔG_T^0 derived from the average values of K are compared with those derived from the standard free energies of formation of liquid oxides (Table 5.2). The difference between the two values is well within the uncertainty ($\pm$ 6.5 kcal/mole MgO) of ΔG_T^0 calculated from published data [14,38]. However, because of the uncertainty in the standard free energy of formation of hypothetical liquid oxides at high temperatures, the validity of the assumed activity coefficients of MgO cannot unfortunately be confirmed.

5.1.2 Effect of pressure on rate

The rate of reduction of MgO from MgO - Al_2O_3 - CaO slags with ferroaluminium increased as the pressure was reduced below the equilibrium values (Figures 4.1 and 4.2). At a given operating pressure, the rate decreased with the depletion of MgO in the slag. Semi-log plots of the form

$$\log \{[(\%MgO)_t - (\%MgO)_{eq}] / [(\%MgO)_0 - (\%MgO)_{eq}]\} = - Kt \qquad (4.11)$$

were satisfactorily fitted to the experimental points as shown in Figure 4.3. The linearity of these plots suggests that the reduction of MgO from molten slags with ferroaluminium at reduced pressures was controlled by transport of reacting species in the slag phase and/or by a first order reversible chemical reaction taking place at the slag/metal interface.

Transport in the metal phase was unlikely to be the controlling mechanism because aluminium was always present in considerable excess at high bulk concentrations. Gas - phase resistance was non-existent because pure magnesium vapour was in contact with all active slag/metal interfaces.

Migration of the magnesium vapour from the reaction zone to the

Table 5.2

Comparison between values of ΔG_T^0 obtained from the average equilibrium constant for reaction (2.18) and those derived from the standard free energies of formation of hypothetical liquid MgO and Al_2O_3

Temp (K)	γ_{MgO}	Average K	ΔG_T^0 (a) (cal/mole MgO)	ΔG_T^0 (b) (cal/mole MgO) $\pm$ 6500 cal/mole
1708	1.0	0.200	5462	- 651
1708	0.1	2.00	- 2352	- 651
1723	1.0	0.212	5311	- 707
1723	0.1	2.12	- 2573	- 707

(a) experimental

(b) derived from the standard free energies of formation of hypothetical liquid MgO and Al_2O_3

condensation zone of the apparatus did not control the overall process since experimental evidence (Figure 4.4) showed that there was no sudden increase of pressure in the furnace tube when Mg vapour evolved. This confirms that the surge tank, connected to the furnace, functioned as an effective sink for the system, so that transport of magnesium vapour to the condenser could take place almost instantaneously by a combination of diffusional and bulk flow.

The values of K equal to the slopes of the straight lines shown in Figure 4.3 are given in Table 4.2.

Due to difference in densities between metal and slag, most of the metal phase existed as a distinct layer at the bottom of the crucible when the 35% Al-alloy was used (Figures 4.7 and 4.8). On the other hand, with the 80% Al-alloy the metal phase formed a dispersion of molten droplets in the slag (Figures 4.5, 4.6 and 4.9). Values of K (= kA/2.303V) were three times higher* for reduction with the 80% Al-alloy than with the 35% Al-alloy. It will be seen from Table 4.2 that the average values for the product kA relative to experiments of series A (experiments A-1 to A-4) and B are 0.616 and 0.131 respectively. Therefore, the rate per unit driving force (= kA) with the 80% Al- was 4.7 times greater than with the 35% Al-alloy. It is reasonable to attribute the higher value of kA obtained with the 80% Al-alloy primarily to the higher slag/metal interfacial area when this alloy is used.

A correlation between constant K and operating pressure, in the range $28 \leq p_{Mg} \leq 50$ mm Hg, was not evident. For the slag/metal systems studied, it is very difficult to isolate the effect of pressure on the constant K because the mass

* except for experiment A-6

transfer coefficient and interfacial reaction area are themselves affected by the operating pressure. For example, for a given alloy composition, lower values of operating pressure will increase the driving force for reaction, so that higher rates of evolution of $Mg_{(g)}$ will be achieved. The generation of higher volumetric flow rates of $Mg_{(g)}$ will stir the melt more vigorously and, at the same time, it will assist the dispersion of metallic droplets in the slag. These two effects would be expected to increase the mass transfer coefficient and the interfacial area respectively.

Table 5.3 shows that there is no evident correlation between the flow rate of $Mg_{(g)}$ and the constant K for the experiments of series A. It is relevant to note that the flow rates of magnesium vapour decrease from the start of reaction and also that the creation of new interfaces probably takes place at the very early stages of reaction when most of the magnesium vapour is released. It will be noted in Figure 4.3 that, in general, the semi-log plots deviate from the linear relationship during the initial stages of reaction. Besides the uncertainty regarding the exact instant at which the reaction started, this deviation from linearity could also indicate that the mass transfer coefficient of the reacting species and the interfacial surface area were not constant during the early stages of reaction.

The effect of the slag/metal volumetric ratio on the rate of reduction was studied in experiments A-4 and A-5. Because different volumes of slag were present, the rates of evolution of magnesium vapour relative to unit volume of slag were compared. Curves of weight of magnesium produced per cubic centimeter of slag against time are plotted in Figure 5.3. The curves show that, between 10 and 40 seconds the rates were close to each other; however, after 40 seconds the rate was higher in experiment A-5 than in experiment A-4.

Figure 5.3 - Evolution of $Mg_{(g)}$ per unit volume of slag in experiments A-4 and A-5

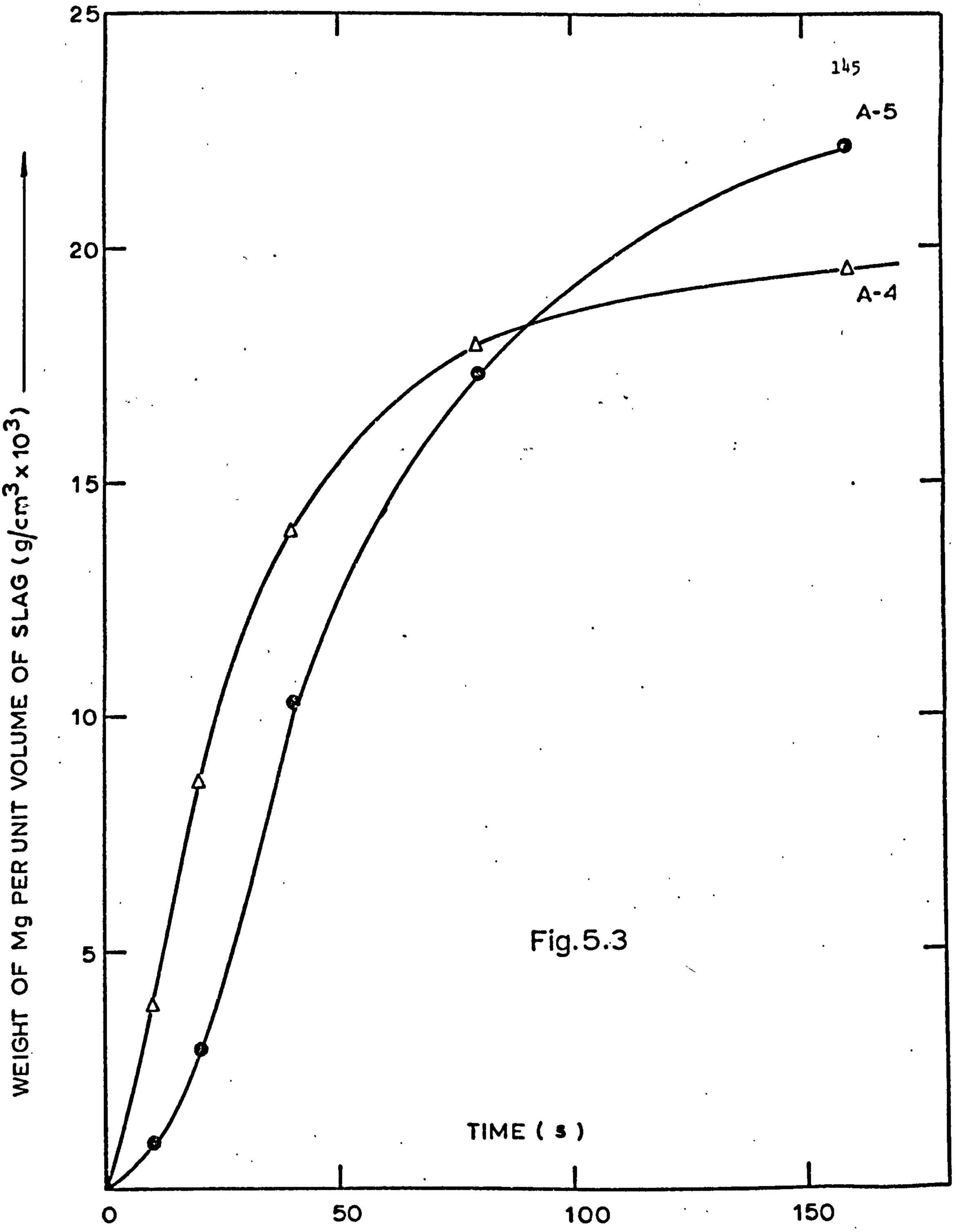

25
20
15
10
5
0
50
100
150
145
A-5
A-4
TIME (s)
WEIGHT OF Mg PER UNIT VOLUME OF SLAG (g/cm3 x 10^3)

Fig.5.3

Table 5.3

Volumetric flow rate of magnesium vapour corresponding to the initial rates of reduction of MgO observed in experiments of series A and B

Experiment	Alloy composition (% Al)	Slag/metal volumetric ratio	Initial rate (% MgO s^{-1})	Weight of slag (g)	Magnesium flow rate (ml s^{-1}, STP)	K=kA/2.303 V (s^{-1})
A-1	80	2.8	0.8×10^{-1}	75.18	33.7	8.28×10^{-3}
A-2	80	2.8	0.7×10^{-1}	75.62	26.9	12.7×10^{-3}
A-3	80	2.8	0.5×10^{-1}	75.74	21.2	8.66×10^{-3}
A-4	80	2.4	0.3×10^{-1}	75.03	12.6	11.57×10^{-3}
A-5	80	6.2	0.2×10^{-1}	176.00	19.7	8.83×10^{-3}
A-6	80	2.7	0.3×10^{-2}	75.38	1.3	7.05×10^{-4}
B-1	35	2.4	0.1×10^{-1}	50.00	3.1	3.40×10^{-3}
Г-2	35	2.4	0.4×10^{-2}	52.51	1.0	3.04×10^{-3}

The total volume of $Mg_{(g)}$ released in experiment A-5 was 2.7 times that in experiment A-4, although the amount of ferroaluminium in both experiments differed by less than 10%. From Table 4.2 it will be seen that the rate per unit driving force in experiment A-5 was 1.8 times that in experiment A-4. This suggests that the actual slag/metal interfacial area was higher in experiment A-5 than in experiment A-4 due to a greater dispersion of the metal phase in the slag which was caused by the greater evolution of bubbles of magnesium vapour.

Because of the high temperatures at which the experiments were carried out, it is reasonable to assume that the rates of chemical reactions involved are very rapid for controlling the overall process[29,77]. However, straight lines as those of Figure 4.3 would also result if the process was controlled by a first order reversible reaction at the slag/metal interface. The overall reaction which produces $Mg_{(g)}$, described by reaction (2.18), is reversible because its equilibrium constant is small (Figure 2.3 and Table 5.1). The determination of the "apparent activation energy" for reduction could have provided additional information useful for the elucidation of the controlling mechanism of the process. However, the effect of temperature on the rate of reduction was not studied due to the limitation imposed by the maximum temperature at which the furnace could be safely operated.

5.1.3 Effect of argon flow rate bubbled through the melt on the rate of reduction of MgO

It was possible to recover magnesium from slags by bubbling argon at atmospheric pressure through the melt. This finding is new. However, the rate was much slower than that obtained at reduced pressures, as shown in Table 5.4. Estimates of the maximum values

Table 5.4

Comparison between orders of magnitude of rate of reduction at reduced pressures and at atmospheric pressure with bubbling of argon through the melt

Reduction	Alloy (% Al)	Rate of reduction (% MgO s^{-1})
Reduced pressures (28-63 mm Hg)	80	$10^{-1} - 10^{-2}$
	35	$10^{-2} - 10^{-3}$
Bubbling of argon at atmospheric pressure (1040-2040 ml.min^{-1}, STP)	80	$10^{-4} - 10^{-5}$
	35	$10^{-3} - 10^{-4}$

of p_{Mg} in the $Ar/Mg_{(g)}$ mixture leaving the melt (Table 5.5) indicate that these were smaller than the operating pressures in the reduced-pressure experiments, so that the thermodynamic conditions for removal of magnesium from the slag/metal interface to the argon bubbles were favourable.

The low rates observed with the bubbling-method may not be simply attributed to the introduction of an additional resistance term to the transport of magnesium vapour, namely, gas-phase resistance. In fact, an evaluation of the criteria to be satisfied for the reaction to take place at reduced pressures and at atmospheric pressure with bubbling of argon through the melt, indicate that at reduced pressures all the slag/metal interfaces are active, whereas reduction of MgO, when the pressure above the melt is maintained at ≈ 760 mm Hg, can occur only at locations where gas, slag and metal meet. Moreover, for magnesium to be released, its partial pressure in the gas phase should be smaller than the equilibrium value corresponding to the local slag composition.

It seems that the entire slag/metal interface was not active in the experiments in which argon was bubbled through the melt. Although the average total flow rate of gas delivered into the melt was in the same range as the average value for $Mg_{(g)}$ flow rate observed in experiments at reduced pressure (A-1 to A-5), the slag/metal/gas contact was poor. It is likely that this was the reason for the low rates observed with argon bubbling.

It is interesting to note that the initial rates of reduction obtained with the 80% Al-alloy (Figures 4.12a and 4.13a) were very close to each other, irrespective of the argon flow rate. For 2040 ml. min^{-1}, however, the highest initial rate was observed. The data points of experiments C-1 to C-4 are located along a mean curve up to approximately 20% yield of magnesium. At higher yields, however, the results showed wide scatter and it is was not possible to relate the

Table 5.5

Calculated values of partial pressure of magnesium in Ar + Mg(g) mixtures. Total pressure ≈760 mm Hg

Experiment	Alloy (% Al)	Slag/metal vol. ratio	Initial rate (% MgO s^{-1})	Weight of slag (g)	Argon flow rate (ml. s^{-1}, STP)	$Mg_{(g)}$ flow rate (ml. s^{-1} STP)	Total flow rate (ml. s^{-1}, STP)	p_{Mg} (mm Hg)
C-1	80	2.6	2.8×10^{-4}	61.14	17.333	0.096	17.429	4.2
C-2	80	2.5	3.2×10^{-4}	75.00	22.083	0.134	22.217	4.6
C-3	80	2.6	1.9×10^{-4}	69.30	22.933	0.074	23.007	2.4
C-4	80	2.8	1.6×10^{-4}	69.35	22.933	0.062	22.995	2.0
C-5	80	2.3	8.0×10^{-4}	70.00	34.000	0.314	34.314	7.0
D-1	35	3.4	1.6×10^{-4}	71.11	17.333	0.617	17.950	26.0
D-2	35	3.2	1.8×10^{-4}	66.61	21.000	0.653	21.653	23.0

rate of reduction with gas flow rate. There is reason to believe that the movement of metal and slag caused by the stream of argon bubbles and by the introduction of the lance could have reduced the total interfacial area. This probably explains the observed low rates in experiments C-1 and C-5.

Higher initial rates were obtained with the 35% Al- than with the 80% Al-alloy (see Figures 4.12b and 4.13b). When the heavier alloy was used the argon bubbles were released in the metal layer, at the bottom of the crucible so that, in general, they had to cross the slag/metal interface. However, a situation could develop in which the stream of bubbles would be in contact with only one liquid phase, in which case the reaction would stop. This seems to have been the case in experiments C-1, D-1 and D-2.

The existing metallothermic processes[3] for recovery of magnesium involve the use of low pressures. The present work has shown that a process for reducing MgO from molten slags could be operated at atmospheric pressure by the gas-bubbling method (Figure 5.4). Rates of reduction could be increased by improving the distribution of bubble streams in the melt and the process could be continuously operated with recirculation of argon. It is interesting to note that the yield of magnesium will not be limited by the static pressure on any slag/metal interface, as would occur with reaction at reduced pressures. Any MgO-bearing raw material could be used for the preparation of suitable slags and aluminium could be obtained relatively cheaply in the form of aluminium alloys, for example, by carbothermic smelting of aluminium - silicate ores. Briquetting of the mixture of reactants would not be necessary. Operation at atmospheric pressure is very desirable for continuous production of magnesium at high temperature because feeding and discharging operations are greatly simplified, the stress on materials of construction is minimized and because magnesium can be condensed as liquid, rather than

Figure 5.4 - Schematic flow diagram for the gas-bubbling process

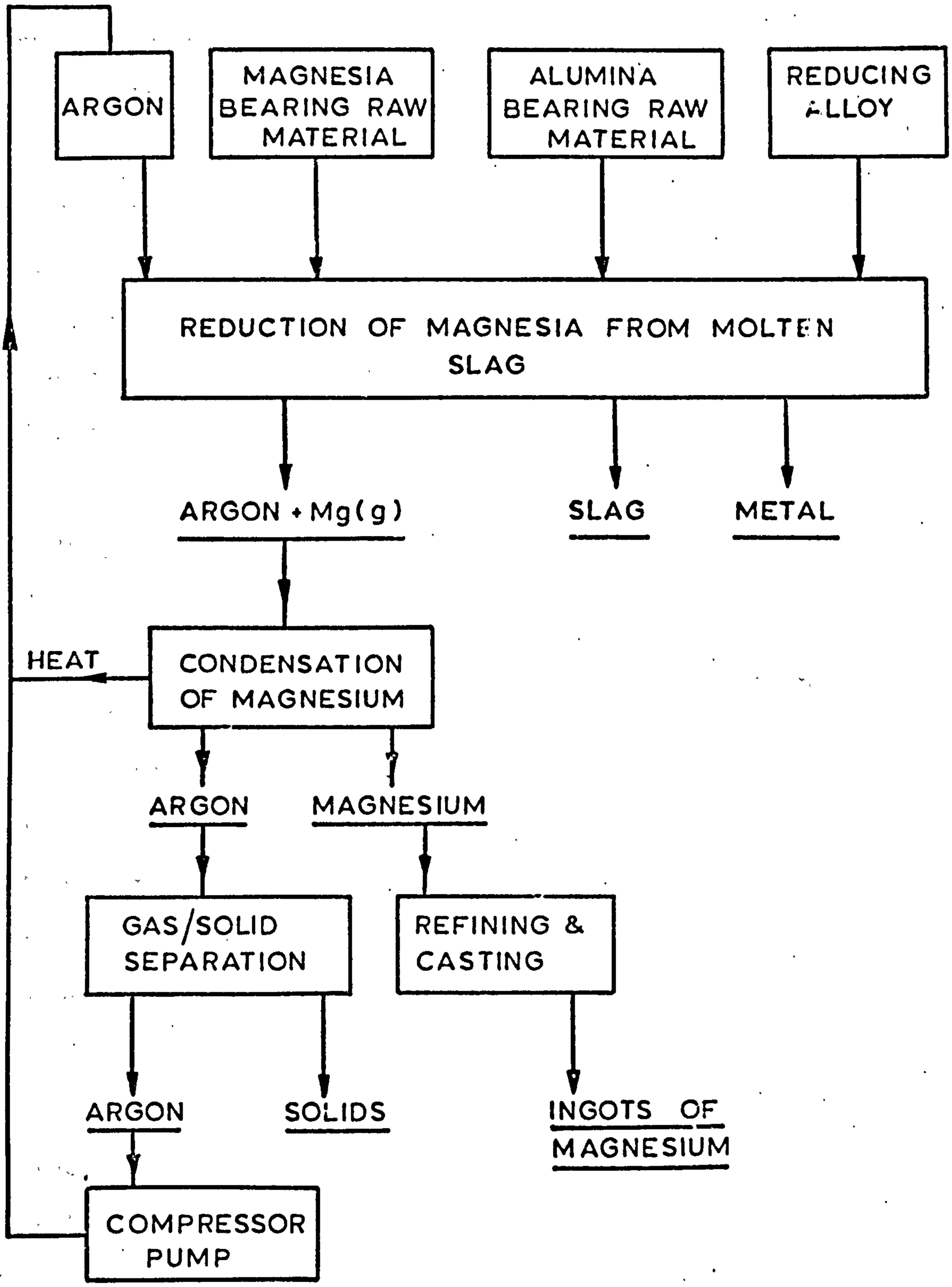

ARGON
MAGNESIA BEARING RAW MATERIAL
ALUMINA BEARING RAW MATERIAL
REDUCING ALLOY
REDUCTION OF MAGNESIA FROM MOLTEN SLAG
ARGON + Mg(g)
SLAG
METAL
HEAT
CONDENSATION OF MAGNESIUM
ARGON
MAGNESIUM
GAS/SOLID SEPARATION
REFINING & CASTING
ARGON
SOLIDS
INGOTS OF MAGNESIUM
COMPRESSOR PUMP

FIG.5.4

as a solid. A heat exchanger located in the condenser could recover heat from the hot argon leaving the furnace, which would be used for pre-heating the recirculated gas.

It is relevant to note that, depending on the operating temperature and the activity of Al in the alloy used, magnesium can be produced at pressures even higher than atmospheric, by reduction of solid MgO of the charge with molten Al-alloy (see Section 2.1.1.1). The equilibrium vapour pressure of magnesium for the reaction of solid MgO, in the presence of CaO, with pure aluminium ($a_{MgO} = a_{Al} = 1$) is higher than 760 mm Hg for temperatures above 1370 C (Figure 2.1).

5.1.4 Purity of the deposits of magnesium

The magnesium produced was more than 98.5 atomic percent pure as the results given in Table 4.3 show. Traces of impurities which were present in the raw materials used for the preparation of slags and alloys, such as chlorine, fluorine and alkalis were detected in the deposits.

At the operating temperatures involved, the vaporization of aluminium from the ferroalloys could have occurred only to a small extent because the values of vapour pressure of Al in ferroaluminium were low. For the 80% Al- and the 35% Al-alloy p_{Al} values are 0.34 and 0.09 mm Hg respectively as will be seen from Figures A2-1 and 2.7.

Reduction of CaO with ferroaluminium may explain the presence of calcium in the deposits of magnesium. Estimates of p_{Ca} for reaction (2.22) at the operating temperatures give less than 7 mm Hg and less than 4 mm Hg for reaction with the 80% Al- and the 35% Al-alloy respectively. Although these values are well below the operating pressures in the experiments, reduction of CaO could have been enhanced by bubbles of $Mg_{(g)}$ or argon. Lime could also react with aluminium to produce calcium aluminides, which would dissolve in the

metal phase, and subsequently $Ca_{(g)}$ would be distilled off.

5.2 REACTION OF MgO DISSOLVED IN SILICATE SLAGS WITH FERROSILICON AT REDUCED PRESSURES

Results given in Table 4.6 show that contamination of the magnesium deposits with silicon and carbon increased with activity of silica in slags. The increase in operating pressure appears to have depressed the evolution of $Mg_{(g)}$ more than that of $SiO_{(g)}$, since the Si/Mg ratio in the deposits increased. The results are supported qualitatively by the conclusions from the thermodynamic assessment for reactions of slags with ferrosilicon in graphite crucibles, discussed in Sections 2.1.2.4 and 2.1.2.5.

Table 5.6 gives values of the equilibrium vapour pressures of $Mg_{(g)}$ and $SiO_{(g)}$ for reactions (2.19) and (2.31) respectively at various temperatures, for the initial slag composition and after 100% recovery of magnesium. For the calculations it was assumed that activity of silicon was constant and equal to 0.86[35]. From the results given in the table it will be evident that the decrease in the values of a_{SiO_2} resulting from alumina additions, is essential for the generation of $Mg_{(g)}$ without the simultaneous evolution of $SiO_{(g)}$. It is also clear that an increase in the operating temperature will increase markedly the equilibrium vapour pressure of $SiO_{(g)}$.

Rate measurements for reduction of slags with ferrosilicon were not attempted mainly because side reactions, which compete with the evolution of $Mg_{(g)}$, would have made interpretation of results even more difficult than for the case of reduction of $MgO - Al_2O_3 - CaO$ slags with ferroaluminium.

Table 5.6

Calculated values for the equilibrium vapour pressures of Mg(g) and SiO(g), mm Hg, for various temperatures and values of a_{MgO} and a_{SiO2} in slags

Vapour	Temp. (K)	Quarternary slag 22.0%SiO_2-25.0%Al_2O_3-43.0%CaO-10.0%MgO		Ternary slag 52.0%SiO_2-35.3%CaO-12.7%MgO	
		% yield of magnesium		% yield of magnesium	
		a_{MgO} = 0.153 a_{SiO_2} = 0.01(*)	a_{MgO} = 0 a_{SiO_2} = 0.025(*)	a_{MgO} = 0.10(*) a_{SiO_2} = 0.4(*)	a_{MgO} = 0 a_{SiO_2} = 0.9(*)
Mg	1700	13.1	0	1.5	0
	1800	19.2	0	2.2	0
	1900	25.9	0	2.9	0
SiO	1700	0.9	1.4	5.5	8.2
	1800	3.0	4.8	19.2	28.7
	1900	8.8	14.0	55.9	83.8

(*) Rein, R.H. and Chipman, J. Ref. (46)

CHAPTER 6

CONCLUSIONS

A technique was developed for measuring the rate of evolution of magnesium vapour when a molten slag containing MgO is reduced with ferroaluminium. Magnesium vapour from the reaction zone was transferred to a condenser which was weighed continuously by means of a load cell. This method was successfully used to study the kinetics of reduction when the process was operated at pressures below atmospheric and when an inert gas at atmospheric pressure was bubbled through the melt.

A. In the reduced-pressure experiments it was found that:

(a) The rate of reduction of MgO from molten MgO - Al_2O_3 - CaO slags with ferroaluminium increased as the pressure was reduced below the equilibrium value. In general the rate per unit driving force (=kA) with the 80% Al-alloy was 4.7 times that with the 35% Al-alloy. This increase was attributed primarily to the larger slag/metal interfacial area when the 80% Al-alloy was used. In this case the metal phase existed as a dispersion of droplets whereas with the 35% Al-alloy it existed as a distinct layer below the slag.

(b) The overall process of reduction appears to be controlled by transport in the slag phase and/or by a first-order, reversible chemical reaction taking place at the slag/metal interface.

(c) The final yield of magnesium decreased as pressure increased. In the range of operating pressures and concentrations of MgO studied, a linear correlation fitted the experimental points reasonably well. However, since the activity of Al_2O_3 increased and the activity of MgO decreased during an experiment, this apparent linear correlation is only valid as a first approximation. It would not be expected to apply for higher yields and lower

operating pressures.

(d) Estimates of ΔG_T^0 at 1708 - 1723 K for the overall reaction

$$(MgO) + \frac{2}{3}\,[Al] \rightarrow Mg_{(g)} + \frac{1}{3}\,(Al_2O_3),$$

derived from experimental results, are within the uncertainty of the calculated values of ΔG_T^0 derived from standard free energies of formation of hypothetical liquid MgO and Al_2O_3. However, the inaccuracies in the published values are too high to allow conclusive confirmation of the assumed values of $a_{Al_2O_3}$ and γ_{MgO} used for calculation of the equilibrium constant from experimental results.

B. In the experiments carried out at atmospheric pressure with bubbling of argon through the melt, it was found that:

(a) It was possible to recover magnesium from slags by bubbling, although rates were one to three orders of magnitude lower than those obtained at reduced pressures. The entire slag/metal interface was not active in these experiments.

(b) Rates obtained with the 35% Al-alloy were approximately 10 times those with the 80% Al-alloy. A correlation between the rate of reduction and gas flow rate, in the range 1040 - 2040 $ml.min^{-1}$ STP, was not evident because of the uncertainty regarding the behaviour of the bubbles and the effective interfacial areas.

(c) A continuous process for producing magnesium from MgO dissolved in molten slags using argon bubbling, could be of potential industrial interest, since operations at atmospheric pressure are very desirable.

C. The deposits of magnesium produced were more than 98.5 atomic percent pure. However, reduction of MgO from SiO_2 - bearing slags with ferrosilicon yielded magnesium which was heavily contaminated with silicon and carbon as a result of reactions of SiO_2 with Si and graphite, which were expected from thermodynamic considerations. Consequently, the kinetics of the reduction of slags with ferrosilicon was not investigated.

APPENDICES

APPENDIX 1

Metallothermic Processes of Production of Magnesium

The metallothermic processes of production of magnesium are based on reduction of magnesium-bearing raw materials with metallic reductants such as ferrosilicon, ferroaluminium, aluminium-silicon and calcium. Presently, there are reduction plants working mainly based on the following processes:[3]

(a) Retort or Pidgeon process;

(b) Rotary furnace process;

(c) Knapsack process;

(d) Magnetherm process.

Retort or Pidgeon Process[66 - 69]

The Pidgeon process is at present the most widely used among metallothermic processes. Briquettes of calcined dolomite (CaO.MgO) and ferrosilicon are reduced in chromium-nickel steel retorts. The daily output of a retort is about 50 kilograms of magnesium. The maximum operating temperature is 1200 C and the residual pressure inside the retorts is maintained at around 0.1 mm Hg. This is a batch process with a cycle time of about 8 hours. The magnesium vapour leaves the charge of briquettes in the hot zone and condenses to a solid crown of crystals, on the internal walls of a water-cooled condenser insert, positioned at the cool end of the retort. The deposit of solid magnesium is removed by pneumatic hammers for melting. The process has a silicon efficiency (weight of magnesium collected/magnesium equivilent of silicon present) of 65 - 70%. The process uses externally heated horizontal retorts. Since the rate-controlling factor in this process is the heat transfer to the solid bed of briquettes[26], any increase in the size of the retorts may result in an increase of the time cycle. An improvement of

the heat transfer conditions of the retort process was achieved by the Amati process[2,70] operating in Bolzano, Italy. It is a version of the retort method in which calcined dolomite is reduced by ferrosilicon in internally heated vacuum retorts with a batch size of over 400 kilograms of magnesium.

Rotary furnace process

The rotary drum furnace process was developed by IG-Farbenisdustrie AG (Bielefeld)[71] in order to overcome the shortcomings of the Pidgeon process which are: low reaction temperature, poor heat transfer conditions and low output. Briquettes of calcined dolomite, ferrosilicon and fluorspar, which have been previously hardened (to avoid desintegration during the rotation of the furnace) are reduced in a rocking resistor furnace with internal electric heating elements. The operating temperature is 1400 C. It is a batch process which produces 1000 kilograms of magnesium per day. The duration of a cycle is 3½ - 4 hours. The Si efficiency is 80%. The furnace works under vacuum similar to the Pidgeon process. The magnesium vapour is condensed in a detachable condenser chamber. The process of hardening the briquettes before the reduction relies upon the initial reaction of CaO and ferrosilicon which produces a liquid Ca - Si - Fe alloy (see Section 2.1.1.2). A metallic network is formed when the liquid Ca - Si - Fe alloy permeates the porous structure of the briquettes. Formation of liquid Ca - Si - Fe alloy starts at approximately 1000 C. It has been found that the mechanical strength of the briquettes may also be improved if the calcination of dolomite is carried out in the presence of small quantities of chlorine. In this case, the pre-hardening treatment of the briquettes may even be omitted [71].

Knapsack-Griescheim process[71 - 73]

In this process a mixture of granulated reactants (calcined dolomite and ferrosilicon) is deposited on top of a layer of reacted material, which has accumulated on a water-cooled moving grate, inside the reactor. The mixture is heated by radiation up to 1600 C and the pressure inside the furnace is maintained between 1 - 50 mm Hg. The magnesium vapour leaves the reaction zone and it goes to a condensation chamber where liquid magnesium is collected. The liquid metal is then removed via a barometric column. Between the reaction zone and the condenser there is a filter of coke and granular dolomite in which the vapour is scrubbed before reaching the condenser. The residue of reaction consists of calcium orthosilicate. An excess of calcined dolomite joins the residue and both are continuously removed. Because of the high temperature at which the reduction is carried out, a large excess of dolomite must be added to the charge in order to prevent it from sintering. It is required merely to act as a heat carrier. The potential advantages of this process are: feeding of coarser dolomite than normally used (0.5 - 20 mm), direct feeding of hot calcined dolomite into the reactor (no need for briquetting), higher values of operating pressures than those normally used in plants operating the Retort process, direct condensation to liquid magnesium. Despite the technical and commercial success with continuous ferrosilicon reduction which appears to have been made by Kanpsack-Griesheim in Germany, it is understood that work on this process has been discontinued [2].

Magnetherm process[4, 30, 31]

The Magnetherm process is a French development which uses an electric furnace and liquid slag. Calcined dolomite is reduced with ferrosilicon. The residuals of reaction are withdrawn in the

liquid slag and magnesium vapour is condensed to the liquid state. The operating temperature and pressure are 1500 C and 5 - 30 mm Hg respectively. Alumina is added to the charge in order to reduce the liquidus temperature of the slag and to control the activity of silicon oxide in the slag (see Sections 2.1.2.4, 2.1.2.5, 2.1.2.7 and 5.2). The operation is semi-continuous. The mixture of calcined dolomite and alumina is fed in portions every 3 minutes and it dissolves in the slag. Ferrosilicon (75% Si) is fed continuously on top of the slag. Charging takes place under vacuum. When the slag has completed its reaction the process is interrupted, the furnace is opened to the atmosphere and part of the slag and all the depleted ferrosilicon are tapped. The concentration of Si in ferrosilicon is about 30% Si at this stage. To continue the reduction further it would be necessary to operate the furnace at higher temperatures. One working cycle takes 12 hours and at the end of each cycle about 1400 kilograms of magnesium are produced. The yield of magnesium is 90%, corresponding to a residual concentration of MgO in the slag of 3%. The Si-efficiency of the Magnetherm process is the same as that of the Pidgeon process and the energy required to produce 1 kilogram of magnesium is 10.8 kWhr, which is about 22% higher than the specific energy consumption of the retort process.[1, 3]

Reduction with aluminium and calcium

Besides ferrosilicon, aluminium alloys and calcium are the other metallic reducing agents which have been considered for reduction of magnesium oxide. From the pure thermodynamic point of view calcium and aluminium are better reducing agents than silicon. However, Si, in the form of ferrosilicon, presents economic advantages in comparison with any other metallic reducing agent [1]. For this reason it has been widely used in the magnesium production industry.

It is interesting to note that calcium vapour can be made available from calcium carbide, by thermal decomposition of CaC_2 and that aluminium alloys can be produced from cheap silicate-aluminium ores which are not suitable for direct production of pure aluminium by the conventional route. The Vereinigte-Aluminiumwerke AG-VAG process[71] uses $Ca_{(g)}$ obtained from calcium carbide for reduction of calcined dolomite in a typical gas-solid reactor. Aluminium alloys (Al-Si and Fe-Al) have been used in proposed processes for production of magnesium at high temperatures[30, 74, 75].

APPENDIX 2

Activity of Aluminium in Fe-Al and Fe-Al-C Alloys

Values for the activity coefficient of aluminium in 80% Al- and 35% Al-alloys were estimated from exisiting data [62 - 64]. The effect of carbon on the activity of aluminium in Fe-Al-C alloys was also considered since graphite was used for making the crucibles.

Figure A2.1 shows the variation of log γ_{Al} with $(1 - x_{Al})^2$ for binary Fe-Al alloys as well as for ternary Fe-Al-C (graphite saturated) alloys at 1600 C. Measured values of a_{Al} in these systems are available for concentrations of aluminium less than 0.36 atom fraction. However, extrapolation of the existing data to higher aluminium concentrations is valid since it appears that Raoult's law can be safely adopted as a limiting law in these cases [63]. Values of a_{Al} for the binary alloys are given in Table A2.1.

For the calculation of a_{Al} in ternary Fe-Al-C alloys, it was assumed that the values of the atom fraction of carbon were much smaller than those of aluminium, so that the same aluminium concentration could be used for the binary and ternary alloys. This assumption is correct because solubility of carbon in Fe-Al decreases significantly as the concentration of aluminium increases (see Figure A2.2). Chipman and Floridis[62] determined the solubility of carbon in Fe-Al alloys up to $x_{Al} = 0.36$ and temperature equal to 1600 C. Their results could be correlated by the equation

$$\log x_C = - 0.68 - 1.17\, x_{Al} , \quad 0 < x_{Al} \leq 0.36 \quad (1600\ C) \quad (A2\text{-}1)$$

When the straight line given by equation (A2-1) is extrapolated to zero atom fraction of aluminium it gives the solubility of carbon in liquid iron at 1600 C, which is in agreement with value reported

Figure A2.1 - Activity coefficient of aluminium for Fe-Al and Fe-Al-C (graphite saturated) alloys at 1600 C. (Ref. 63, 64)

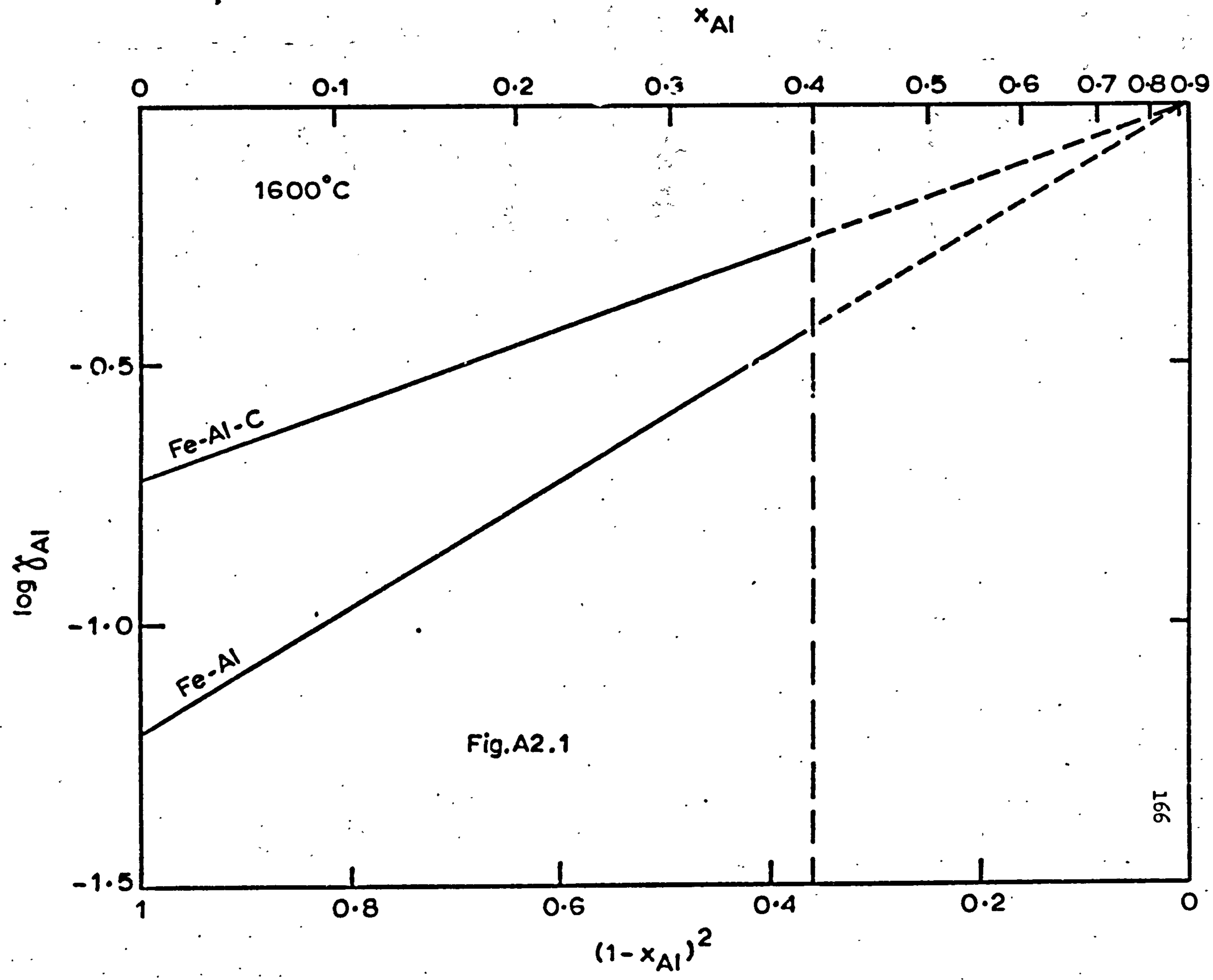

x_{Al}
0
0·1
0·2
0·3
0·4
0·5
0·6
0·7
0·8
0·9
1600°C
Fe-Al-C
Fe-Al
$\log \gamma_{Al}$
-0·5
-1·0
-1·5
1
0·8
0·6
0·4
0·2
0
$(1-x_{Al})^2$
166

Fig.A2.1

by Chipman et al.[65]. The slope of the solubility line shown in Figure A2.2 probably increases with increasing aluminium and decreasing carbon concentrations [62]. A second line was plotted for the concentration range $0.36 \leq x_{Al} \leq 0.999$. The value of solubility of carbon in pure aluminium is very small (≈ 0.05% or $x_C \approx 0.001$ at 1300 - 1500 C) [51]. The corresponding equation for the second line is

$$\log x_C = - 0.03 - 2.973\, x_{Al} , \quad 0.36 \leq x_{Al} \leq 0.999 \qquad (A2\text{-}2)$$

Chipman and Floridis[62] also studied the effect of carbon on the activity coefficient of aluminium in Fe-Al-C alloys. This effect was expressed by the equation

$$\log \gamma_{Al}^{(C)} = \log \gamma_{Al} - \log \gamma'_{Al} \qquad (A2\text{-}3)$$

where γ_{Al} and γ'_{Al} represent the activity coefficient of aluminium in Fe-Al-C and Fe-Al alloys respectively. Figure A2.3 shows the variation of $\log \gamma_{Al}^{(C)}$ with the concentration of carbon [62].

Values of activity of aluminium in Fe-Al-C alloys of the compositions $x_{Al} = 0.89$ and $x_{Al} = 0.53$ were derived by following the procedure:

(a) calculation of γ'_{Al} at a given value of x_{Al} by using the curve for binary Fe-Al in Figure A2.1;

(b) calculation of the atom fraction of carbon from the solubility curve of Figure A2.2 adopting the same value for x_{Al} as in (a);

(c) calculation of $\gamma_{Al}^{(C)}$ from Figure A2.3 for the molar fraction of carbon obtained in (b);

(d) calculation of the activity coefficient of aluminium, γ_{Al}, in the ternary alloy using equation (A2-3);

(e) calculation of activity of aluminium in the ternary alloy by the equation

Figure A2.2 - Solubility of carbon in Fe-Al alloys at 1600 C

(Ref. 62)

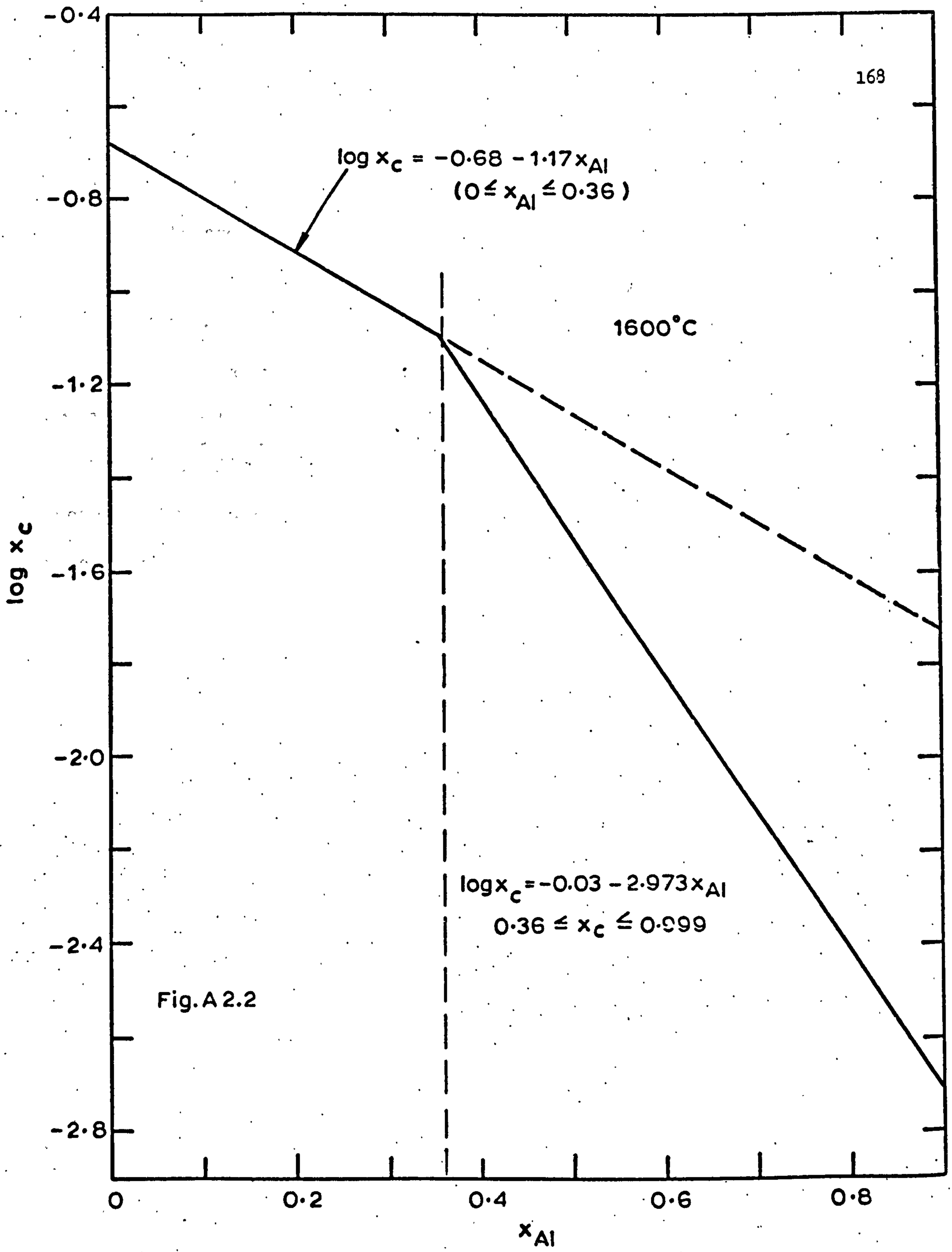

-0·4
-0·8
-1·2
-1·6
-2·0
-2·4
-2·8
log x_c
$\log x_c = -0.68 - 1.17 x_{Al}$
$(0 \leq x_{Al} \leq 0.36)$
1600°C
$\log x_c = -0.03 - 2.973 x_{Al}$
$0.36 \leq x_c \leq 0.999$
0
0·2
0·4
0·6
0·8
x_{Al}

Fig. A 2.2

$$e_{Al} = \gamma_{Al} \cdot x_{Al} \qquad (A2\text{-}4)$$

Calculated values of a_{Al} for the ternary alloy are given in Table A2.1. They confirmed those derived from the extrapolated line of Figure A2.2. Values of a_{Al} determined at 1300 C for the binary Fe-Al alloys for $0.42 \leq x_{Al} \leq 0.75$ are close to the corresponding values determined at 1600 C (Figure 2.2). Consequently, it is reasonable to adopt values determined at 1600 C for the equilibrium calculations at 1435 - 1450 C.

It will be seen from Table A2.1 that carbon does not effect the activity of aluminium in the 80% Al-alloy, whereas an increase of 21 - 28% in the value of a_{Al} would be expected due to saturation of the 35% Al-alloy with carbon. However, this variation does not increase the values of p_{Mg} for reaction with the 35% Al-alloy by more than 17.6%.

Figure A2.3 - Effect of carbon on activity coefficient of aluminium (Ref. 62)

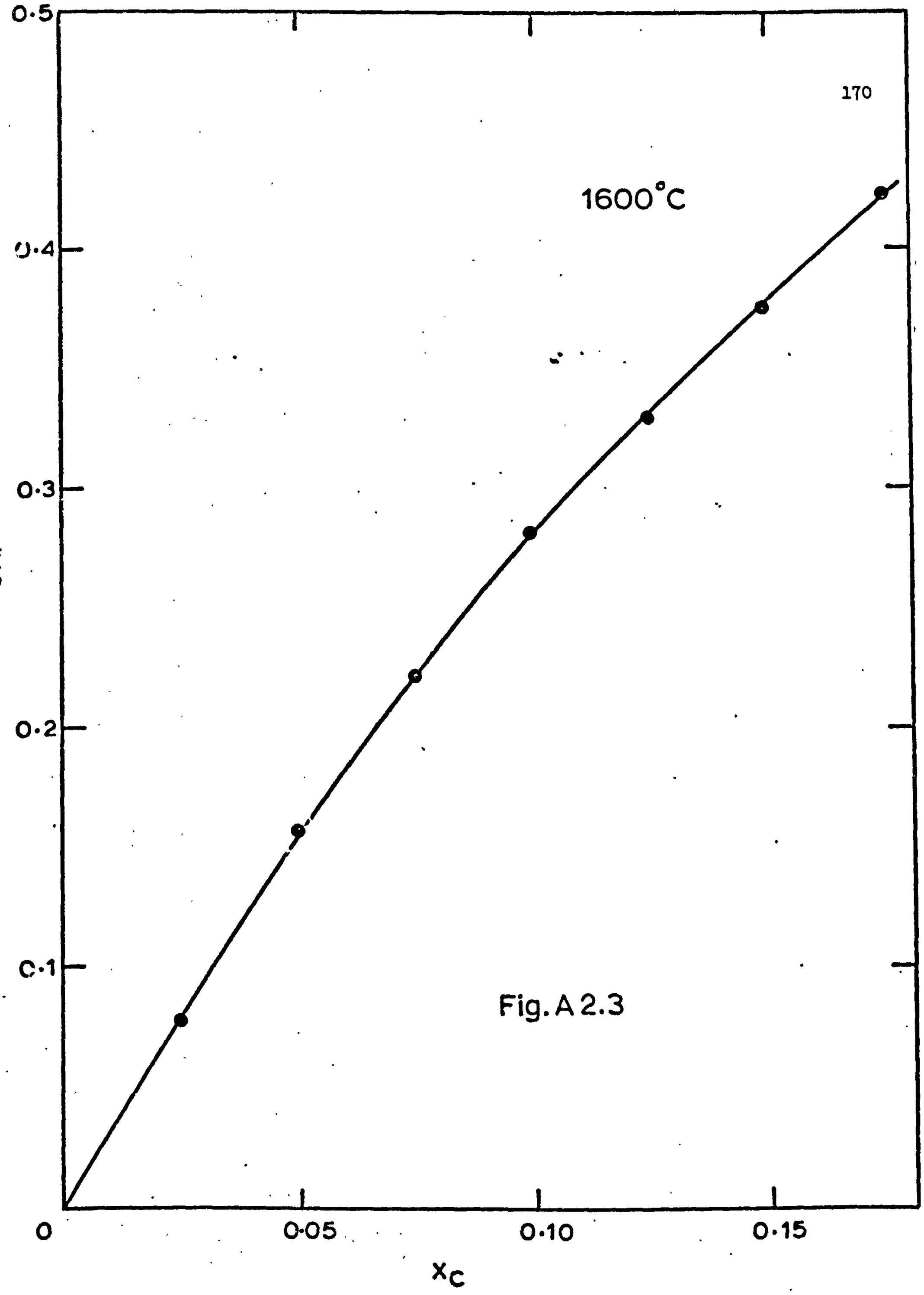


Fig. A 2.3

Table A2.1

Activity of aluminium in Fe-Al and Fe-Al-C (graphite saturated) alloys at 1600^{0}C

Alloy	% Al	x_{Al}	a_{Al}	Calculation method
Fe-Al	35	0.53	0.29	Figure A2.1
Fe-Al	80	0.89	0.87	Figure A2.1
Fe-Al-C	35	0.53	0.37	Figure A2.1
Fe-Al-C	80	0.89	0.87	Figure A2.1
Fe-Al-C	35	0.53	0.35	Equation A2.4
Fe-Al-C	80	0.89	0.88	Equation A2.4

APPENDIX 3

Power Supply

Silicon carbide elements increase in resistance during their life. Consequently a means of varying the applied voltage must be provided, for example, by using a multi-tapped double-wound transformer.

The elements were connected in seven branches of two elements in series and the nominal resistance of each new element was 2 ohms. Therefore, the resistance of the network of heating elements, R, was:

$$R = 4/7 = 0.571 \text{ ohms} \qquad \text{(A3-1)}$$

The estimated required power for the furance was:

$$W = 10{,}000 \text{ watts} \qquad \text{(A3-2)}$$

The nominal full-load voltage, V, is determined as follows:

$$V = (WR)^{0.5} = (10{,}000 \times 0.571)^{0.5} = 75.56 \text{ volts} \qquad \text{(A3-3)}$$

The manufacturers of Crusilite heating elements (Morganite Electroheat Limited) recommend that a voltage reserve of 100% should be allowed to cater for ageing of the elements operating at temperatures up to 1500 C or higher. Therefore, the maximum output voltage of the transformer should be

$$V_{max} = 2V = 2 \times 75.56 = 151.12 \text{ volts} \qquad \text{(A3-4)}$$

For controlling the rate of heating during the temperature cycle of the furnace, it was necessary to extend the voltage range below the nominal initial voltage required for full-power. Therefore, tappings were used to span the secondary output of the transformer from 55 to 155 volts in 5 volts steps, as recommended by the suppliers of the

heating elements.

APPENDIX 4

Phase Diagrams

Diagrams of the systems CaO - MgO - Al_2O_3, Fe-Al and Fe-Si are given in Figures A4.1, A4.2 and A4.3 respectively.

Figure A4.1a - CaO-MgO-Al_2O_3 system (Reference 76a)

Figure A4.1b - CaO-MgO-Al_2O_3 system (Reference 76b)

Figure A4.2 - The Fe-Al system (Reference 51)

Figure A4.3 - The Fe-Si system (Reference 51)

$CaO - MgO - Al_2O_3$

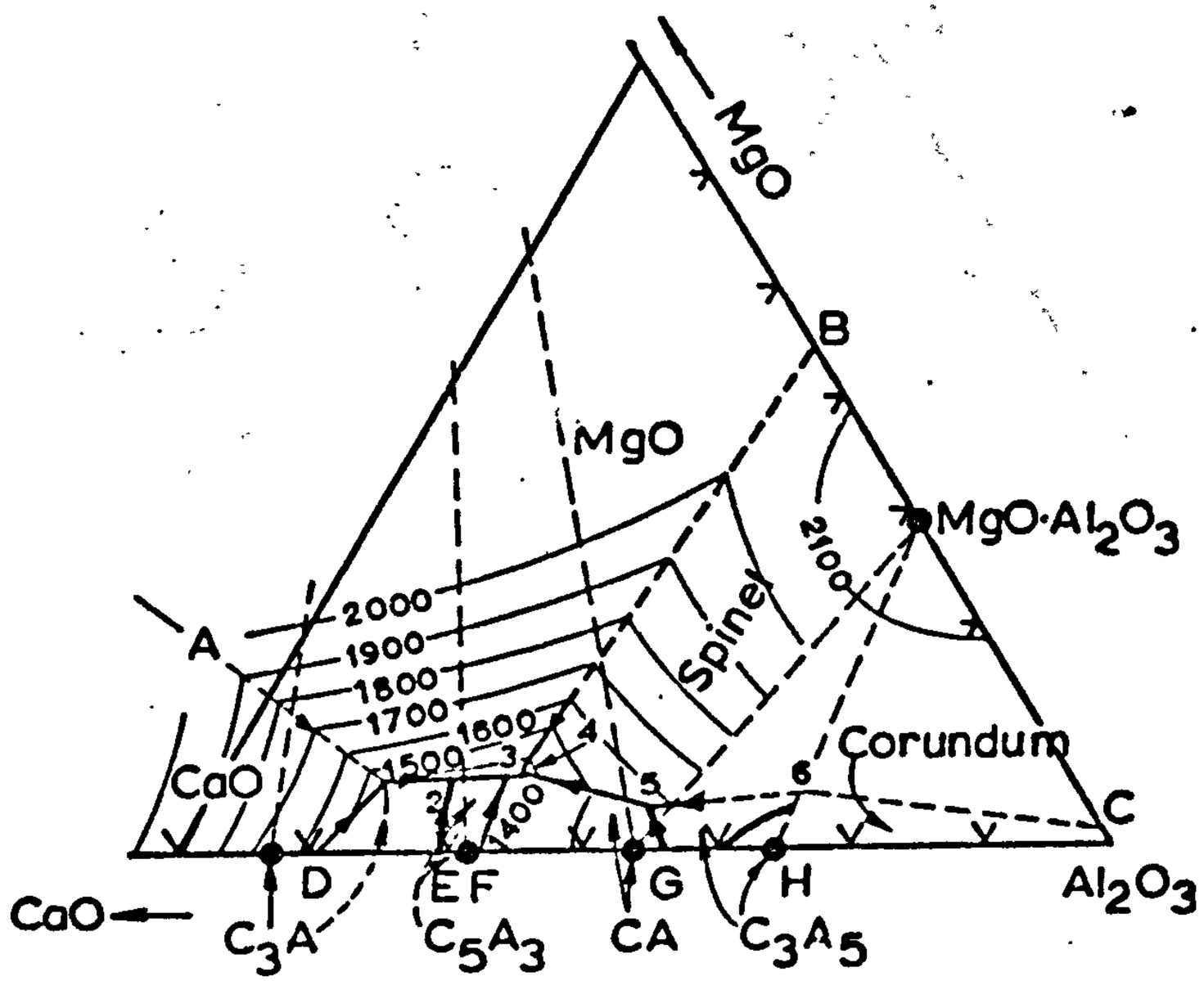


Fig. A4.1a

Pt	Crystal phases	CaO	MgO	Al_2O_3	TEMP.
A	C,M	67	33		2300
B	M,MA		45	55	2030
C	MA,A		2	98	1925
D	C, C_3A	59		41	1535
E	C_3A C_5A_3	50		50	1395
F	C_5A_3 CA	47		53	1400
G	CA.C_3A_5	33·5		66·5	1590
H	C_3A_5, A	24		76	1700
	1.M,C,C_3A	51·5	0·2	42·3	1450
	2*M,C_3A,C_5A_3	46	6·3	47·7	1345
	3*M,C_5A_3,CA	41·5	6·7	51·8	1345
	4 M,MA,CA	45·7	6·9	52·4	1370
	5 MA,CA,C_3A_5	33·3	3·5	63·2	1550
	6 C_3A_5,MA,A	21·0	5·0	74	1680
	5CaO·3Al_2O_3	47·8		52·2	1455
	CaO·Al_2O_3	35·4		64·6	1600
	3CaO·5Al_2O_3	24·8		75·2	1720
	MgO·Al_2O_3		28·4	71·6	2135
	3CaO·Al_2O_3	62·2		37·8	1535
	PERICLASE		100		2800
	LIME	100			2570
	CORUNDUM			100	2050

* eutectic

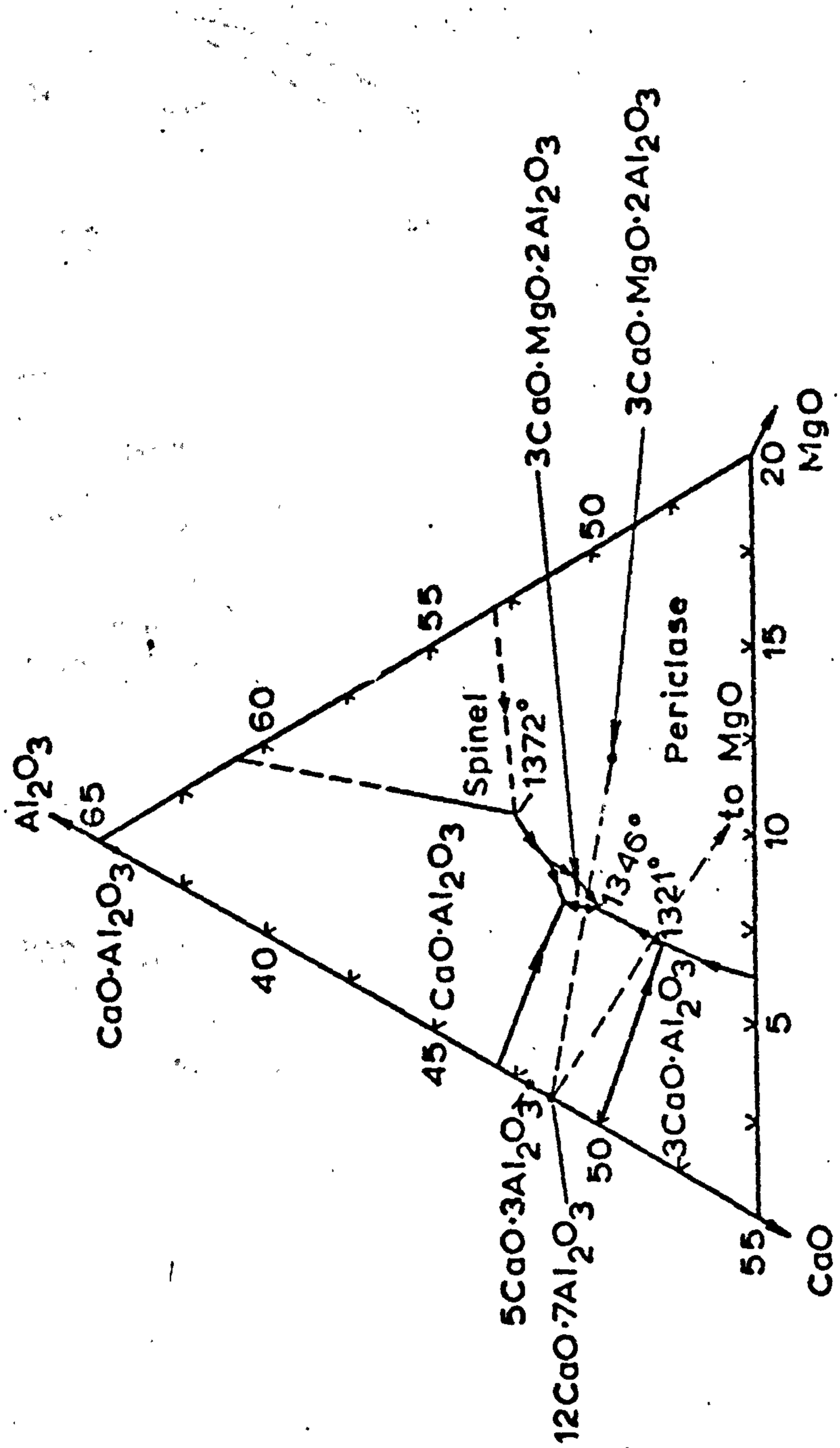

Al_2O_3
65
60
55
50
20
MgO
$3CaO \cdot MgO \cdot 2Al_2O_3$
$3CaO \cdot MgO \cdot 2Al_2O_3$
Spinel
1372°
Periclase
to MgO
15
10
5
$CaO \cdot Al_2O_3$
40
45
$CaO \cdot Al_2O_3$
1346°
1321°
$3CaO \cdot Al_2O_3$
$5CaO \cdot 3Al_2O_3$
$12CaO \cdot 7Al_2O_3$
50
55
CaO

Fig.A4.1b

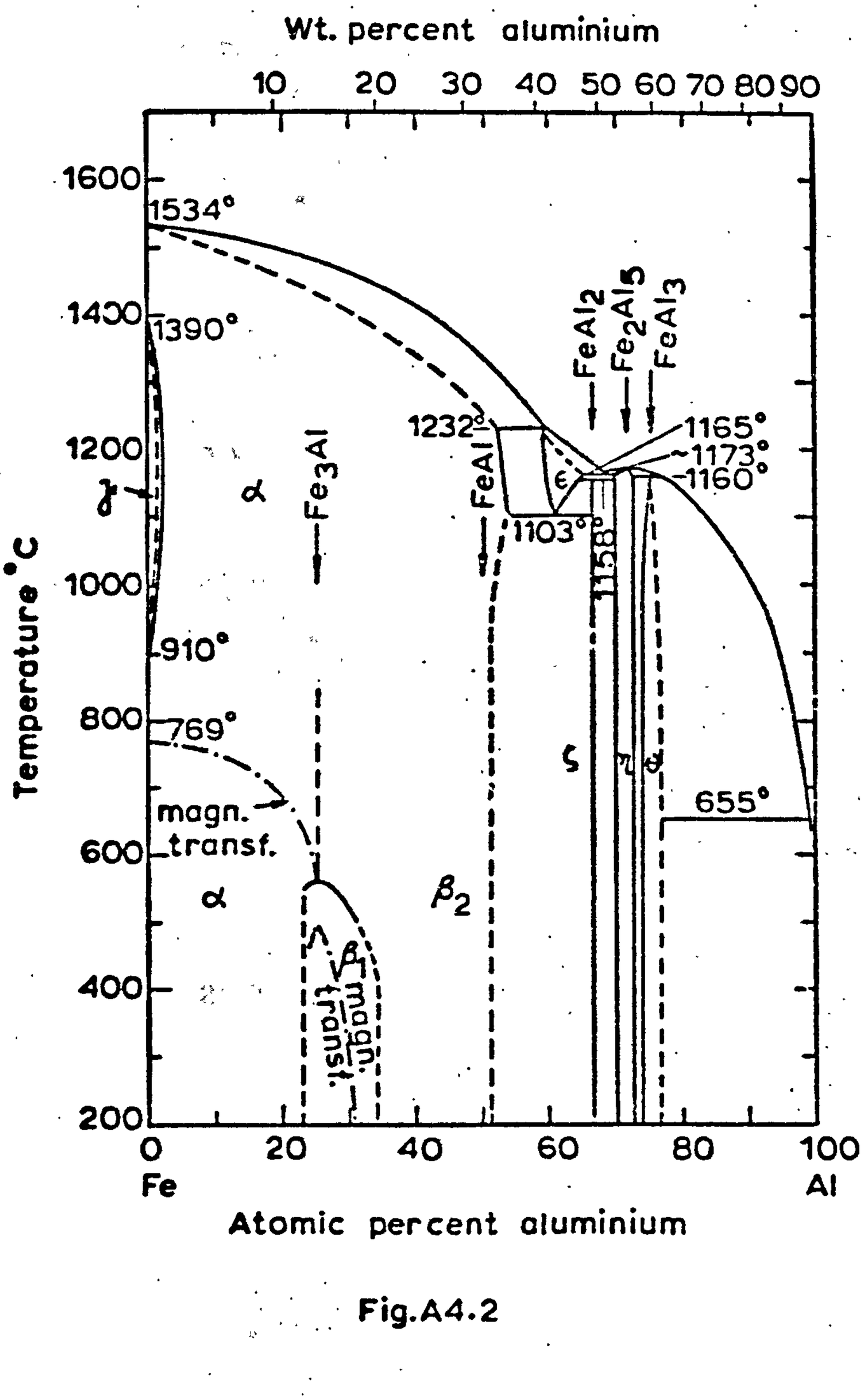

Wt. percent aluminium
10 20 30 40 50 60 70 80 90
1600
1400
1200
1000
800
600
400
200
Temperature °C
1534°
1390°
910°
769°
magn. transf.
γ
α
Fe3Al
FeAl
1232°
1103°
FeAl2
Fe2Al5
FeAl3
1165°
1173°
1160°
1158°
ε
ζ
η
α
655°
α
β2
magn. transf.
β
0 20 40 60 80 100
Fe
Al
Atomic percent aluminium

Fig.A4.2

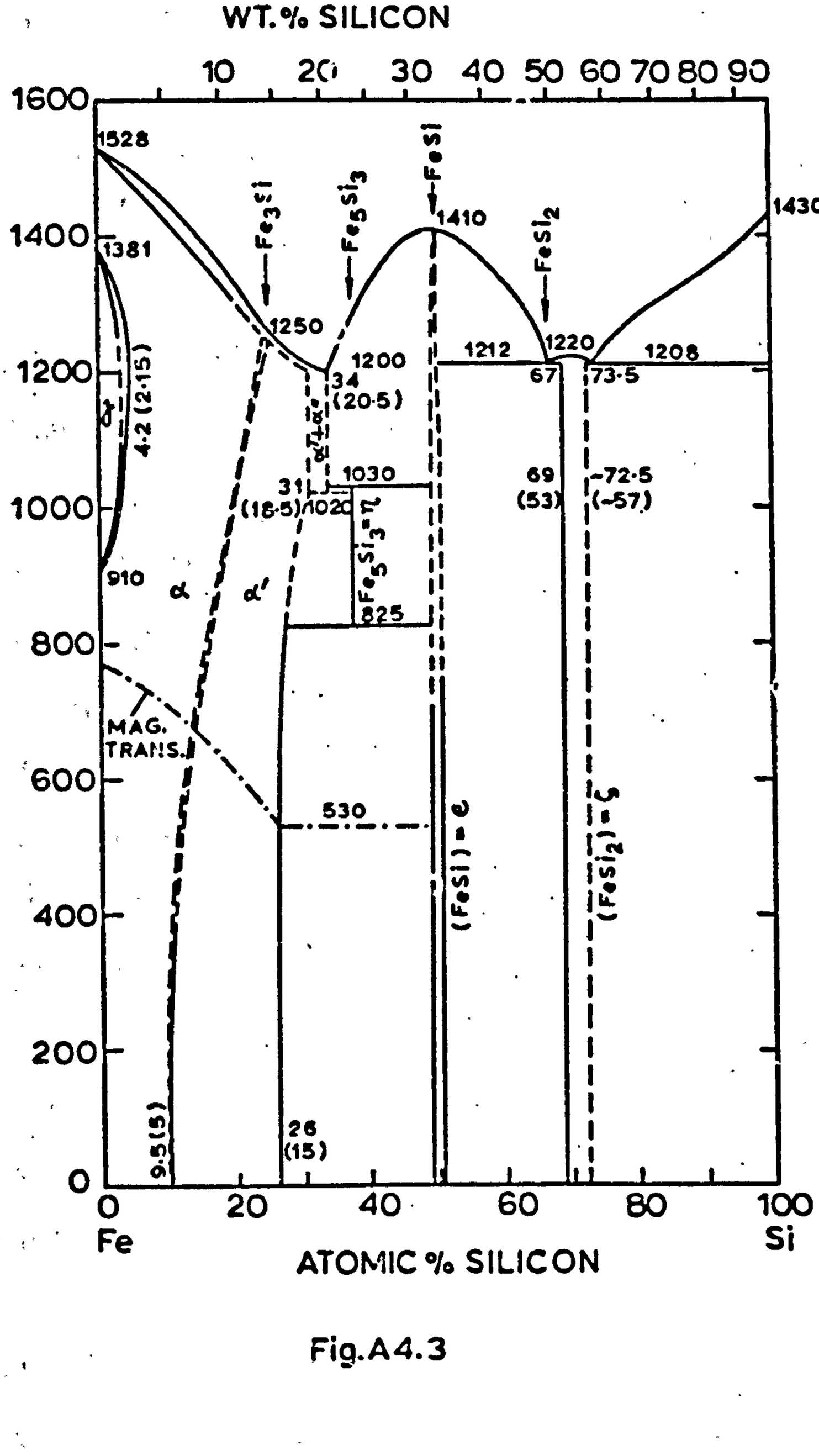

WT.% SILICON
10 20 30 40 50 60 70 80 90
1600
1400
1200
1000
800
600
400
200
0
TEMPERATURE °C
1528
1381
910
1410
1430°
1250
1200
34
(20·5)
1212
1220
67
1208
73·5
1030
31
(18·5)
1020
825
69
(53)
~72·5
(~57)
530
9·5(5)
26
(15)
4·2 (2·15)
α
α'
MAG.
TRANS.
0 20 40 60 80 100
Fe
Si
ATOMIC % SILICON

Fig.A4.3

REFERENCES

(1) DEAN, K.C., ELKINS, D.A. and HUSSEY, S.J. - An economic and technical evaluation of magnesium production methods (Part I - Metallothermic), Bureau of Mines (United States Department of the Interior), R.I. 6656 (1965).

(2) ENLEY, E.F. - Principles of magnesium technology - Pergamon Press (1966).

(3) WINKLER, O. and BAKISH, R. (Editors) - Vacuum Metallurgy - Elsevier Publishing Company (1971).

(4) U.S.P. 2,971,833 (1961).

(5) U.S.P. 3,129,094 (1964).

(6) U.S.P. 3,114,627 (1963).

(7) GRJOTHEIM, K., HEARSTEAD, O. and TOGURI, J.M. - Can. Min. and Metall. Trans ., 65, 1962, 221.

(8) TAITZ, A. Yu. - Tsvetn. Metall., 30, 1957, 56.

(9) KOMATSU, R.-J. - Mining and Metallurgical Institute of Japan - 77, 1961, 899.

(10) KOMATSU, R. and SENDA, O.-J. - Mining and Metallurgical Institute of Japan, 78, 1972, 341.

(11) VIGNIAL, P. and ANDRIEUX, J.L. - Compt. Rend., 242, 1956, 709.

(12) AKERMAN, K. and ORMAN, M. - Acta Tech. Acad. Sci. Hung., 15, 1956, 179.

(13) KUBASCHEWSKI, O.,-EVANS, E.LL. and ALCOCK, C.B. - Metallurgical Thermochemistry - 4th Edition (1967), Pergamon Press Ltd.

(14) JANAF Thermochemical Tables, 2nd Edition - NSRDS-NBS37 - U.S. Department of Commerce, Nat. Bureau of Standards (1971).

(15) ELLIOTT, J.F. and GLEISER, M. - Thermochemistry for Steelmaking - Addison-Wesley, 1960.

(16) SCHNEIDER, A. and Hesse, E. - Z. Elektrochemie, 46, 1940, 279.

(17) PIDGEON, L.M. and KING, J.A. - Disc. Faraday Soc., 4, 1948, 197.

(18) TOGURI, J.M. and PIDGEON, L.M. - Can. J. Chem., 39, 1961, 540, 1769.

(19) KROLL, W.J. - U.S. Bureau of Mines - I.C. 7327 (1945).

(20) KROLL, W.J. - Rev. Met., 48, 1951, 929.

(21) MIKULINSKILL, A.S. and RYABCHIKOV, I.V. - Izv. Vysskikh Uchebnykh Zavedinii (Chernaya Metallurgiya), 6, 1962, 44.

(22) RYABCHIKOV, I.V. and MIKULINSKII, A.S. - Zhurnal Prikldnvi Khimii, 35, (8), 1962, 1656.

(23) RYABCHIKOV, I.V. and MIKULINSKII, A.S. - Russian Metallurgy, 2, 1963, 5.

(24) SCHNEIDER, A. - Z. Metallkunde, 41, 1950, 205.

(25) SCHNEIDER, A., CORDES, J.F., KRIBE, H. and RUNGE, H. - Z. Erzgerbau Metallhuttenw., 12, 1959, 103, 164, 167.

(26) HUGHES, W.T., RANSLEY, C.E. and ENLEY, E.F. - Reaction Kinetics in the production of magnesium by the dolomite-ferrosilicon (Pidgeon) process - Advances in Extractive Metallurgy (Proc. Symp. IMM, London, 1967, 429).

(27) AKERMAN, K., BRAFMAN, M., BIALA, N., KIERZEK, J., TABOR, W., LAPUZSEK, H. and NIZIOLEK, L. - Rev. Met. 64, (11), 1967, 1001.

(28) KRÜGER, J. - Vacuum Metallurgy (Reference 3).

(29) RICHARDSON, F.D. - Physical Chemistry of Melts in Metallurgy (2 volts) - Academic Press, 1974.

(30) KIERSEBON, G.N. - Light Metals Industry, 27, 1964, 44.

(31) FAURE, C. and MARCHAL, J. - J. of Metals, 16, 1964, 721 - Metallurgia Ital., 58, 1966, 82.

(32) TRANCMÉ, F. - The Magnetherm process, Marignac, France - Advances in Extractive Metallurgy and Refining, Proc. Symp. IMM (London), 1971, Paper 24.

(33) GROSS, P., LEVI, D.L., DEWING, E.W. and WILSON, G.L. - The Activities of Aluminium in Al-Fe Alloys - Phys. Chem. of Process Metallurgy, Interscience Publishers, 403, (1961).

(34) HULTGREN, R., ORR, R.L., ANDERSON, P.D. and KELLY, K.K. - Selected values of thermodynamic properties of metals and alloys - Addison-Willey, 1963.

(35) ELLINGSAETER, B. and ROSENQVIST, T. - J. of Metals, 212, 1956, IIII.

(36) CHIPMAN, J., FULTON, J.C., GOKCEN, N. and CASKEY, G.R. - Acta Metallurgica, 2, 1954, 439.

(37) SANBOGI, K. and OHTANI, M. - Science Reports Research Inst., Tohoku Univ., Japan, v. A5, 1953, 350.

(38) Thermodynamic Data Bank, Chemical Standards Division, National Physical Laboratory, Teddington, Middlesex, G.B., 1976.

(39) SCHICK, H.L. - Thermodynamics of certain refractory compounds, Academic Press, 1966.

(40) SHPIL'RAIN, E.E., KAGAN, D.N. and BARKHATOV, L.S. - High temperatures, High pressures, 4 (6), 1972, 605.

(41) KAY, D.A.R. and TAYLOR, J. - Trans. Faraday Soc., 56, 1960, 1372.

(42) OSBORN, E.F., DEVRIES, R.C. and KRANER, H.M. - Trans. Met. Soc. AIME, J. of Metals, Janaury 1954, 33.

(43) KUZLOV, V.A. and MIKULINSKII, A.S. - Izv. Akad. Naut. SSSR, Metal., 1968 (5), 14-8 (Russ), in Chem. Abstr. 70, 1969, 161.

(44) RÈIN, R.H. and CHIPMAN, J. - Trans. Met. Soc. AIME, 233, 1965, 415.

(45) HENDERSON, D. and TAYLOR, J. - J. of Iron and Steel Inst., 204, 1966, 39.

(46) REIN, R.H. and CHIPMAN, J. - Trans. Met. Soc. AIME, 227, 1963, 1193.

(47) TAYLOR, J. - J. of Iron and Steel Inst., 202, 1964, 420.

(48) ELKINS, D.A., PLACEK, P.L. and DEAN, K.C. - An economic and technical evaluation of magnesium production (Part 2 - Carbothermic), Bureau of Mines (U.S. Dept. of the Interior), R.I. 6946, 1967.

(49) CHANDRASEKHARAIAH, M.S. - The characterization of high temperature vapours - MARGRAVE, J.L. (Ed.), J. Willey and Sons Inc., 1967.

(50) TOPOROV, N.A. and BARZAKOVSKII, V.P. - High temperature chemistry of silicates and other exide systems - Consultants Bureau, New York, 1966.

(51) HANSEN, M. and ANDERKO, K. - Constitution of binary alloys, McGraw Hill Book Co., 1958.

(52) TURKDOGAN, E.T., GRIEVESON, P. and BEISLER, J.F. - Trans. Met. Soc. AIME, 227, 1963, 1265.

(53) FULTON, J.C. and CHIPMAN, J. - Trans. Met. Soc. AIME, 215, 1959, 888.

(54) POMFRET, R.J. and GRIEVESON, P. - Some further considerations of the reduction of silica by molten carbon-saturated iron - Symp. High Temperature Chemical Reaction Engineering, The Instn. of Chem. Engrs., Symp. Series 43, 1975, Paper 27.

(55) DAVENPORT, W.G., BRADSHAW, A.V. and RICHARDSON, F.D. - J. of Iron and Steel Inst., 205, 1967, 1034.

(56) PORTER, W.F., RICHARDSON, F.D. and SUBRAMANIAN, K.N. - Some studies of mass transfer across interfaces agitated by bubbles. HILLS, A.W.D. (Ed.), Heat and mass transfer in Process Metallurgy, IMM (London), 1967, 79.

(57) SUBRAMANIAN, K.N. and RICHARDSON, F.D. - J. of Iron and Steel Institute, 206, 1968, 576.

(58) BRIMACOMBE, J.K. and RICHARDSON, F.D. - Trans. Instn. Min. Met. (Section C), 80, 1971, C140.

(59) BRIMACOMBE, J.K. and RICHARDSON, F.D. - Trans. Instn. Min. Met. (Section C), 82, 1973, C63.

(60) ROBERTSON, D.G.C. and STAPLES, B.B. - Model studies on mass transfer across a metal-slag interface stirred by bubbles. JONES, J.J. (Ed.), Process Engineering of Pyrometallurgy, IMM (London), 1974, 51.

(61) SHARMA, R.A. and RICHARDSON, F.D. - J. Iron and Steel Inst., 198, 1961, 386.

(62) CHIPMAN, J. and FLORIDIS, T.P. - Acta Metallurgica, 3, 1955, 456.

(63) DARKEN, L.S. - Trans. Met. Soc. AIME, 239, 1967, 80.

(64) DARKEN, L.S. - Trans. Met. Soc. AIME, 239, 1967, 90.

(65) CHIPMAN, J., ALFRED, R.M., GOTT, L.W., SMALL, R.B., WILSON, D.C., THOMPSON, C.N., GUERSEY, D.L. and FULTON, J .C. - Trans. Am. Soc. Met., 44, 1952, 1215.

(66) PIDGEON, L.M. and ALEXANDER, W.A. - Trans. Met. Soc. AIME, 159, 1944, 315.

(67) MAYER, A. - Trans. Met. Soc. AIME, 159, 1944, 363.

(68) HUMES, W.B. - Trans. Met. Soc. AIME, 159, 1944, 353.

(69) Brit. Pat. 606, 637, 606, 644.

(70) HANAWALT, J.D. - J. of Metals, 16, 1964, 559.

(71) WEISS, P. - Erzmetall., 20, 1967, 249.

(72) RITTER, F. and JAEKEL, G. - Magnesium. WINNACKER, K. and KUCHLER, L. (Eds.), Chemischie Technologie, Vol. 5, Metallurgie/Allgemeines, Hanser Verlag, Munich, 1961, 106.

(73) U.S.P. 3,151,977.

(74) U.S.P. 3,441,402.

(75) ROSENQVIST, T. - Principles of extractive metallurgy - McGraw Hill Book Company, 1974.

(76) LEVIN, E.M., ROBINS, C.R. and McMURDIE, H.F. - Phase Diagram for Ceramists - The American Ceramic Society.

(a) 1964

(b) supplement 1969

(77) BODSWORTH, C. and BELL, H.B. - Physical Chemistry of iron and steel manufacture - Longman Group Limited, 2nd Edition, 1972.

(78) SHUNK, F.A. - Constitution of Binary Alloys (2nd Supplement), McGraw Hill Book Co., 1969.

(79) LITVINOVA, T.I.; KRAVCHENKO, V.A.; BARZAKOVSK'II, V.P. AND RAICHENKO, T.F. Chemical Abstracts, 69 (1968), 6734, 72037 g.

ACKNOWLEDGEMENTS

I am greatly indebted to Dr. V. Rajakumar for his excellent supervision. His suggestions and criticisms were essential for the progress of my research. I am grateful to Professor A.V. Bradshaw and Dr. R.J. Tait for their supervision during the initial stages of this work. I am also glad to acknowledge the very helpful discussions I have had with Professor F.D. Richardson.

I am most grateful to Mr. A. Willis for his assistance during the experimental campaign and to Mr. A. Neve for his interest and suggestions. I am grateful to Mr. J. Herbertson and other members of the John Percy Research Group for useful discussions.

I thank Mr. J. Rossdale and Miss P. Martin for the assistance I received in the preparation of several illustrations and Mr. A.J. Tipple for his expert work on the diagrams. I also thank Miss Anne Usher, Mrs. Anne de Sayrah and Miss Susan Hayden for their work in producing the typescript.

I gratefully acknowledge the financial support of Fundação ao Amparo à Pesquisa do Estado de São Paulo and the Instituto de Pesquisas Tecnológicas do Estado de São Paulo S/A.

Finally, thanks are due to my family for tolerating long periods of separation and to many friends, in particular to Mr. H.P. Rizzo, for the useful help I received on many occasions.